Elimination of reactive nitrogen in continental shelf sediments measured by membrane inlet mass spectrometry.

Dissertation
zur Erlangung des Doktorgrades der Naturwissenschaften.

Eingereicht im
Department Geowissenschaften,
Fakultät für Mathematik, Informatik und Naturwissenschaften,
Universität Hamburg.

vorgelegt von

Andreas Neumann

aus
Magdeburg

Hamburg
2012

Als Dissertation angenommen vom Department für Geowissenschaften,
Fakultät für Mathematik, Informatik und Naturwissenschaften,
Universität Hamburg auf Grund der Gutachten von

Prof. Dr. Kay-Christian Emeis

und

Dr. Justus van Beusekom

Hamburg, den 14. 5. 2013

Prof. Dr. Jürgen Oßenbrügge
Leiter des Department Geowissenschaften

Überblick

Stickstoff ist eines der Hauptelemente aller Organismen, und deshalb ein wichtiger Nährstoff pflanzlicher Primärproduzenten. In den letzten einhundert Jahren wurden mittels industrieller Stickstofffixierung exponentiell anwachsende Mengen reaktiven Stickstoffs erzeugt, und als Dünger auf landwirtschaftlichen Flächen ausgebracht. Diese anthropogene Stickstofffracht erreicht hauptsächlich als Nitrat in Flüssen wie der Elbe auch die Küstengewässer. Dort führt sie zu Eutrophierung, die im Weiteren unerwünschte Algenblüten, sauerstoffarme Bodenwässer und Massensterben verursachen kann. Dem anthropogenen Stickstoffeintrag stehen mikrobielle Prozesse wie Denitrifikation und Anammox gegenüber, die reaktiven Stickstoff in N_2 zurückwandeln und somit aus dem Ökosystem entfernen. Ziel der vorliegenden Arbeit war es, die Eliminierung reaktiven Stickstoffs in den Sedimenten des Elbe-Ästuars und der anschließenden Deutschen Bucht zu messen, um die Faktoren zu identifizieren, die diese Eliminierung kontrollieren.

In Kapitel zwei wird eine bisher kaum genutzte Methode zur Messung von N_2-Profilen im Sediment mittels Membraneinlass-Massenspektrometrie aufgegriffen und für Routinemessungen in den Sedimenten der Deutschen Bucht angepasst. Die neu entwickelte Membranspitze weist eine größere mechanische Festigkeit auf als bisher vorgestellte Bauformen, und erlaubt Messungen mit geringerer Störung im Sediment. Zusätzlich wurden mögliche Störfaktoren identifiziert und eine Möglichkeit zur Korrektur der Messwerte vorgeschlagen.

Der entwickelte Membraneinlass für N_2-Profilmessungen im Sediment wurde entlang des Salinitätsgradienten des Elbe-Ästuars und der Elbwasserfahne in der Deutschen Bucht eingesetzt (Kapitel 3). Die erhaltenen N_2-Flüsse aus dem Sediment in die Wassersäule sind ein Maß für die Eliminierung reaktiven Stickstoffs im Sediment. Die gemessenen N_2-Produktionsraten korrelierten mit der Nitratkonzentration im Bodenwasser und dem TOC-Gehalt des Sedimentes. Eine Sauerstoff- oder Temperaturabhängigkeit wurde dagegen nicht beobachtet. Die aus Nitratprofilen errechneten Nitratflüsse aus der Wassersäule ins Sediment zeigten ein ähnliches Muster, deckten sich aber nicht mit den N_2-Produktionsraten. Besonders in permeablen Sanden wurde deutlich mehr N_2 produziert als Nitrat gezehrt wurde, sodass gekoppelte Nitrifikation-Denitrifikation als wahrscheinlichste Quelle der zusätzlichen N_2-Produktion erscheint.

Im vierten Kapitel wurden die im Elbe-Salzgradienten gefundene Abhängigkeit der benthischen Nitratzehrung und N_2-Produktion von Nitratkonzentration und TOC-Gehalt als Grundlage benutzt, um eine Schätzfunktion für die beiden Reaktionsraten

herzuleiten. Diese Schätzfunktion beschreibt den angenommenen Einfluss von Nitratkonzentration, Sauerstoffkonzentration und TOC-Gehalt auf Nitratzehrung und N_2-Produktion. Kalibriert wurde die Funktion sowohl mit Daten von 70 Stationen im Elbeestuar, dem Nordfriesischen Wattenmeer und der Deutschen Bucht, als auch mit veröffentlichten Daten von verschiedensten Ökosystemen des Atlantiks. Beide Kalibrierungen wurden mit Verteilungskarten von Nitrat, Sauerstoff und TOC verwendet, um die Nitratzehrung und N_2-Produktion in den Sedimenten der Elbfahne zu schätzen. Im Winter (Februar, März 2009) wurden 1 % der Nitratfracht direkt durch Denitrifikation entfernt. Durch gekoppelte Nitrifikation-Denitrifikation wurde N_2 produziert, dass 3-7 % der Nitratfracht entsprach. Im Sommer (August, September 2009) blieb die Nitratentfernung durch direkte Denitrifikation bei 2-3 % der Elbefracht, wogegen die N_2-Produktion durch gekoppelte Nitrifikation-Denitrifikation 19-43 % der Elbefracht entsprach. Die Stickstoffquelle für die dominante Nitrifikation-Denitrifikation ist organische Substanz, dessen Stickstoff bei der Primärproduktion als Nitrat aus dem Wasser aufgenommen wurde. Somit wurde letztlich die Assimilation von Nitrat durch Primärproduzenten als wesentlicher Prozess zur Entfernung von Nitrat aus der Wassersäule identifiziert, dass teilweise durch anschließende Ammonifikation-Nitrifikation-Denitrifikation im Sediment als N_2 eliminiert wird.

Die in der Nordsee verwendeten Methoden zur Profilmessung von N_2 und Nährstoffen wurden zusätzlich im Benguela-Auftriebsgebiet vor Namibia (Südliches Afrika) eingesetzt (Kapitel 5). Auch in diesem Ökosystem hatte die gekoppelte Nitrifikation-Denitrifikation einen höheren Anteil an der N_2-Produktion als die direkte Denitrifikation von Nitrat aus der Wassersäule. Anders als in der Nordsee konnte im Auftriebsgebiet vor Namibia ein deutlicher Einfluss von Temperatur und Sauerstoffkonzentration auf die Remineralisierung nachgewiesen werden, wogegen der TOC-Gehalt des Sedimentes keinen nachweisbaren Effekt hatte. Als Ursache für diesen scheinbaren Widerspruch konnte die hohe Variabilität der unter vergleichbaren Bedingungen gemessenen Nitratzehrung beziehungsweise N_2-Produktion identifiziert werden, die die Effekte von Parametern mit nur geringer Variation verdeckte.

Overview

Nitrogen is one of the mayor building blocks of organisms and thus an important nutrient of primary producers. During the last century, exponentially increasing amounts of reactive nitrogen were produced by industrial nitrogen fixation and subsequently dispersed as agricultural fertilizer. This anthropogenic reactive nitrogen is partially leached from the soil, transported mainly as nitrate by rivers such as Elbe, and finally reaches the coastal ecosystem. The nitrate load contributes to eutrophication and may cause harmful algae blooms, bottom water anoxia and mass extinctions. However, the anthropogenic nitrogen fixation is opposed by microbial processes such as denitrification and anammox, which convert reactive nitrogen back into N_2 and thus effectively remove the nitrogen from the ecosystem. The objective of the present study was measuring the elimination of reactive nitrogen in the sediment of the Elbe estuary and the adjacent German Bight (North Sea), and identifying the controlling environmental factors.

The second chapter presents a rarely employed method of N_2-profile measurements with membrane inlet mass spectrometry, which was adopted for measurements in North Sea sediment. The newly developed membrane tip featured improved mechanical durability and enabled measurements with less sediment disturbance than previously presented types. Potential interferences of N_2/Ar measurement by sediment properties were identified, and a correction of biased measurements was proposed.

The newly-developed membrane-inlet for N_2-profiling in sediments was employed along the salinity gradient of Elbe estuary and the adjacent Elbe plume (chapter 3). The obtained N_2 fluxes from the sediment into the water column are a proxy of elimination of reactive nitrogen within the sediment. The N_2 fluxes correlated with the bottom water nitrate concentrations and sediment TOC content, respectively. An impact of oxygen or temperature was not evident. The calculated nitrate fluxes from the water column into the sediment based on nitrate concentration profiles had a similar pattern, but did not match exactly the N_2 fluxes. Especially in permeable sediment, N_2 fluxes significantly exceeded the nitrate consumption, and coupled nitrification-denitrification was identified as most probable source of additional N_2 production.

The correlation of benthic nitrate consumption and N_2 production with the availability of nitrate, oxygen and TOC, as found in the salinity gradient of the Elbe (chapter 3), was used as basis for the derivation of an estimation function of both reaction rates (chapter 4). This estimation function describes the assumed effect of nitrate, oxygen

and TOC on benthic nitrate consumption and N_2 production. The function was calibrated with the data of 70 stations in the Elbe estuary, North-Frisian Wadden Sea and German Bight, and additionally with compiled published data comprising various ecosystems of the Atlantic. Both calibrations were used in combination with distribution maps of nitrate, oxygen and TOC to estimate the rates of nitrate consumption and N_2 production in sediments of the Elbe plume. During winter (February, March 2009), direct denitrification removed 1 % of the Elbe nitrate load. Coupled nitrification-denitrification produced N_2 equal to 3-7 % of the nitrate load. During summer (August, September 2009), direct denitrification removed 2-3 % of the nitrate load, whereas coupled nitrification-denitrification produced N_2 equal to 19-43 % of the nitrate load. The nitrogen source of coupled nitrification-denitrification is organic matter, which contains nitrogen assimilated as nitrate during primary production. Thus assimilation was identified as the dominant nitrate-removing process. The assimilated nitrogen is subsequently partially eliminated as N_2 by ammonification-nitrification-denitrification.

The methods employed for profiling of N_2 and nutrients in North Sea sediment were additionally used in sediments of the Benguela Upwelling System off Namibia, southern Africa (chapter 5). Likewise to North Sea sediment, coupled nitrification-denitrification had a higher contribution to benthic N_2 production than direct denitrification of water column nitrate. In contrast to the North Sea, a substantial impact of temperature and oxygen on remineralisation was found in sediments of Benguela Upwelling System, whereas the bulk sediment TOC content had no evident effect. The reason for this apparent contradiction of results from North Sea and Benguela was the high variability of nitrate consumption and N_2 production observed under similar conditions, which disguised the effects of parameters with little variance.

Table of content

1. Introduction

1.1 The nitrogen cycle: human impacts and consequences

The importance of reactive nitrogen as an essential nutrient for the primary production and thus a powerful adjustment factor for the entire biosphere has been recognized at the latest in the 19th century by von Liebig (1840). Since the development of the Haber-Bosch process in the early 20th century to industrially fixate atmospheric dinitrogen, man is introducing exponentially increasing amounts of reactive nitrogen into the global nitrogen cycle. After just a century, fertilizer made of industrially fixated nitrogen is providing approximately 50 percent of the world's food production and projections for the future assume a further increase (Erisman et al. 2008). However, only a fraction of the deployed nitrogen fertilizer is assimilated by the plants or stored in the soils, the rest is drained directly into surface waters and aquifers. A major fraction of the plant assimilated nitrogen is released into the water bodies via manure and sewage in the following. Thus, there is a significant correlation between population density and its ecological wealth, and discharge of reactive nitrogen from river catchments (Howard et al. 1996). In consequence, anthropogenic sources have doubled the turnover rates of the global nitrogen cycle (Gruber & Galloway 2008).

In pace with global trends, the nitrogen loads of the rivers discharging into the southern North Sea have increased tenfold during the last five decades (Behrendt and Opitz 1999). This anthropogenic reactive nitrogen is driving primary production in the open North Sea (Owens et al. 1990) as well as the coastal Wadden Sea (van Beusekom et al. 2001, van Beusekom & de Jonge 2002), where the turnover rates have increased fivefold compared to the assumed background intensities (van Beusekom 2005). This eutrophication led to several severe effects on the coastal marine system: Shifts of the nutrient stoichiometry, massive phytoplankton blooms and oxygen depletion in the southern North Sea and the Wadden Sea, the decline of seagrass and shifts of the species composition of plankton and benthos (Lancelot et al. 1987, van Beusekom et al. 2001, van Beusekom et al. 2005). These and other undesirable effects of the eutrophication have been acknowledged and led to new water management policies, as for example the 'Convention for the Protection of the Marine Environment of the North-East Atlantic' (OSPAR), the 'Baltic Marine Environment Protection Commission' (HELCOM) and the 'European Water Framework Directive' (WFD). Most recently the EU Marine Strategy Framework Directive (MSFD) requests a comprehensive management of human activities to minimize their impacts on marine systems to re-establish a "good environmental

status". However, successful realization of water management policies demands exact and quantitative knowledge on the different processes of nitrogen cycling in the ambience and their rates under varying conditions.

A simplified overview about the known nitrogen pathways is illustrated in figure 1.1. Dinitrogen gas (N_2) in the atmosphere is the largest nitrogen pool on Earth and is present in the aquatic systems in the magnitude of several hundred micromoles per litre. Because its N≡N triple bond is very energy-rich, it is inert and can be converted to reactive form only by specialized microorganisms by nitrogen fixation. Briefly, these organisms use the nitrogenase enzyme complex to catalyze the addition of hydrogen to the N_2 molecule and to produce ammonium as the final product (Postgate 1998). Once the nitrogen has been assimilated, it is released as ammonium when the organic nitrogen compounds are remineralized. This ammonium can either be re-assimilated or oxidized to nitrite and further to nitrate via aerobic nitrification (Winogradsky 1892). Alternatively, ammonium can be oxidized anaerobically to nitrate by manganese reduction (Hulth et al. 1999, Bartlett et al. 2008). Nitrate is reduced back to ammonium via dissimilatory nitrate reduction in combination with fermentation or sulphide oxidation (Brunet & Garcia-Gil 1996, An & Gardner 2002). Nitrate can also be consumed by respiratory denitrification to oxidize organic carbon, methane (Islas-Limaa et al. 2002) or ferrous iron (Straub et al. 1996) and thus becomes an important oxidant under environmental conditions when molecular oxygen (O_2) is unavailable. Both nitrate and ammonium form the major inorganic compounds of reactive nitrogen, with nitrate prevailing under aerobic conditions and ammonium being typical for anaerobic conditions. In contrast, nitrite (NO_2^-) is an intermediate of many metabolic pathways involving nitrogen as for example the nitrification of ammonium or the denitrification. The nitrite acts as a hub for reactive nitrogen and rarely accumulates due to rapid utilisation. Further, nitrite has been identified as substrate of some recently discovered pathways, such as the anaerobic ammonium oxidation (Mulder et al. 1995) or the heterotrophic production of molecular oxygen (Ettwig 2010). Bulla et al. (1970) reported non-biological reduction of nitrite with ferrous iron. Some of the recently described new pathways of nitrogen cycling are still subject of debate, as for example the anaerobic ammonium oxidation to dinitrogen coupled to manganese reduction (Luther et al. 1997, Thamdrup & Dalsgaard 2002).

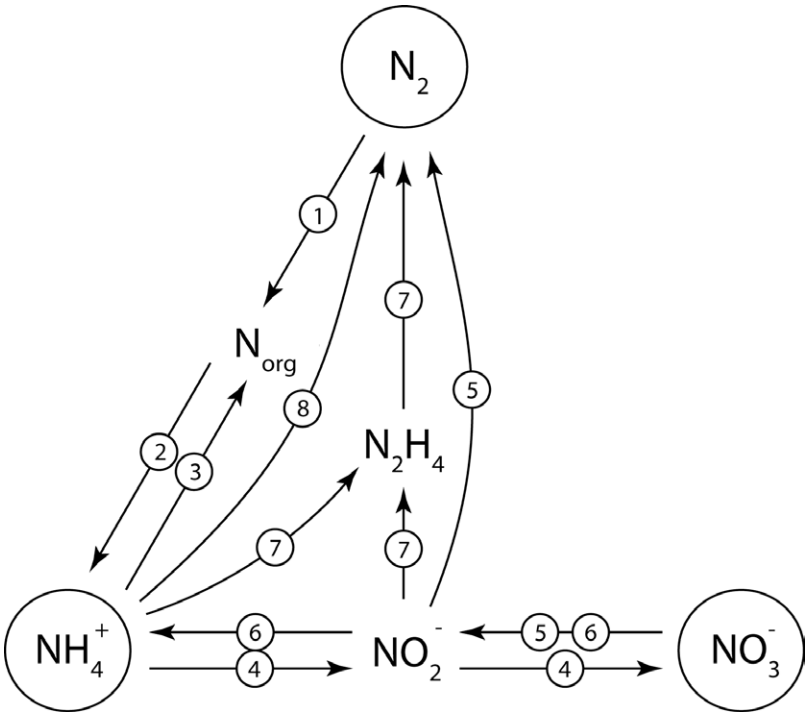

Fig 1.1: Simplified scheme of nitrogen pathways. 1: nitrogen fixation, 2: ammonification, 3: assimilation, 4: nitrification, 5: respiratory denitrification, 6: dissimilatory nitrate reduction to ammonium (DNRA), 7: anaerobic ammonium oxidation (Anammox), 8: manganese catalyzed ammonium oxidation. See text for details.

Especially within sediments, all pathways tend to be intimately coupled and reversible, because the redox gradients are steep. Examples are the coupling between nitrification and denitrification or between nitrate reduction and anammox (Thamdrup & Dalsgaard 2002, Kartal et al. 2007). Thus, nitrogen changes between the various reactive species and rapidly reacts to changes of geochemical conditions. This dynamic behaviour expands the classic nitrogen cycle to a complex metabolic network with interfaces to other 'cycles', as for example those of carbon, sulphur, iron and manganese. As the beginning, the end of many processes is the formation of dinitrogen gas, because the reversal process nitrogen fixation is energetically expensive and should occur exclusively when reactive nitrogen compounds are otherwise unavailable. Thus, the measurement of dinitrogen fluxes from individual compartments of an ecosystem enables to account for the elimination of reactive nitrogen in the system. Other accounting tools, such as the determination of nitrification or denitrification rates from observation of ammonium and nitrate concentrations do not allow distinguishing between elimination, rapid internal turnover by coupled nitrification-denitrification, storage (within sulphur bacteria, Sayama 2001, Preisler et al. 2007) or masking by adsorption to silicates or humic substances.

1.2 Working area 1: Elbe estuary and Wadden Sea

The North Sea is a semi- enclosed marginal sea and sensitive to eutrophication due to the long residence times of the water masses. The criteria of the OSPAR identify the North Sea as a problem area with high nutrient concentrations and high N:P ratios (van Beusekom et al. 2001, OSPAR 2003). The high nitrogen load is caused by the high population density and the intensive agriculture in the catchment area. This antropogenic nitrogen reaches the German Bight via the river Elbe, which is the major freshwater discharge into the German Bight. This led to increasing loads of inorganic nitrogen compounds (DIN) and other pollutants. The concentrations of these pollutants reached a maximum in the 1980's and various efforts reduced these loads since then. The Elbe has annually introduced 840 x 10^3 tons of nitrate during peak discharges in 1987 and 280 x 10^3 tons of nitrate in 2008 (ARGE), after several managerial and political measures have been introduced to curb eutrophication. However, the reduction of the different nutrient loads was not simultaneous. The concentration of phosphate has been decreasing since the 1980's when the concentration of DIN was still increasing, thus shifting the N:P molar ratio from 50 in 1982 to > 200 around the year 2000. Additionally, increasing oxygen levels and decreasing concentrations of toxic trace compounds (e.g. Pb, Hg) enabled higher nitrification rates which shifted the ratio between ammonium and nitrate almost completely towards nitrate (ARGE 2007) as illustrated in figure 1.2.

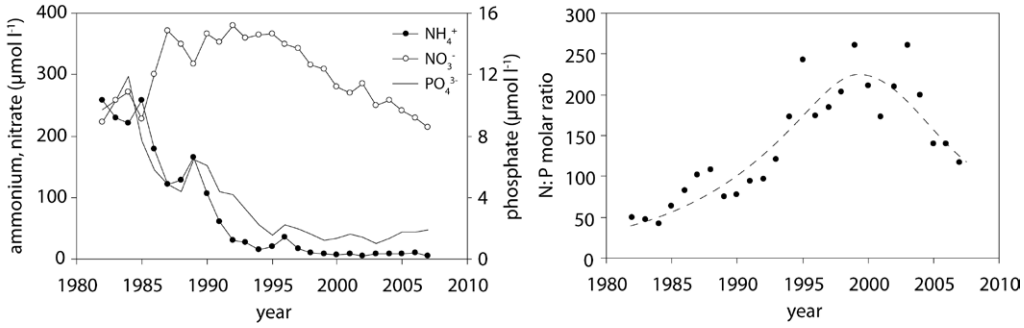

Fig. 1.2: Temporal variation of the nitrogen load of the river Elbe. Left panel: Annual mean concentrations of nutrients in the Elbe estuary at Seemannshöft. Right panel: Molar N:P ratio of DIN and DIP. Data from ARGE 2007.

The North-Frisian Wadden Sea is a part of the German Bight and is directly affected by the river Elbe loads of nutrients, because the plume of the Elbe is deflected northward and is seen in low salinity and high nutrient concentrations along North-Frisian coast (Fig. 1.3). Here, tidal oscillation drives the exchange of water and matter between the Wadden Sea and the Elbe plume, injecting nitrate as well as particulate organic carbon (POC) into this area of extensive back- barrier tidal flats. According to Cornwell et al. (1999), denitrification rates are dependent on the sedimentary

inventory of organic matter, the nitrate concentration in the bottom water in contact with the sediment, the physical exchange rates between water column and sediment interstices, and some secondary factors like the presence of macrofauna or iron sulphide. These factors are generally believed to be advantageous in the shallow North Sea and particular in the mud flats of the Wadden Sea because high nitrate concentrations meet high fluxes of total organic carbon (TOC) into the sediment, whereas hydrodynamic forcing accelerates the transport of nitrate from the water column into the sediment, where denitrification occurs below the zone of oxygen penetration. Thus, the shallow North Sea sediments and mud flat sediments are likely to be effective sinks for reactive nitrogen.

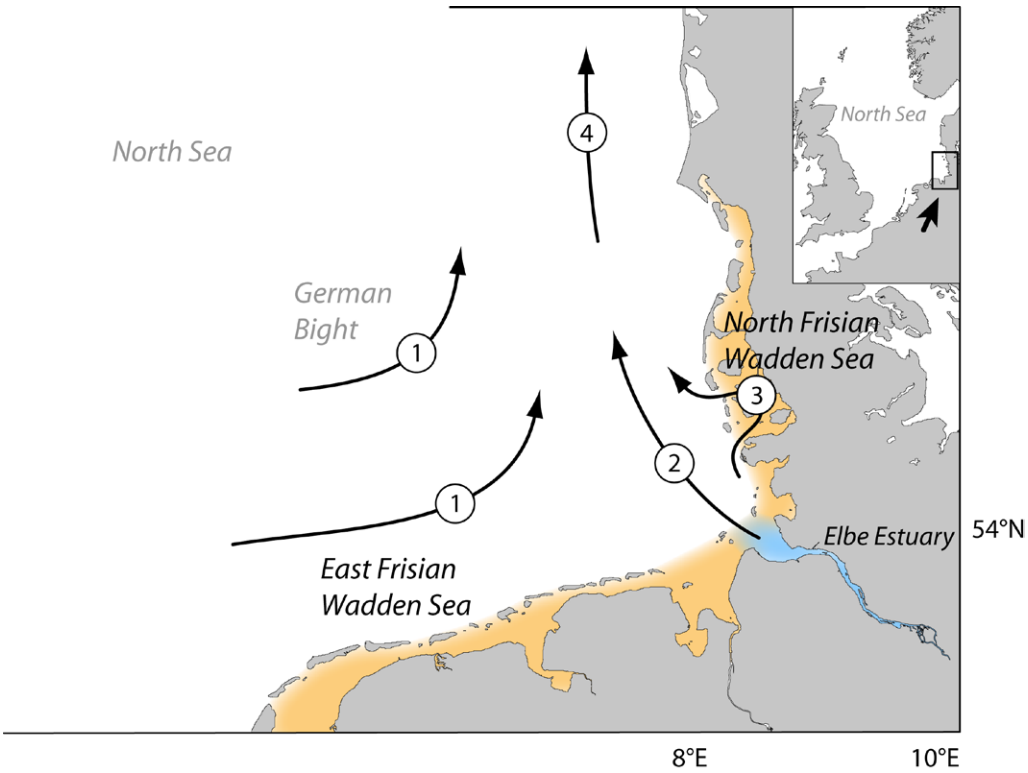

Fig. 1.3: Map of working area 1. The Elbe estuary is highlighted with blue hue, and the North-Frisian Wadden Sea is highlighted with orange hue. The arrows illustrate major currents in the German Bight: Dominant counter-clockwise circulation (1), northward deflected Elbe plume (2), tide-driven exchange between Elbe plume and North Frisian Wadden Sea (3), Jutland current (4). Illustration based on Breton & Salomon (1995).

1.3 Previous studies examining North Sea and Wadden Sea sediments

Sediment denitrification rates have been estimated for the North Sea based on mass balances calculations on the difference between sources and sinks with the difference being assumed as coupled nitrification-denitrification, or based on the biological oxygen consumption (Seitzinger & Giblin 1996). These approaches yielded values in the range of 580 x 10^3 tN a^{-1} (Hydes et al. 1999) and 2080 x 10^3 tN a^{-1} (Brion et al. 2004) or 0.02 mmol m^{-2} d^{-1} and 0.13 mmol m^{-2} d^{-1}, respectively. Further assuming a total introduction of 2436 x 10^3 tN a^{-1} of reactive nitrogen from fluvial and atmospheric sources, the thus estimated rates of denitrification would eliminate all fluvial nitrogen loads and additionally between 12% and 37% of the oceanic nitrogen advected into the North Sea (Brion et al. 2004). Pätsch et al (2010) used an ecosystem model of the North Sea to simulate the nitrogen fluxes of the German Bight and accounted 868 x 10^3 tN a^{-1} to benthic denitrification, which equals an average denitrification rate of 1.35 mmol m^{-2} d^{-1}. The denitrification rates in the Wadden Sea should be even higher than the estimated 0.02 to 1.35 mmol m^{-2} d^{-1} because the physical, chemical and biological properties of the Wadden Sea sediments combine to conditions ideal for denitrification.

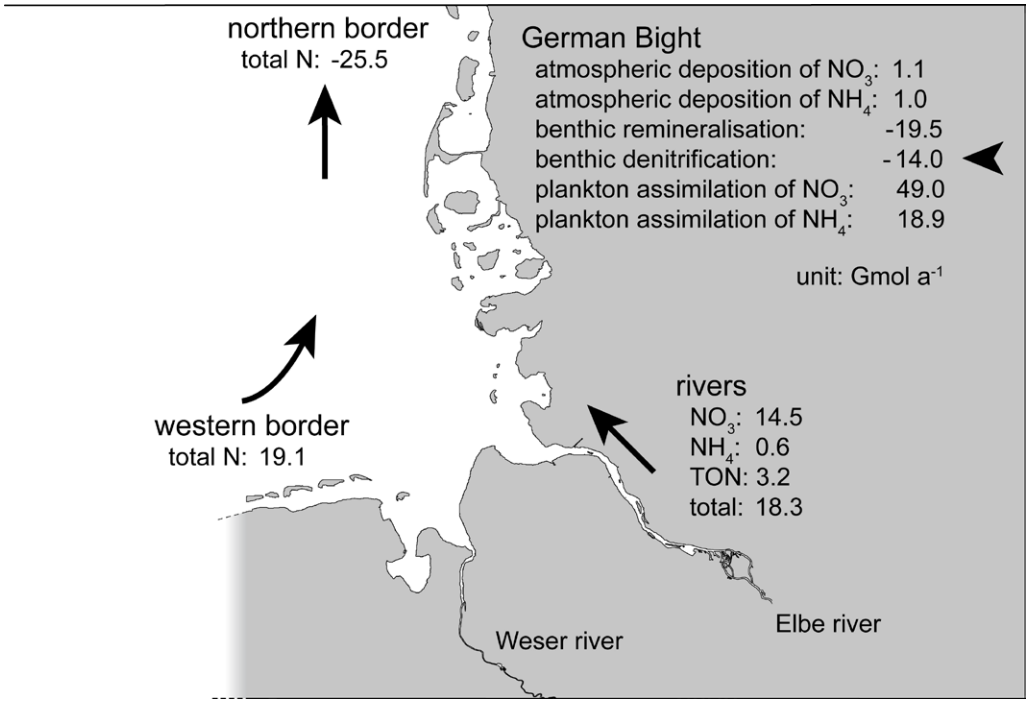

Fig. 1.4: Sources, sinks and turn-over processes of reactive nitrogen in the German Bight as simulated by Pätsch et al. (2010).

The denitrification potential of sediments in the Wadden Sea has been addressed by few studies yet. Dick et al. (1999) used a mass balance approach for the North-Frisian Wadden Sea and estimated a daily nitrate deficit between 48 and 464 tons of nitrate per day for the entire area. This would imply a denitrification rate between 0.8 and 8.3 mmol m^{-2} d^{-1}, if the complete nitrate deficit is attributed to denitrification. Van Beusekom and de Jonge (1998) estimated a denitrification rate of 2.5 mmol m^{-2} d^{-1} for the Ems estuary in the Dutch Wadden Sea, which would eliminate 19% of the total nitrogen input to this area. This result based on budget calculations is significantly above the estimated denitrification rates of sediments in the open North Sea, which are assumed to be in the range of 0.3 to 0.7 mmol m^{-2} d^{-1}. Direct measurements of benthic denitrification rates in the Elbe estuary and the adjacent German Bight are also rare. Schroeder et al. (1996) established denitrification rates in the Elbe estuary between 1984 and 1989 and observed denitrification rates between 1 and 9 mmol m^{-2} d^{-1} depending on location and season. Lohse et al. (1993) examined North Sea sediments in 1991 and 1992 and reported denitrification rates that ranged from 0 mmol m^{-2} d^{-1} to 0.2 mmol m^{-2} d^{-1}. Beddig et al. (1997) subsequently used these empirical results for a reactive nitrogen mass balance of the German Bight. In this model, the sources of DIN exceeded the sinks by 100 x 10^3 tN a^{-1} and the authors suggested that Lohse et al. (1993) underestimated the true denitrification rates. The nitrogen balance of Beddig et al. (1997) has been reviewed by Beusekom et al. (1999) in the light of newer denitrification studies. They propose that the denitrification rates in the German Bight and the adjacent Wadden Sea are high enough to balance the sources of reactive nitrogen. Recently, Gao et al. (2010) examined permeable sediments from the East-Frisian Wadden Sea and reported denitrification rates as high as 11.3 mmol m^{-2} d^{-1}. However, the direct measurements of denitrification rates in the North-Frisian Wadden Sea or the German Bight are at least 15 years ago and have been conducted in a period of rapid environmental changes (Fig. 1.2). Since then, the Elbe estuary has undergone further changes as for example a decrease of the nitrate load and a shift of the N:P ratio. A consequence of these changes might be the transition of the estuary from a nitrogen sink to an inert channel, as the results of Dähnke et al. (2008) suggest.

Tab 1.1: Summary of published denitrification rates of North Sea sediments.

area	year	denitrification rate (mmol m^{-2} d^{-1})	method	reference
Elbe estuary	1984-1989	1 - 9	benthic chamber	Schroeder et al. 1996
Dogger bank	1988	0.2	pore-water profiles	Van Raaphorst et al. 1990
southern North Sea	1988-1989	0.02	mass balance	Hydes et al. 1999
southern North Sea	1991-1992	0 – 0.2	acetylene inhibition	Lohse et al. 1993
North Sea	-	0.6	estimated from primary production	Seitzinger & Giblin 1996
Ems estuary	1992-1993	2.5	mass balance	van Beusekom and de Jonge 1998
southern North Sea	1994	0.2 – 0.3	isotope pairing incubation	Lohse et al 1996a
North-Frisian Wadden Sea	1994	0.2 – 1.2	isotope pairing incubation	Jensen et al. 1996
North-Frisian Wadden Sea	1994-1995	0.8 – 8.3	mass balance	Dick et al. 1999
German Bight	1995	1.4	ecosystem model	Pätsch et al 2010
North Sea	1995	0.1	mass balance	Brion et al 2004
East-Frisian Wadden Sea	2007-2008	4.5 - 11.3	isotope-pairing incubation, micro-profiling, N_2/Ar incubations	Gao et al. 2010

1.4 Working area 2: The Benguela Upwelling System off Namibia

The second working area is the continental shelf and slope influenced by the coastal upwelling off Namibia in the southern Africa (Fig. 1.5). Namibia is sparsely populated and the almost uninhabited coast is dominated by the Namib Desert. Only minor and often transient rivers discharge into the Benguela system, thus the antropogenic input of reactive nitrogen is insignificant.

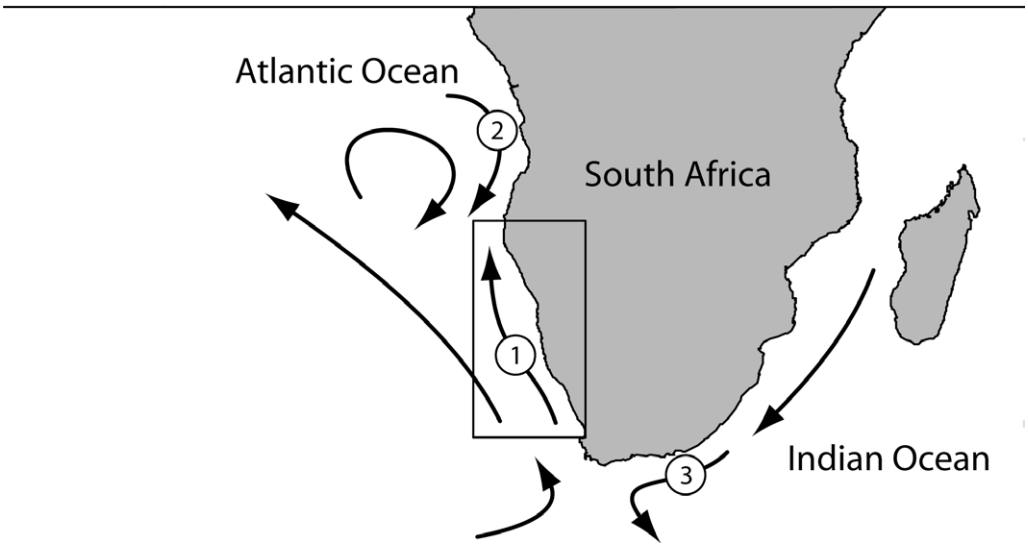

Fig. 1.5: Overview of major surface currents off the south african coast: 1: Benguela Coastal Current, 2: Angola Current, 3: Agulhas Current. The rectangle indicates the working area 2 off the Namibian coast. Illustration based on Peterson & Stramma (1991).

The major source of reactive nitrogen is instead the coastal upwelling of nutrient-rich deep water onto the shelf driven by strong easterly trade winds. These winds blow parallel to the coastline and the wind-driven Ekman-transport displaces the warm, nutrient-depleted surface water away from the coast toward the open South Atlantic. In the following, cold and nutrient-rich deep water replaces the water deficit at the coast and thus reaches the surface. This coastal upwelling is illustrated in figure 1.6.

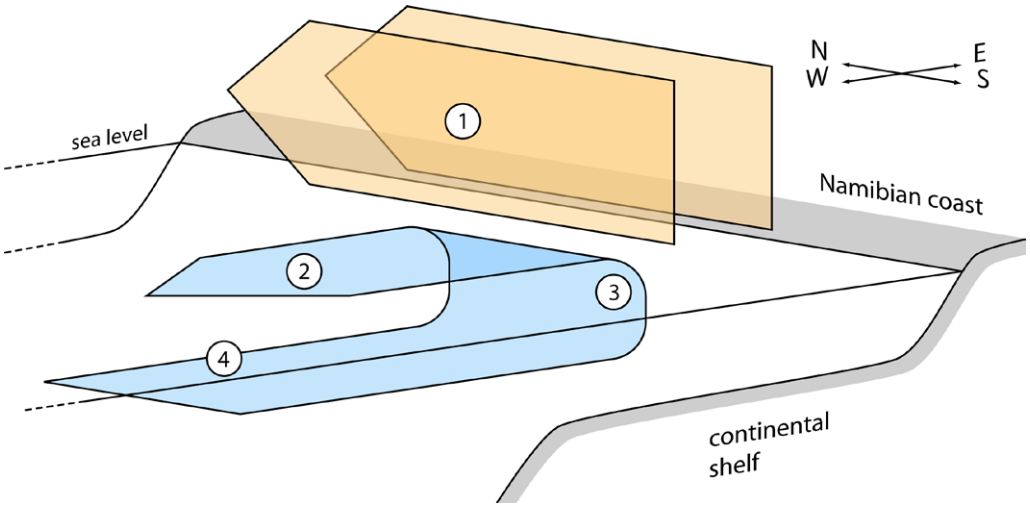

Fig. 1.6: Conceptual illustration of the wind-driven coastal upwelling off the namibian coast. South-easterly winds blow along the coast (1) and displace the surface water westward away from the coast and toward the open Atlantic (2). The water deficit at the coast is replaced by the upwelling (3) of deep water (4).

As a consequence, nutrients transported onto the continental shelf by the upwelling water provide intense primary production and sustain one of the most productive ecosystems. The intense primary production is deposited on the shelf sediments and results in sediments with very high organic matter content. Here, the further fate of the reactive nitrogen is governed by the variable hydrodynamic conditions. During intensive upwelling, the oxygen consumed by remineralisation of the organic matter is constantly replaced and the bottom water remains oxic. Ammnoium that is released by the remineralisation is nitrified to nitrate and further fuels the primary production in the surface water. In contrast, during weak or absent upwelling, all available oxygen is consumed and the water column becomes anoxic. This condition promotes the elimination of reactive nitrogen by denitrification and anammox, and thus curbs the primary production in the surface water. The significance of nitrate as an alternative electron acceptor to consume the high concentration of organic carbon in the sediment may be highlighted by the abundant bacteria such as Beggiatoa, Thioploca or Thiomargarita (Schulz & Schulz 2005). Microorganisms of this kind are adopted to exploit the occurrence of nitrate, hydrogen sulphide and methane in anoxic sediment.

However, despite the low input of anthropogenic reactive nitrogen into the Benguela Current, this system is by no means pristine. Human activity severely impacts this system by intensive fishing and marine mining. As an example, the commercial fishing collapsed in the 1990's and Lynam et al. (2006) observed a shift in the abundance of top-level predators from vertebrates such as sardines and tuna toward preying cnidaria. The geochemical consequences are still unclear.

1.5 Previous studies examining Benguela Current sediments

The hydrodynamic conditions in the Benguela system are not as simple as introduced above. Instead, the system is very variable and governed by various factors such as the wind field, the position of the front between the Angola Current and the Benguela Current and the passing of an Agulhas ring, which is a patch of Indian Ocean water detached from the Agulhas Current. These factors influence the primary production in the surface water, which is the main source of labile organic carbon and thus the fuel for the benthic remineralisation. The intensity of the deep-water upwelling controlled by the mentioned forces also determines the supply of oxygen and nutrients and thus the balance between recycling and elimination of reactive nitrogen. The feed-back between primary production and remineralisation in combination with the variable hydrodynamic control potentially induces a pronounced non-linear behaviour of the system. The implied variability of the rates of benthic remineralisation processes such as nitrate consumption is not yet fully covered by the few published studies.

Hensen et al. (2000) examined the surface sediments of the continental margin off Namibia between the 1300 m isobath and the abysal plain of the Cape Basin. They reported nitrate fluxes between 0.2 and 0.6 mmol m^{-2} d^{-1} and nitrate penetration depths < 10 cm. The sediments along the 1300 m isobath have also been studied by Niewöhner et al. (1998) and they reported that sulphate reduction occurs several meters deep in the sediment with reaction rates between 60 and 160 µmol m^{-2} d^{-1}. Fossing et al. (2000) found similar results with the methods applied by Niewöhner et al. (1998) but yielded six-fold higher sulphate reduction rates when expanding the applied diffusion-reaction model with an irrigation function.

1.6 Review of methods to determine sediment denitrification rates

Numerous methods have been established to measure benthic denitrification rates, with most of them relying on incubations of undisturbed sediments in enclosures (Devol 1991, Jansen et al. 2005), undisturbed sediment cores (Lohse et al. 1993), or homogenized slurries (Würgler Hansen et al. 2000). In most experimental setups, the concentration variations of substrates or products over the time are assumed to directly reflect the reaction rates. A sub-set of these methods utilises inhibitors or labelled substrates to distinguish between processes of nitrification and denitrification, which are often coupled. The acetylene inhibition technique (Sørensen 1978, Christensen et al. 1989) uses the gas acetylene (C_2H_2) to inhibit the complete denitrification to N_2 and suppresses the final reduction step. Instead, the intermediate N_2O accumulates, which can be quantified easily by gas chromatography. Acetylene also inhibits the nitrification and thus allows isolating denitrification. As demonstrated by Lohse et al. (1996), however, acetylene inhibition can lead to severe underestimations of the denitrification rates if denitrification is tightly coupled to nitrification. In contrast, the isotope-pairing method established by Nielsen (1992) and expanded by Risgaard-Petersen et al. (2003) does not need any inhibitor. This method uses substrates enriched in the stable nitrogen isotope ^{15}N to label the substrates during the incubation whereas ^{14}N dominates in natural substances. The products of the labelled substrate can be identified by a deviation of the natural $^{15}N/^{14}N$ ratio of the products. The isotope-pairing method enables distinguishing between denitrification and anammox (Risgaard-Petersen et al. 2003) and to enumerate the effect of nitrification on denitrification.

All these incubation techniques necessarily confine the sediment and thus isolate it from the naturally occuring hydrodynamic conditions. This confinement especially affects permeable sediments, which are characteristic for mnay coastal and shelf sea environments, such as the Wadden Sea (Figge 1981, Köster 1998). Precht and Huettel (2003), Cook et al. (2006) and others have demonstrated that the interaction of wave oscillations and currents with sediment bed forms drives an advection of the pore water into the surface sediment and thus enhances the transport of solutes and particles (Fig. 1.7). Although this hydrodynamic action is often simulated in incubations with stirrers that agitate the incubated water volume, it does not sufficiently compensate for the inhibition of natural water movements at the sea floor (de Beer et al. 2005). Alternative setups, such as flexible enclosures as described in Risgaard-Petersen et al. (1999) or the isotopic labelling of whole water bodies (Axler & Reuter 1996) are either an insufficient approximation of natural conditions, or not feasible in tidal environments. In summary, confined incubations are prone to shifts of the geochemical conditions at the sediment-water interface,

because the availability of substrates and the distribution of added inhibitors are sensitive to fluctuations of the hydrodynamic forces. Thus, the reaction rates within the confinement tend to deviate from in-situ conditions with time.

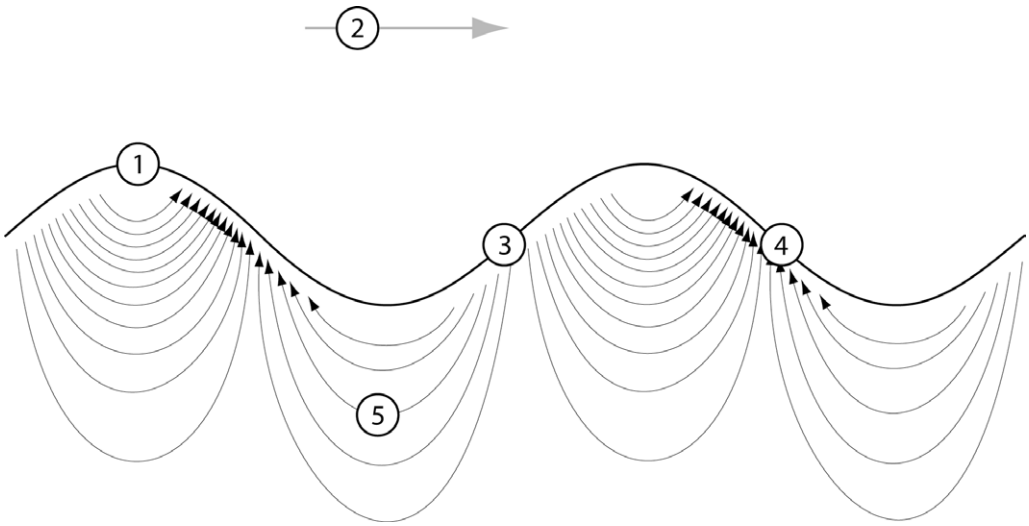

Fig. 1.7: Conceptual drawing of flow induced pore water advection in permeable sediments. A sediment surface (1) with bedforms (e.g. ripple marks) is sheared by a current (2). Areas of increased pressure are formed at each flow-exposed side (3) and areas of decreased pressure are formed at each lee side (4). As a result, the pore water is forced from the exposed side to the lee and thus percolating the sediment surface (5). The arrows represent the stream lines of the pore water advection. Drawing based on Elliott & Brooks (1997).

An alternative to confined incubations is the measurements of concentration profiles across the sediment-water interface and the interpretation of such profiles with a suitable numerical model (Berg et al. 1998). Microscale sensors for the direct measurements of concentration profiles are available for ammonium (de Beer & van den Heuvel 1988), nitrous oxide (Revsbech et al. 1988) and nitrate (Larsen et al. 1996), and other relevant compounds such as oxygen (Revsbech 1989, Klimant et al. 1995) or methane (Damgaard & Revsbech 1997) among others. However, most of these microsensors are sensitive to a single compound only. Simultaneous or successive profiling with multiple microsensors for different compounds is faced with temporal or spatial inhomogeneities of the sediment, because the different profiles are either temporally or spatially apart. A solution to these problems of traditional techniques may be an experimental setup where several gaseous compounds are determined simultaneously in the same water or sediment pore water sample with a quadrupole mass spectrometer equipped with a membrane inlet system, a technique which is known as membrane inlet mass spectrometry (MIMS).

This MIMS technique was introduced to geochemistry by Kana et al. (1994) and is in increasing use since then. The use of miniaturised membrane inlet probes sturdy enough for insertion into sediments would potentially enable direct measurements of dinitrogen concentration profiles along the sediment column, which is not possible with other microsensors. Additionally, MIMS also permits simultaneous measurements of nitrous oxide, methane, carbon dioxide and hydrogen sulphide in the same single profile. The employment of mass spectrometry further enables to measure isotopic ratios in gaseous compounds, which is also impossible with other microsensors. Lloyd et al. (1996) and Hartnett and Seitzinger (2003) have published prototypes of such membrane probes suitable for insertion into sediments, but the membrane probes have not been used in routine yet.

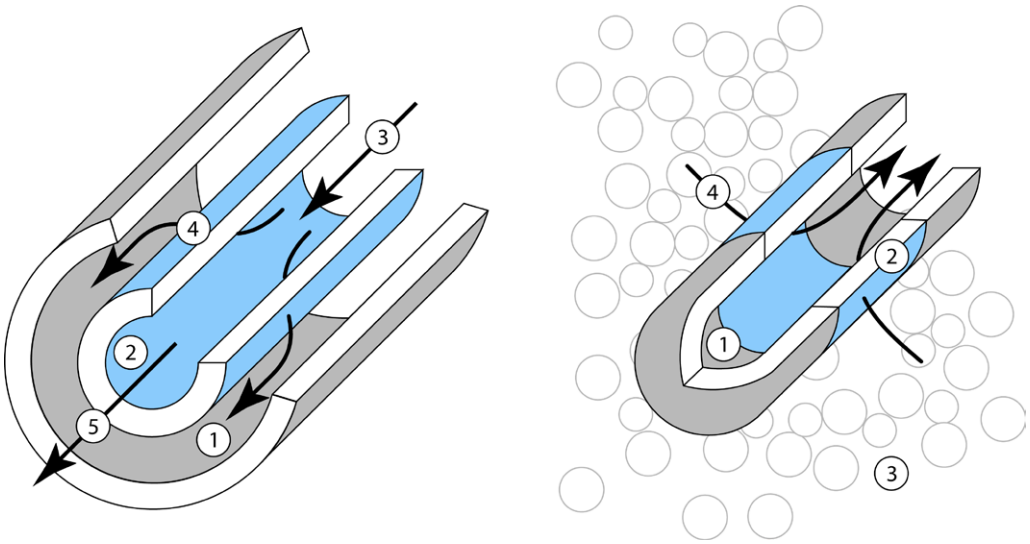

Fig. 1.8: Principal configurations of membrane inlets. Left panel: A flow-through inlet with vacuum vessel (1) and inner membrane tube (2). The aqueous sample (3) is fed through the membrane tube, which is permeated by the dissolved gasses (4). The water and non-volatile solutes are held back by the membrane and leave the inlet (5). Right panel: A membrane probe with a narrow evacuated tube (1) and an orifice covered with the membrane (2). The dissolved gasses diffuse through the sediment (3) and permeate through the membrane.

A typical membrane inlet for mass spectrometry is depicted in figure 1.8 (left panel) and corresponds to the inlet described in Kana et al. (1994). The inlet is a combination of a vacuum tight outer vessel usually made from glass or metal, and an inner membrane tube. The membrane material is often silicone. The space between the vacuum vessel and the membrane tube is evacuated and is connected to the sample port of the mass spectrometer. The aqueous sample is fed through the membrane tube. Dissolved gases and other volatile compounds permeate the membrane, evaporate into the surrounding vacuum and enter the mass spectrometer. The water and non-volatile solutes are held back by the membrane and leave the

inlet as retentate. The configuration of a membrane probe is inverse (Fig. 1.8 right panel). A vacuum-tight narrow tube with closed end is connected to the sample port of a mass spectrometer. Close to the tip of this tube is an orifice which is covered with the membrane material. The dissolved gases diffuse through the sediment, permeate the membrane and evaporate into the vacuum within the probe. Cold traps installed along the capillary between the membrane inlet and the mass spectrometer to reduce the amount of water vapour entering the mass spectrometer.

1.7 Objectives and thesis outline

The central assumption of this study is that sediments of Wadden Sea and German Bight are efficient sinks for reactive nitrogen via denitrification. This assumption is based on discrepancies in nitrogen budgets of mass flux estimations and stabile isotope measurements as well as preliminary results of the nitrogen isotopic ratio of surface sediments (Serna).

The particular objectives of the present study were:

- Establishment of a routine method for direct measurements of the benthic N_2-fluxes based on membrane inlet mass spectrometry (MIMS). The technique was to be appropriate for employment in remote laboratories and aboard of research vessels.

- Employment of this technique for determination of benthic N_2 fluxes across the sediment-water interface. The sampled stations were to represent as much as possible of the temporal and spatial variability of potential determinants such as nitrate concentration, TOC content, temperature to ensure that the results contain sufficient contrast for subsequent statistical analyses.

- Statistical analyses of assembled data for identification of major determinants of nitrate consumption and N_2 production and assessment of their relative contribution.

- Estimation of the total nitrate consumption and N_2 production of German Bight sediment on the basis of interpolated spot measurements.

Thesis outline

The present thesis is based on four manuscripts intended for publication. Each of them comprises introduction, methods, results and discussion, thus some recurrences occur.

2nd Chapter: Needle-type membrane inlet for sediments.

As a first step, a robust needle-type membrane inlet was developed for the measurement of dissolved gases in water saturated sediments. A measurement routine was established for the estimation of benthic denitrification rates using N_2/Ar profiles of undisturbed sediment cores.

3rd Chapter: Rates of benthic nitrate consumption along the salinity gradient of the Elbe estuary.

The established method of denitrification measurement using N_2/Ar profiles was applied to a series of sediment cores from the Elbe estuary and the adjacent North-Frisian Wadden Sea. The results are compared to denitrification rate estimates obtained in parallel by pore water nutrient profiles, a flow-through isotope pairing incubation, and a batch isotope pairing incubation.

4th Chapter: Benthic elimination of reactive nitrogen in the German Bight (southern North Sea)

Based on results of chapter 3, a simple transport-centered model of nitrate uptake and N_2 release was derived and fitted with measurements from Elbe estuary and German Bight sediments. The fitted model was employed for interpolation of spot measurements of nitrate consumption and N_2 production.

5th Chapter: Benthic remineralisation rates of the shelf and slope sediments off Nambia.

In an additional application, The N_2/Ar profiling method was utilised to estimate the benthic remineralisation rates of the shelf and the slope sediments influenced by the Benguela current off the Namibian coast. The results of MIMS profilings are compared with the results of parallel pore water nutrient profiles and batch isotope pairing incubation.

6th Chapter: Conclusions and future work.

This section summarizes main results and conclusions of the previous chapters. Possible future application and development of miniaturized membrane probe and prediction model are sketched.

2. A robust needle-type membrane inlet for dissolved gas analysis in sediments

Abstract

The microbially mediated transformations of reactive nitrogen results produce a diverse spectrum of nitrogen compounds. Many of these transformation processes are reversible and interconnected, which enables nitrogen cycling to this metabolic network. In this respect is the production on N_2 by e.g. denitrification and anammox a unique reaction, because the reversal process (N-fixation) is very energy consuming and thus restricted to nitrogen-limited conditions. The N_2 production efficiently eliminates nitrogen from the ecosystem. The measurement of N_2 is challenging due to its low reactivity and a high atmospheric background. A solution is the employment of membrane inlet mass spectrometry. This chapter presents a newly developed needle-type inlet for the measurement of N_2 profiles across the sediment-water interface. The presented membrane inlet permits N_2 profiling with significantly less sediment irrigation and improved mechanical robustness compared to published inlet types.

2.1 Introduction

Numerous methods have been established to measure benthic denitrification rates, which found on incubations of undisturbed sediments in enclosures (Devol 1991, Jansen et al. 2005), undisturbed sediment cores (Lohse et al. 1993) or homogenized slurries (Würgler Hansen et al. 2000). Utilized methods are for example nitrate-depletion (Lohse et al. 1993), acetylene block (Sørensen 1978), N_2 flux (Seitzinger et al. 1980), ^{15}N-tracer techniques (Nishio et al. 1983, Nielsen 1992, Risgaard-Petersen et al. 2003) or changes in N_2/Ar ratios (Kana et al. 1994). All these incubation techniques confine the sediment and thus isolate it from the natural hydrodynamic conditions. This confinement affects especially permeable sediments, which are characteristic for the Wadden Sea (Figge 1981, Köster 1998). Precht and Huettel (2003), Cook et al. (2006) and others have demonstrated that the interactions of wave oscillations and currents with sediment bed forms drive advection of pore water and thus enhance the transport of solutes (Huettel at al. 1998) and particles (Huettel and Rusch 2000). In contrast to these incubations, measurements of concentration gradients across the water-sediment interface in combination with a transport-reaction model (e.g. Berg et al. 1998) allow the estimation of in-situ fluxes without incubation under confined conditions.

Micro-scale electrodes with appropriate resolution for steep concentration gradients are available for ammonium (de Beer & van den Heuvel 1988), nitrous oxide (Revsbech et al. 1988) and nitrate (Larsen et al. 1996) but not for the remineralisation endmember dinitrogen. An alternative for the electro-chemical detection is the membrane inlet mass spectrometry (MIMS) which uses a hydrophobic membrane to separate dissolved gases from aqueous samples and a mass spectrometer to analyse the resulting gaseous samples. Kana et al. (1994) introduced the N_2/Ar method to measure small N_2 variations against the high atmospheric background and utilized a flow-through membrane inlet. This N_2/Ar method was adapted by Hartnett and Seitzinger (2003) for a needle-type membrane probe to measure small-scale N_2 concentration gradients in surface sediments. Similar membrane probes have been described previously by Thomas & Lloyd (1995), Lloyd et al. (1996) and Cartaxana & Lloyd (1999). Especially the combination of fast quadrupol mass spectrometers and membrane inlets offer the advantage to determine several geochemically interesting gases simultaneously and thus to obtain concentration profiles of N_2, CO_2, CH_4 and H_2S without interference of temporal or spatial variability. Surprisingly, this method was rarely used as routine method yet.

A reason might be that the inevitable characteristic of needle-type membrane inlets contradicts the design principles of vacuum systems. Gas transport in high vacuum

is governed by molecular diffusion if the characteristic dimension of the vacuum vessel is less than the pressure-dependent mean free path (Hoffman et al. 1997). On that condition, gas particles interact more often with the vacuum vessel than with other gas particles. Hence, net transport is dependent on the spatial dimension of the vacuum system and led to the design principle to build vacuum conduits as short and wide as possible (Hoffman et al. 1997). However, this principle is not applicable for membrane probes because the conduit between membrane and mass spectrometer needs to be long and flexible enough to provide sufficient movement for profiling. Additionally, a long and wide conduit mounted upstream of a narrower conduit acts as a reservoir, resulting in unwanted tailing of the signal. For this reason, the transfer conduit of the membrane probe to be presented here had 1.1 mm outer diameter and 0.6 mm inner diameter. This dimension provided sufficient flexibility and was below of the inner diameter of the internal conduits of the employed GAM-200 (InProcess Instruments) mass spectrometer (1.2 mm). The consequences of the long and narrow vacuum conduit are long residence times of the gas samples within the system and long response times. The inlet probes of Thomas & Lloyd (1995), Lloyd et al. (1996) and Cartaxana & Lloyd (1999) had response times in the magnitude of 15 - 20 minutes, which accumulated to several hours measuring time for a single profile. The inlet of Hartnett & Seitzinger (2003) reduced the response time to 5 - 7 minutes.

An essential element of the membrane probe is obviously the membrane, which separates dissolved gases from water by permitting gas permeation and blocking liquid water. A common membrane material for membrane inlet mass spectrometry is silicone (e.g. Polydimethylsiloxane) because it combines hydrophobicity, high mechanical strength and high gas permeability. High gas permeability of this non-porous polymer is result of the transient opening of voids between the highly mobile and flexible polymer chains. These voids move through the polymer and can enclose or release single gas molecules if they open at the polymer surface (Bernardo et al. 2009). As the movement of the voids is random, the overall movement of the gas molecules within the polymer is best described as diffusion (see Fig. 2.1). But unlike to diffusion, the mobility of a permeating compound is not a function of molecule mass but a function of molecule size, because a given void can enclose and transport more small molecules than larger ones. A direct consequence is that the permeability of argon is higher than the permeability of dinitrogen (Stern et al. 1977). A mixture of argon and dinitrogen permeating through a silicone membrane is enriched in argon.

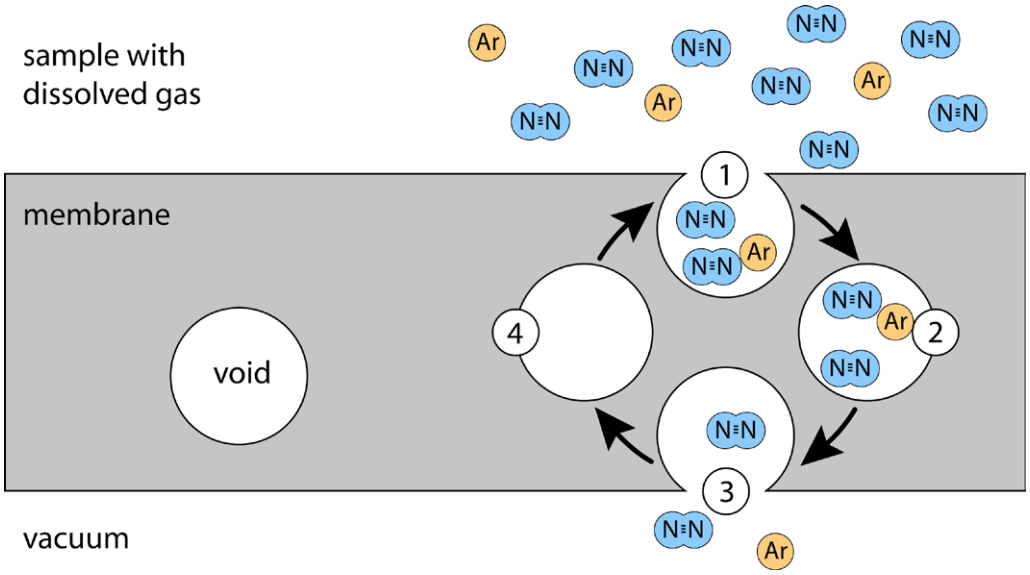

Fig. 2.1: Gas permeation through a non-porous polymer. Individual void spaces between the polymer molecules (solid gray) randomly open and close at the surface and release (3) or enclose (1) gas molecules. The diffusion of the void spaces through the polymer is enabling the passage of gas molecules (2).

Transport of dissolved gases within sediment interstices toward the membrane and from the membrane through the vacuum system is a similar diffusive transport. But in contrast to the membrane permeation described above, diffusivity is controlled by molecule mass and diffusivity of argon is 10 % higher than argon diffusivity (Broecker & Peng 1974). Thus, the ratio of N_2 and Ar may drift over time as a result of different diffusivities. Further, diffusivity within porous media such as sediment is controlled by porosity, tortuosity and pore connectivity (Ullman & Aller 1982, Glover & Walker 2009) of the sediment interstices. The combined effect of these factors can be measured as electrical resistivity and expressed as formation resistivity factor (Manheim & Waterman 1974, Ullman & Aller 1982).

In summary, diffusion-type transport in sediment, membrane and vacuum line bias the measured N_2/Ar ratio, which thus may deviate from the initial N_2/Ar ratio to be measured in the sediment. Mass-dependent diffusion in sediment and vacuum increases the apparent N_2/Ar ratio and size-dependent diffusion in solid membrane decreases the apparent ratio. This chapter presents a newly-developed membrane tip suited for rigid sediment, establishes the extent of the net-bias of the measured N2/Ar ratio, and proposes a correction.

2.2 Material and Methods

Needle-type membrane inlet

The membrane tip of the self constructed needle-type membrane inlet was manufactured from a stainless steel capillary (1.1 mm OD, 0.6 mm ID) and a pressure fitted silicone tube (Silastic, Dow Corning) as membrane. An additional jacket made from stainless steel was mounted to the tip to protect the membrane from peeling-off or buckling. This tip was connected to a stainless steel transfer capillary (1.6 mm OD, 0.9 mm ID) with an inline cryogenic trap. The cryogenic trap was made from stainless steel tubing with an outer diameter of either 1.6 mm (series 1) or 3.2 mm (series 2). See also figure 2.2 and 2.3.

N_2/Ar measurements

The pore water concentrations of dissolved dinitrogen and argon have been profiled with a needle-type membrane inlet for membrane inlet mass spectrometry. This probe was connected to the mass spectrometer via a 1/16” stainless steel transfer tube with an inline cryogenic trap. The trap was not cooled during laboratory measurements described here. The resulting gas stream was analysed with a quadrupole mass spectrometer (GAM-200, InProcess Instruments) using the N_2/Ar method of Kana et al. (1994). The N_2 was measured as m/z 28 and argon as m/z 40 and both signals were measured with a dwell time of 1 second. The cycle time to measure all observed mass/charge ratios was 3 seconds. The profiles were obtained by positioning the probe in 3 mm intervals with an autonomous micromanipulator (MU-1/300, Pyroscience), holding each position for 5 minutes to allow the stabilisation of the N_2/Ar ratio. After this time, the values of 10 consecutive measurement cycles have been averaged. Each profile was calibrated individually with argon as reference for the correction of the dinitrogen signal. See also figure 2.2.

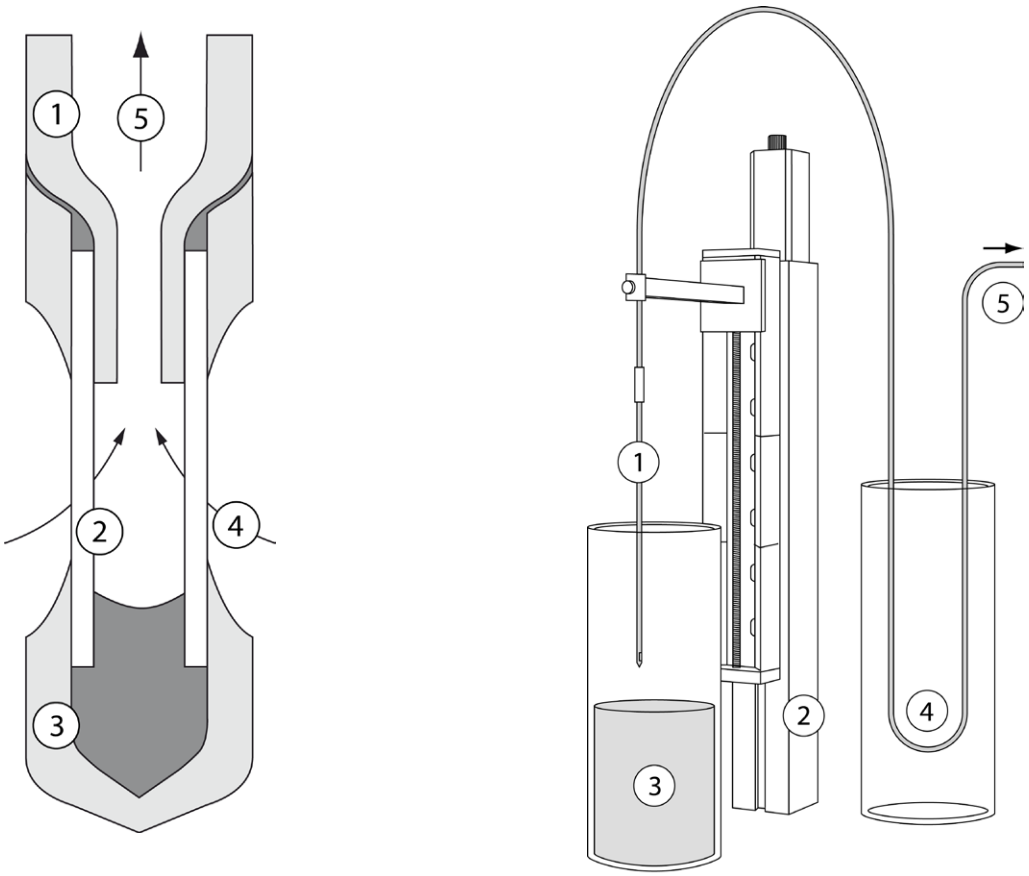

Fig. 2.2: Left panel: diagram of the membrane tip. An evacuated tube (1) carries a membrane tube (2) at its tip, which is protected by a sheath (3). The dissolved gases (4) diffuse to the membrane, permeate the membrane and are transferred toward the mass spectrometer (5). Right panel: simplified diagram of the setup. The membrane probe (1) is positioned by an autonomous micromanipulator (2) into a sediment core (3). The resulting gas stream from the membrane probe is passing through an inline cryogenic trap (4) and transferred into the sample port of the mass spectrometer (5).

Calibration

The standard solutions for N_2/Ar were mixtures of natural seawater and deionized water with a final salinity from 0 PSU to 35 PSU. These solutions have been air-equilibrated for 24 h at constant temperature. These thermo-haline standards have not been aerated with an air pump to avoid supersaturation. These standards were have been used to establish a calibration curve to convert the signal ratio of m/z 28 for N_2 and m/z 40 for Ar to the molar ratio of N_2 and Ar in the sample. Finally, the N_2 concentration was calculated by multiplying the molar N_2/Ar ratio with the equilibrium concentration of argon provided by Hamme & Emerson (2004).

Sediment tests

The necessary force to push a membrane inlet made according Hartnett & Seitzinger (2003) and a membrane inlet developed for this study was measured to estimate the mechanic stress affecting the membrane and the sediment during the insertion. The raw tubes used to fabricate the inlets have also been tested for comparison. The inlets and tubes have been pushed into a water saturated, fine sand (D_{50} = 120 µm) with a constant velocity of 1 mm s^{-1} using an autonomous micromanipulator (MU-1/300, Pyroscience). The force applied to the sediment was measured as weight with a lab balance and converted to a force unit with equation 2.1.

(2.1) $$F = m \times g$$

F: sediment insertion force
m: apparent weight during insertion
g: gravity, 9.81 m s^{-2}

The effect of grain size and water content of the sediment on the N_2/Ar ratio was examined with natural sediment samples collected along the coast of the North-Frisian Wadden Sea. The samples have been washed thoroughly with deionized water to remove any salt and dissolved inorganic nitrogen. Afterwards, the samples were combusted for 12 h at 550 °C to remove any organic carbon. The different sediment samples have been saturated with deionized water and combined to artificial sediment cores. These sediment cores were allowed to equilibrate with air prior to the measurements. The profiles were obtained by positioning the probe in 3 mm intervals with an autonomous micromanipulator (MU-1/300, Pyroscience), holding each position for 5 minutes to allow the stabilisation of the N_2/Ar ratio. Additional rehydrated sediment samples have been dried at 40 °C to determine the water content and sieved through a sieve series to calculate the grain size distribution using Gradistat (Blott & Pye 2001).

2.3 Results

Sediment insertion force

The force necessary to push a needle-type inlet made according to Hartnett & Seitzinger (2003) 20 mm deep into fine quartz sand was 243 ± 22 mN, the insertion force of the raw tube used to build the inlet (0.8 mm OD) was 30 ± 5 mN. The insertion force of this study's inlet into the same sediment was 84 ± 10 mN and the force for the raw tube (1.1 mm OD) was 89 ± 10 mN respectively. See also figure 2.3. The measured inlets are displayed in figure 2.4.

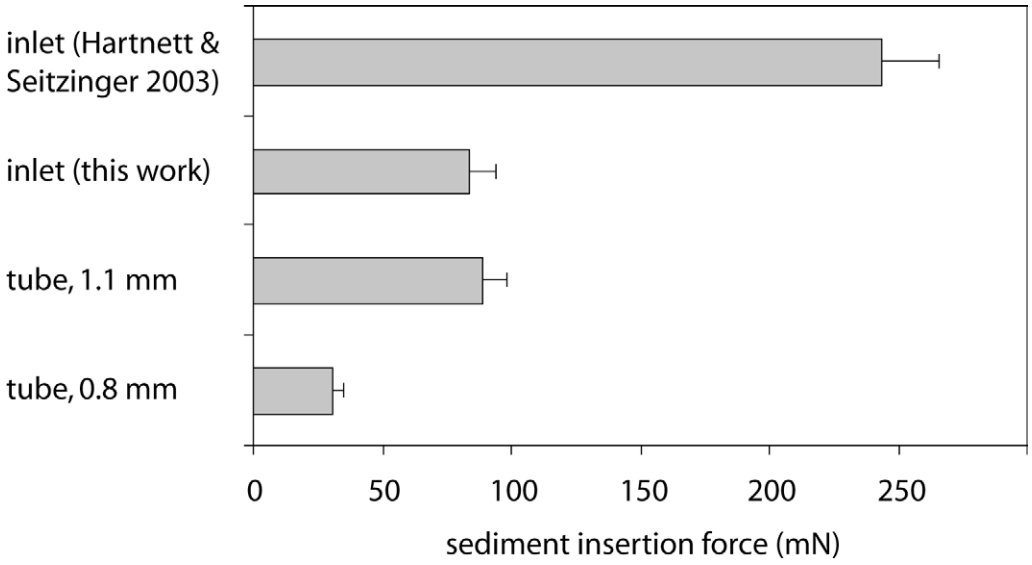

Fig. 2.3: Mean forces (n = 10) necessary to insert different needle-type membrane inlets and raw tubes 20 mm into fine sand with a velocity of 1 mm s^{-1}. Errorbars indicate 1 standard deviation.

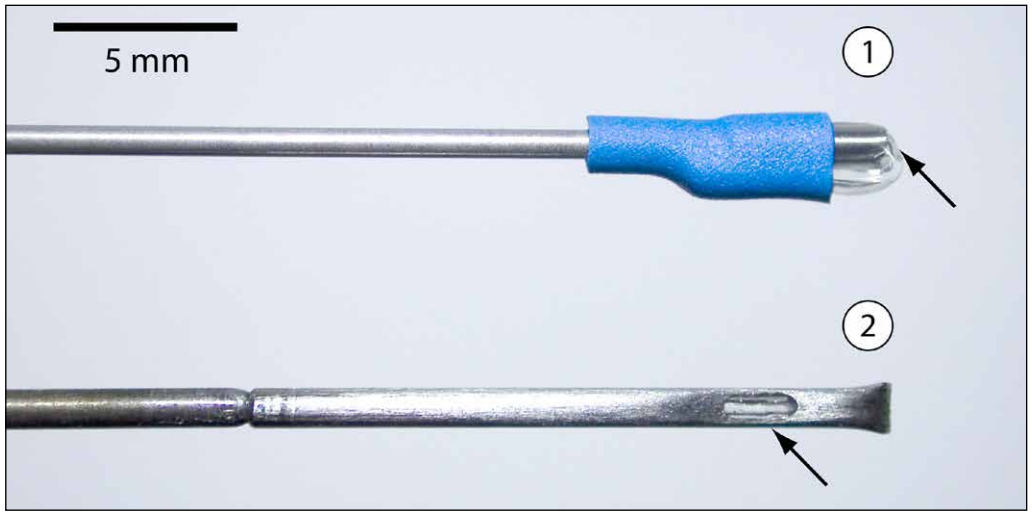

Fig. 2.4: Photograph of the membrane inlets of Hartnett & Seitzinger 2003 (1) and this study (2). The arrows indicate the membrane covered orifices.

Response time and stirring effect

The effect of stirring on the signal ratio m/z 28 to m/z 40 has been examined. The N_2/Ar signal ratio was generally higher when stirred than unstirred. The N_2/Ar signal ratio of deionized water at 26 °C was 43.7 ± 0.1 when stirred and 42.4 ± 0.1 when unstirred. The molar ratio N_2/Ar of the sample was in both cases 39.0. The N_2/Ar signal ratio of seawater with 36 PSU at 26°C was 43.1 ± 0.1 when stirred and 41.7 ± 0.1 when unstirred. The molar ratio N_2/Ar of the sample was in both cases 38.3. The N_2/Ar signal ratio was stable within 2 minutes after start of stirring or cease respectively.

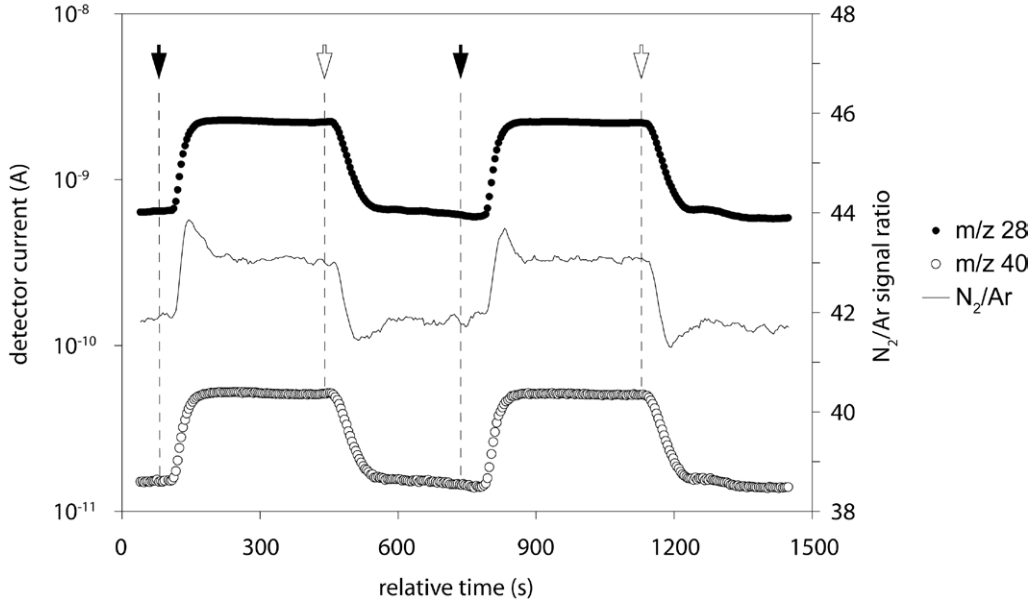

Fig. 2.5: Response time of the developed needle-type membrane inlet. The black arrows indicate start of stirring, the white arrows indicate cease of stirring.

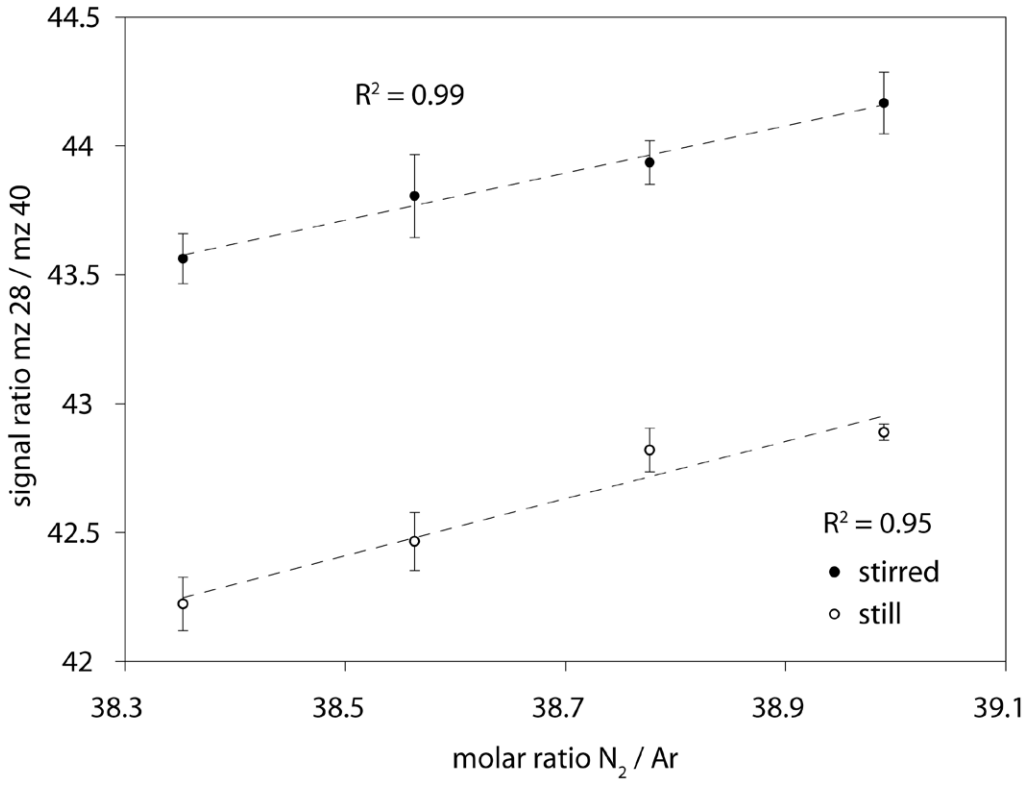

Fig. 2.6: Effect of stirring on N_2/Ar signal ratio of constantly stirred standards (full circles) and non-stirred standards (open circles). Errorbars indicate standard deviation (n=5).

Effect of grain size and water content

The function 2.2 was fitted to published data on measured formation resistivity of surface sediment (Manheim & Waterman 1974, Ullman & Aller 1982) to estimate efficient diffusion coefficients (D_{eff}) on the basis of sediment porosity (Fig. 2.7). The obtained estimation function is

(2.2) $$F = 1.21 \times \Phi^{-1.90}$$

F: formation resistivity factor
Φ: porosity

Analogous to the stirring effect, the influence of sediment grain size and water content on the signal ratio mz 28 / mz 40 was examined by measuring artificial sediment columns (tab 2.1). The signal ratio mz 28 / mz 40 was 43.1 in the supernatant and dropped to 39.4 ± 0.1 when the inlet was positioned in the coarse sand. The signal ratio further increased to 39.8 ± 0.1 in medium sand and 41.1 ± 0.3 in fine sand. The signal ratio within the transition zones between different sediment types was intermediate (Fig. 2.8). The actual molar ratio of N_2 and Ar was in all cases 39.0. The measured signal ratios were further plotted against the formation resistivity factors, which were estimated with equation 2.2. The N_2/Ar signal ratio correlated

with the formation resistivity factor (R^2 = 0.91), and this correlation was employed to derive equation 2.3 to correct the measured N_2/Ar signal ratio for the porosity effect (Fig 2.9). A significant influence of the grain size has not been observed.

$$\left(N_2 / Ar\right)_{corr} = 0.0098 \times F \times \left(N_2 / Ar\right)_{meas} + 0.993 \quad (2.3)$$

$(N_2/Ar)_{corr}$: corrected N_2/Ar ratio
$(N_2/Ar)_{meas}$: measured N_2/Ar ratio
F: formation resistivity factor

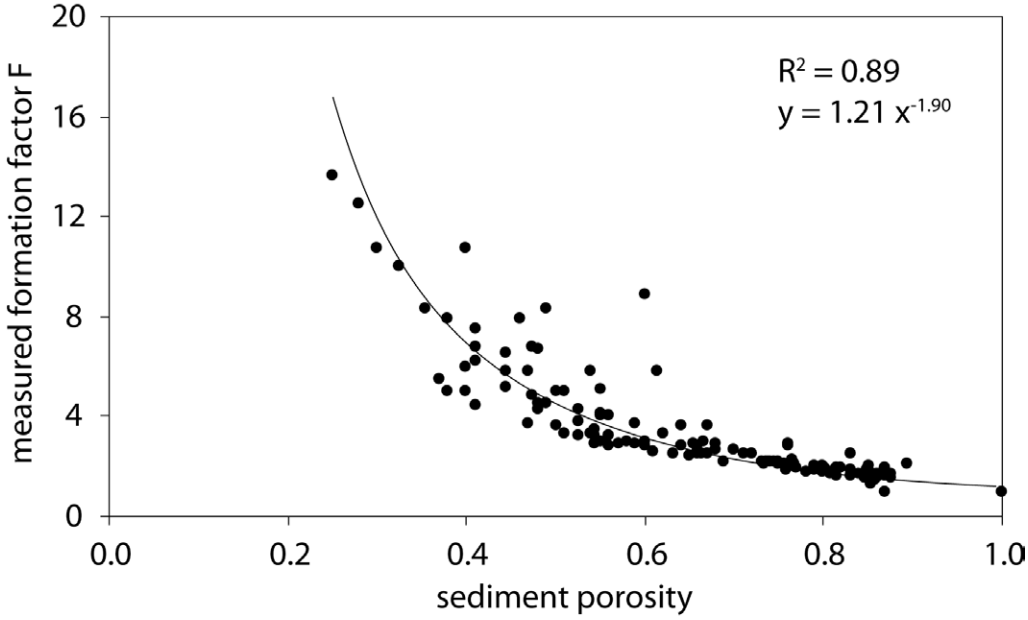

Fig. 2.7: Measured formation resistivity factor (F) vs. sediment porosity. Data from Manheim & Waterman (1974) and Ullman & Aller (1982).

Tab. 2.1: Properties of the sediment used for the artificial sediment columns.

	coarse sand	medium sand	fine sand
grain size (µm)	760	245	86
porosity (v/v)	0.33	0.32	0.45
formation factor	8.2	8.7	4.6

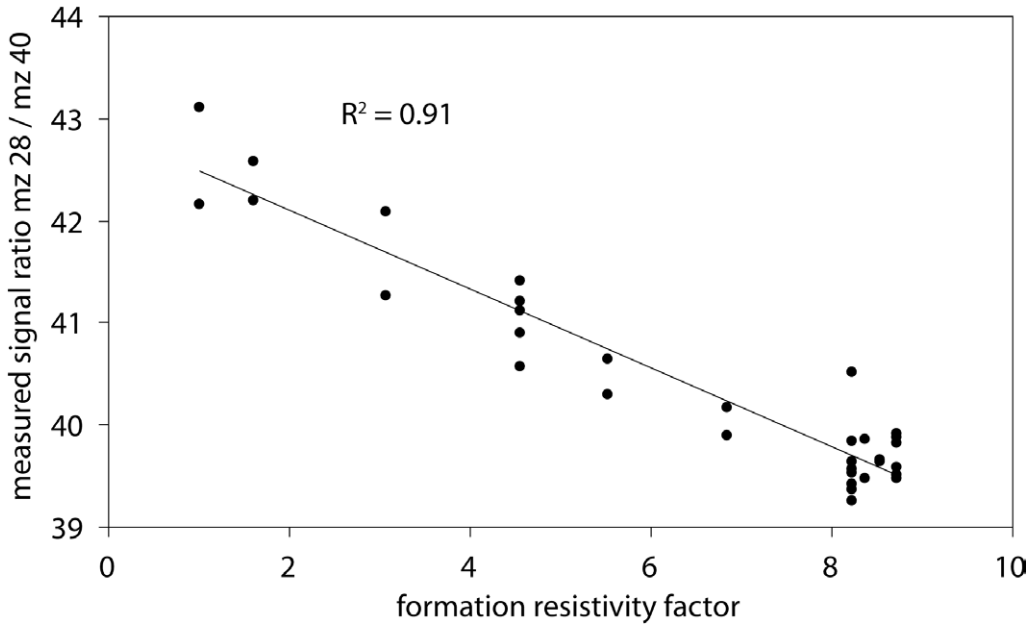

Fig. 2.8: Effect of porosity expressed as formation resistivity factor (equ. 2.2) on N_2/Ar signal ratio.

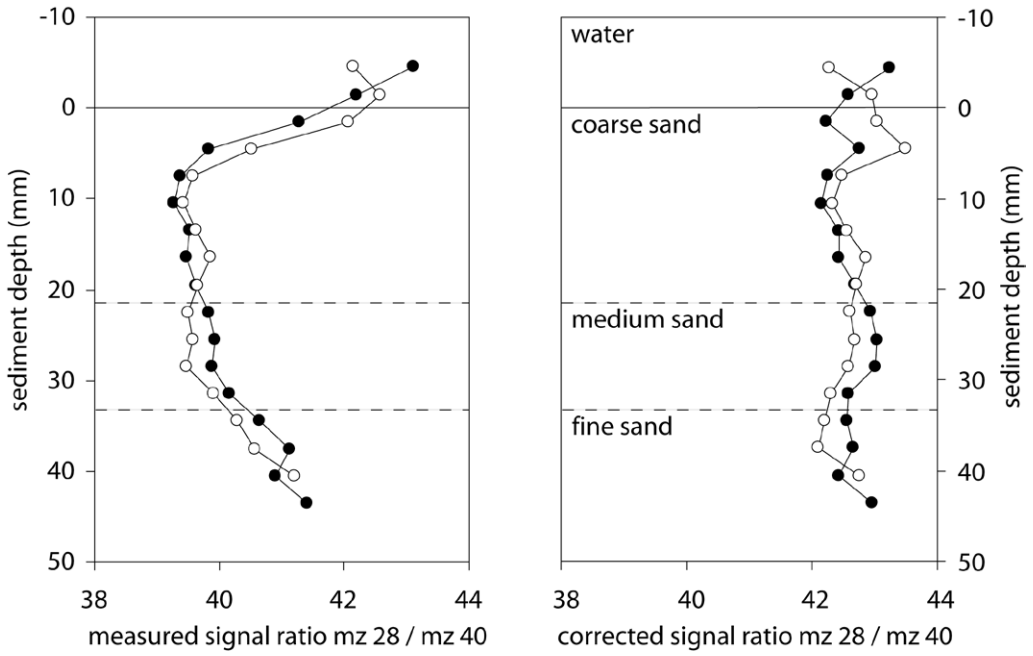

Fig. 2.9: Effect of porosity on N_2/Ar signal ratio. Left panel: Two N_2/Ar profiles of an artificial sediment core with variable water content. Right panel: Corrected N_2/Ar profiles after application of correction equation 2.3. Details of sediment used for artificial sediment column are summarized in table 2.1.

2.4 Discussion

The needle-type membrane inlet developed for this study withstands the mechanical stress during the insertion into compacted fine sands typical for the intended study area. In direct comparison, the newly-developed inlet probe experienced only one third of the insertion force of an inlet probe made according Hartnett & Seitzinger (2003). The insertion force is the result of friction between inlet and sediment particles and thus a proxy for the mechanic stress impinging the inlet. Hence, reducing the insertion force concomitantly reduces the risk of damage to the inlet due to abrasion or shear. Since the silicone membrane of the Hartnett & Seitzinger inlet is at the very front, most of the mechanic stress is directly affecting this membrane. In a preliminary experiment, this membrane was ruptured during the insertion into sediment. This led to the development of this study's inlet which is protected by a steel jacket to minimize the risk of peeling-off or punctuation of the membrane.

This study's inlet probe was sensitive to stirring of the aquateous samples. This behavior is well known from microelectrodes, which also consume the measured compound. Due to this consumption, availability of the measured compound at the sensor is regulated by the diffusion from the sourrounding sample toward the sensor. Stirring of the sample is keeping concentration gradients steep and compound fluxes high, promoting high signals. The membrane inlet probe also consumes the gases to be measured and thus has the same stirring sensitivity illustrated in figures 2.5 and 2.6. This stirring sensitivity of inlet probes was also observed by Lloyd et al. (1995). However, it is unfavorable for the N_2/Ar method that the availability of N_2 and Ar are diffusion controlled, because the diffusivities of both compounds differ and the molar ratio at the membrane is shifting over time. In this context it appears questionable that Hartnett & Seitzinger (2003) used stirred standards for calibration of measurements in unstirred pore waters.

Furthermore, the diffusion-control of the molar N_2/Ar ratio at the membrane also explains the impact of sediment porosity on measured N_2/Ar ratio. Figure 2.9 illustrates the measured N_2/Ar ratio in an artificial sediment column made from sands with different grain sizes and porosities. The measured N_2/Ar ratio was decreasing togehther with the porosity although the initial molar ratio was identical at all depths. Biological interference can be excluded because combustion has eliminated denitrifying bacteria and all organic carbon. The sediment property which is best explaning the relation between porosity and measured N_2/Ar ratio is the formation resistivity factor (F), which was estimated on the basis of measured resistivities (Manheim & Waterman 1974, Ullman & Aller 1982) as equation 2.2. This factor is related with porosity and tortuosity and describes the generic conductivity

of the sediment interstices. Higher values of the formation resistivity factor indicate lower conductivity. Consequently, dissolved gases consumed by the inlet probe are replaced slower. As the diffusivity of N_2 is higher than the diffusivity of argon, N_2 near the membrane is consumed faster than argon, and the N_2/Ar ratio at the membrane is decreasing over time. In sediments with high conductivity and low formation factor, the diffusive flux toward the membrane compensates the consumption of the inlet probe and keeps the N_2/Ar ratio close to the initial value, whereas low sediment conductivity results in insufficient replacement of consumed gases and gradually decreasing N_2/Ar ratio at the membrane.

The extent of this porosity sensitivity of the measured N_2/Ar ratio might be dependent on the used mass spectrometer and the inlet dimensions because the porosity effect is less considerable in the study of Hartnett & Seitzinger (2003). However, the porosity effect observed with the newly-developed inlet was significant and needs to be corrected using equation 2.3. This implies that the precision of N_2/Ar measurements is additionally dependent on measurements of porosity or formation resistivity.

3. Rates of benthic nitrate consumption along the salinity gradient of the Elbe estuary.

Abstract:

Membrane inlet mass spectrometry permits analysing dissolved gasses in aqueous samples. Using miniaturised needle-type membrane inlets enables measuring N_2 profiles across the sediment-water interface, which was rarely used before as routine method. This chapter presents results of a first field test of the newly developed needle-type membrane inlet in sediment of the Elbe estuary (southern North Sea). The Elbe estuary was selected as proving ground because it offers a wide spectrum of sediment grain sizes and nitrate concentrations in the bottom water. The obtained N_2 fluxes were compared with simultaneously measured nitrate fluxes and isotope pairing incubations. Production of N_2 scaled in pace with nitrate flux and agreed well with the results of the isotope pairing methods at low nitrate concentrations, but disagreed at high nitrate concentrations. The results further suggest that coupled nitrification-denitrification fuelled the majority of N_2 production in sandy sediment with low nitrate concentration. Benthic denitrification was found dependent on the concentrations of nitrate, oxygen and TOC, but appeared independent of the temperature.

3.1 Introduction

The significance of nitrogen cycle is undisputed. Still, research is faced with uncertainity because reaction rates cannot be determined directly but have to be estimated on the basis of static state variables and their temporal or spatial variability. This problem is further intensified by the discovery of additional metabolic pathways like Anammox (Thamdrup & Dalsgaard 2002), anaerobic nitrification (Bartlett et al. 2007) or various dissimilatory nitrate reductions using reduced sulphur (Myers 1972) or iron (Straub et al. 1996). Further pathways are still subject of debate as for example the ammonium oxidation to dinitrogen (N_2) coupled to reduction of manganese oxide (Luther et al. 1997, Thamdrup & Dalsgaard 2000). Especially within sediments, these pathways tend to be reversible and coupled temporally or spatially, and thus the nitrogen cycle is expanded to a metabolic network with interfaces to other “cycles”, as for example, those of carbon, sulphur, iron and manganese. An exception is the formation of N_2 because the reverse process nitrogen fixation is energetically expensive and thus should occur exclusively when reactive nitrogen compounds are unavailable. Thus, the measurement of dinitrogen fluxes enables to quantify the net-elimination of reactive nitrogen, whereas the observation of ammonium and nitrate alone does not allow distinguishing between elimination of reactive inorganic nitrogen and other causes of decreasing concentrations of reactive nitrogen, such as assimilation, storage (within sulphur bacteria, Sayama 2001, Preisler et al. 2007) or masking by adsorbtion.

The measurement of N_2 is challenging as the compound is inert and present at high background concentrations compared to microbial reaction rates. Recently, a suitable method emerged using mass spectrometers equipped with membrane inlets, which has been applied for various measurements of water and sludge, often in combination with isotope pairing incubations (e.g. An et al. 2001, Gao et al 2010). However, application of this method to measure N_2 concentration profiles of undisturbed sediment samples to estimate N_2 fluxes are rare. Lloyd et al. (1996) and Hartnett & Seitzinger (2003) developed different needle-type membrane-inlet probes and proved the concept on test measurements, but to our knowledge routine applications for N_2 profiling in sediments as a quantitative measure of N_2 production have not been published so far.

Aim of this study was establishing mass spectrometric N_2 measurements with a needle-type membrane inlet as a routine method for undisturbed sediment cores and to assess its applicability by comparison with the results of independent measurements. The estuary estuary of the river Elbe (northern Germany) was chosen as a test field for the newly developed needle-type membrane inlet because it offers

a combination of high nitrate loads and a wide spectrum of different sediment types that span organic carbon rich, soft sediments to coarse sands with very low organic carbon concentrations. Despite the high nitrate load, the Elbe estuary apparently shifted within one decade from a sink for reactive nitrogen (Schroeder et al. 1996) to an inert channel (Dähnke et al. 2008) due to extensive hydraulic engineering. Thus, besides exploring a method to analyze a method of N_2 Production in sediments, this study also seeks to further elucidate the significance of remaining estuarine sediments as a sink for reactive nitrogen.

All stations were sampled simultaneously by Deek (2011) hence the compiled results enable comparison of four different methods for the estimation of nitrate consumption rates. The present study uses one-dimensional modelling of concentration profiles of nitrate and N_2 respectively, while Deek et al. (2011) applied isotope-pairing incubations of sediment cores in both batch and flow-through configuration. The flow-through incubation is also described in Deek et al. (2011). Since all these methods have their own short comings, it is difficult to choose one of them as basis for the comparison of the results. Here, we propose to compare the results of the afore-mentioned methods on the basis of station parameters such as temperature, oxygen penetration depth, bottom water nitrate concentration and the concentration of organic carbon in the surface sediment. A suitable set of parameters will be selected with a regression analysis. Previous studies of benthic denitrification already found a correlation of the denitrification rate and the availability of nitrate or organic carbon respectively (Lohse et al. 1993, Seitzinger & Giblin 1996).

3.2 Material and methods:

Study site and sampling

The sampling campaigns were carried out between March 2009 and February 2010 with RV Ludwig Prandtl and RV Heincke (Tab. 3.1) along the Elbe estuary and adjacent North Sea (Fig. 3.1).

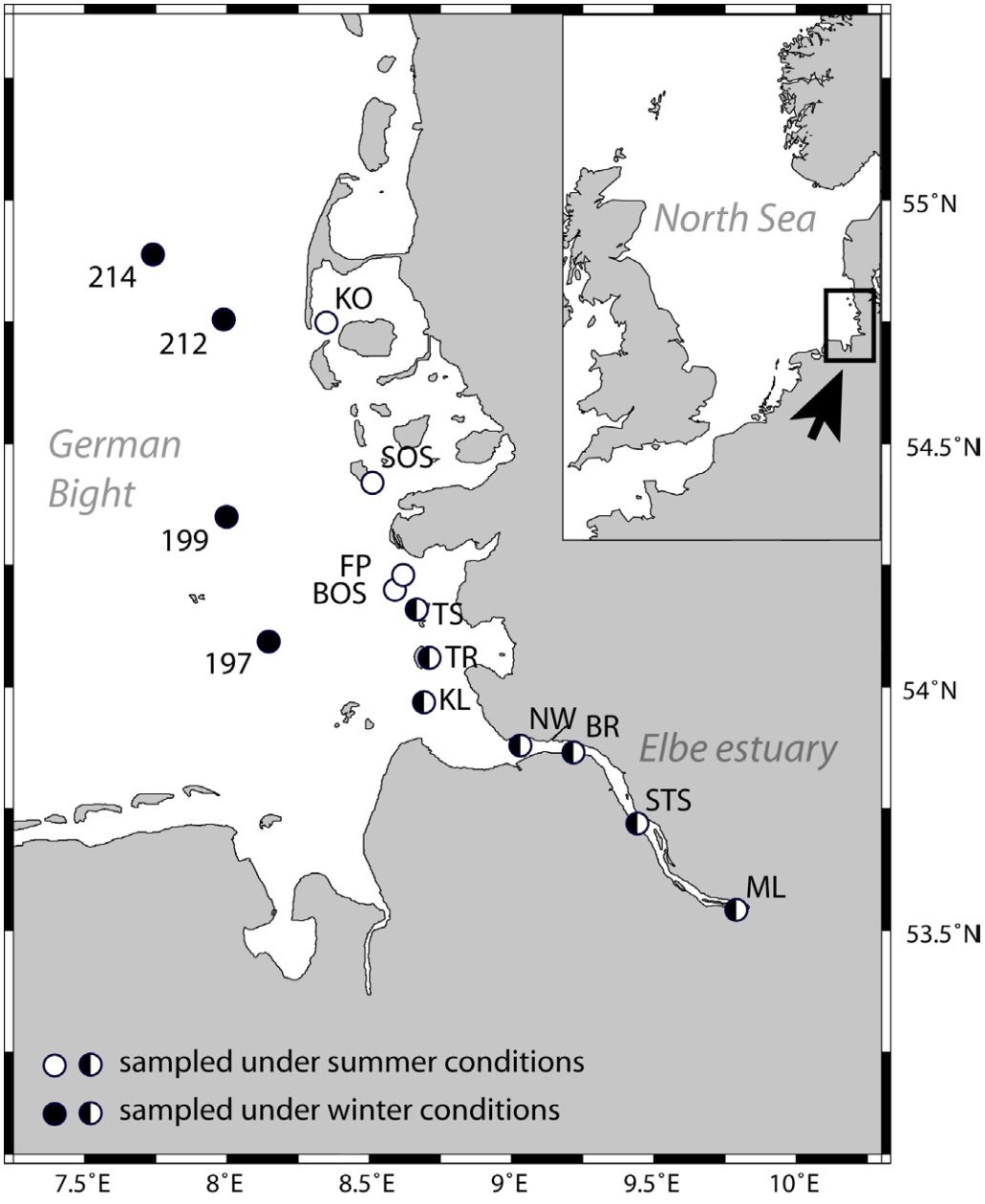

Fig. 3.1: Study area with sampled stations. The insert shows the location of the study area within the North Sea.

The same stations have been sampled and analyzed by Deek (2011) in parallel and we inherit the station designations. An OTS 1500 multiprobe (Meerestechnik-Elektronik) was deployed to measure temperature, salinity and oxygen saturation

of the bottom water. Sediment cores were retrieved with a Multicorer equipped with acrylic glass (PMMA) tubes (60 cm long and 10 cm wide). A subset of these tubes was prepared for pore water sampling by drilling holes in a 1 cm interval and sealing them with adhesive tape prior to deployment. Directly after retrieval, the supernatant of the pore water cores was removed carefully and pore water was extracted with Rhizon core solution samplers (Rhizosphere Research) connected to disposable syringes (see Meijboom & van Nordwijk 1992 and Seeberg-Elverfeldt et al. 2005 for details). The first few hundred microliters of pore water were discarded to remove any air bubbles to prevent oxygenation of the pore water. Samples were then transferred to evacuated Exetainers (Labco) and stored frozen until nutrient analysis. The sediment cores used for O_2 and N_2 profiling were capped with rubber stoppers without any headspace and kept cool during the transport to the land-based laboratory. Lastly, one core of each station was sliced in 1 cm intervals and stored frozen until analysis of the sediment characteristics.

Sediment characteristics

Frozen sediment slices were freeze-dried, and the resulting weight loss was used to calculate the water content. Volumetric porosity was calculated from water content, assuming a mean grain density of 2.65 g cm^{-3}. A subsample of the dry residues was then sieved through mesh sizes of 1000 µm, 500 µm, 250 µm, 125 µm and 63 µm to establish the grain size distributions using Gradistat (Blott & Pye 2001) and the permeabilities using the formula of Beyer (1964). Further subsamples of dry sediment were used to determine the concentrations of total nitrogen and organic carbon with an Elemental Analyzer (Thermo Flash EA) calibrated against acetanilide.

Oxygen measurements

Immediately after arrival at the temperature-controlled laboratory kept at in-situ temperature, at least three oxygen profiles were measured across the sediment-water interface on duplicate cores with needle-type microoptodes (Oxy50, Presens) connected to a Microx TX3 (Presens). After decapping, temperature and oxygen saturation were measured in the bulk supernatant and compared to the values measured in situ with the multiprobe to assess the alterations during the transport. The supernatant was then adjusted to 10 cm height and aerated with an air pump until steady state prior to the profiling. During profiling, the sensor was positioned with an autonomous micromanipulator (Pyroscience). The sensor readings in the aerated supernatant (100 % air saturation) and down in the anoxic sediment (0 % air saturation) were used to calibrate the optodes for each profile individually to account for the constant abrasion of the sensor tip.

N_2 / Ar Profiles

Pore water concentrations of dissolved N_2 were profiled with a needle-type membrane inlet for membrane inlet mass spectrometry developed here. This probe was manufactured from stainless steel capillaries and carried a short silicone tube (Dow Corning) as membrane (see chapter 2 for details). The probe was connected to the mass spectrometer via a 1/16" stainless steel transfer tube with an inline cold trap. The trap was cooled with a mixture of 85 g $MgCl_2$ and 100 g crushed ice to approximately -30 °C, mainly to block fluid water in case of a membrane failure. The resulting gas stream was analysed with a quadrupole mass spectrometer (GAM 200, InProcess Instruments). N_2 was measured according to the N_2/Ar method (Kana et al. 1994) at mass-charge ratio (m/z) 28 and argon as a reference at m/z 40. Additionally, isotopically labelled $^{29}N_2$ and $^{30}N_2$ was detected as m/z 29 and m/z 30, respectively. Vertical profiles were obtained by positioning the probe in 3 mm intervals with an autonomous micromanipulator (Pyroscience), dwelling each position for 5 minutes to allow stabilisation of the N_2/Ar ratio. After this time, values of 10 consecutive measurement cycles were averaged. Each profile was calibrated individually with argon as reference for the correction of the dinitrogen signal. These calculations base on the equilibrium solubilities of N_2 and Ar provided by Hamme & Emerson (2004).

Pore water nutrient analysis

Pore water samples were kept frozen in septum capped Exetainers (Labco). After fast thawing in a water bath at room temperature, the samples were acidified with 6 mol l^{-1} hydrochloric acid (1 % v/v final concentration) to stabilize any gaseous ammonia as ammonium. Aliquots were then taken with syringes through the septum and analyzed with a nutrient autoanalyzer (AA3, Seal Analytical) with methods according to Grasshoff et al. (1983) to establish vertical concentration profiles of dissolved nitrate, nitrite, ammonium, and phosphorous across the sediment-water interface and within the uppermost 14 cm of sediment.

Calculations

Reaction rates and diffusive fluxes across the sediment-water interface were calculated on the basis of the concentration profiles and sediment porosities using the procedure of Berg et al. (1998), assuming steady state profiles, which ultimately employs Fick's first law of diffusion. The local effective diffusion coefficients were corrected for porosity and temperature. Bottom water concentrations were excluded

from flux calculations because the modelled flux over the sediment-water interface and thus the total reaction rate is very sensitive to errors in the bottom water concentration and the porosity of the top layer.

The statistical analysis was conducted with the software SPSS. For correlation analysis, the Spearman‘s rank correlation was preferred to Pearson correlation as a measure of correlation because Spearman‘s rank correlation is more robust against outliers and does not presume linearity.

3.3 Results

Station characteristics and seasonal variations

Riverine nitrate concentrations reached up to 303 µmol l^{-1} (station STS) during winter and 111 µmol l^{-1} (station NW) during summer. During summer, nitrate concentrations had a significant maximum at the estuarine turbidity maximum which was less distinctive during winter (Fig. 3.2). Assimilation, consumption and mixing with nutrient depleted North Sea water reduced the nitrate concentration in the Elbe plume to 20 µmol l^{-1} in winter and 0 µmol l^{-1} in summer, respectively. Additionally, higher fresh water run-off during winter shifted the estuarine mixing zone further downstream towards the North Sea. Using the nitrate concentrations at station ML in combination with the discharge measurements at “Teufelsbrück” (Arge Elbe, 2009) 4 km upstream of station ML, a nitrate load of 1890 t nitrate per day was estimated for March (c = 237 µmol l^{-1} NO_3^-, Q = 1.29 x 10^8 m^3 d^{-1}) and 200 t nitrate per day in September, respectively. All water column characteristics are tabulated in 3.1.

Analyzed sediments comprise coarse silt (station ML), fine sand, and medium sand (stations STS, SOS, KO) with most stations consisting of moderately well sorted, fine sand with low concentrations of total nitrogen (< 0.1 % dry weight) and organic carbon (< 1 % dry weight). The content of organic carbon scaled with fines content (< 63 µm) and can be expressed as $\log_{10}(C_{org}) = 0.88 \times \log_{10}(\text{fines content}) - 1.43$ (n = 68, $R^2 = 0.84$). The calculated permeability was on the order of 10^{-12} m^2, the permeability of sediments with the coarsest grain sizes (stations STS, SOS, KO) estimated at 10^{-11} m^2. As an exception, the stations ML and NW are located in areas with increased deposition of fine material, which resulted in higher contents of nitrogen and organic carbon, poor grain size sorting and very low permeability. All sediment characteristics are summarized in table 3.2.

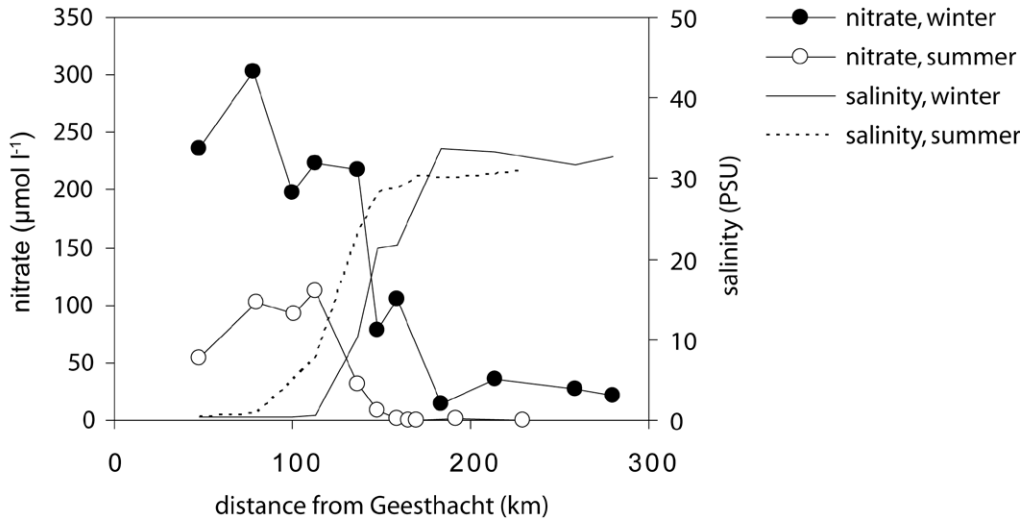

Fig. 3.2: Salinity and concentrations of nitrate in the bottom water (1cm above sediment) along the estuarine salinity gradient. The weir in Geesthacht is the artificial upstream margin of the Elbe estuary.

Tab. 3.1: Sampled positions and water column characteristics.

cruise	station	latitude (°N)	longitude (°E)	date	water depth (m)	salinity (PSU)	temperature (°C)
Pr-0309	ML	53.55	9.80	Mar 2009	2	0.3	6.4
	STS	53.73	9.43	Mar 2009	3	0.4	6.4
	BR	53.87	9.21	Mar 2009	3	0.5	4.5
	NW	53.88	9.03	Mar 2009	4	0.6	6.3
	KL	53.97	8.69	Mar 2009	5	10.3	6.5
	TR	54.06	8.71	Mar 2009	10	21.4	6.2
	TS	54.16	8.67	Mar 2009	6	21.8	5.8
He-318	197	54.09	8.16	Feb 2010	17	33.7	2.1
	199	54.35	8.00	Feb 2010	18	33.2	1.9
	212	54.75	8.00	Feb 2010	17	31.8	0.5
	214	54.88	7.75	Feb 2010	22	32.7	1.4
Pr-0909	ML	53.55	9.80	Sep 2009	2	0.4	18.1
	STS	53.73	9.43	Sep 2009	3	0.8	18.8
	BR	53.87	9.21	Sep 2009	3	5.0	18.1
	NW	53.88	9.03	Sep 2009	4	7.7	18.0
	KL	53.97	8.69	Sep 2009	5	22.9	18.5
	TR	54.06	8.71	Sep 2009	10	28.3	16.1
	TS	54.16	8.67	Sep 2009	6	28.9	16.3
	BOS	54.20	8.59	Sep 2009	5	29.4	16.1
	FP	54.23	8.62	Sep 2009	4	30.3	16.1
	SOS	54.42	8.51	Sep 2009	5	30.1	15.7
	KO	54.75	8.35	Sep 2009	4	30.9	15.9

Tab. 3.2: Sediment characteristics

cruise	station	D_{50} (µm)	sorting (D_{90}/D_{10})	permeability K (10^{-12} m^2)	class	N_{tot} (mg/g)	TOC (mg/g)
Pr-0309	ML	100	109.9	0.0	very coarse silt	2.7	28.0
	STS	390	3.4	73.7	medium sand	< 0.1	0.4
	BR	89	111.0	0.0	very coarse silt	1.3	15.5
	NW	83	15.5	0.0	very fine sand	0.3	3.4
	KL	113	3.1	5.4	very fine sand	0.8	8.1
	TR	149	3.5	5.7	fine sand	0.2	2.1
	TS	150	2.9	6.9	fine sand	< 0.1	1.4
He-318	197	113	283.1	0.0	fine sand	0.2	1.9
	199	256	2.6	25.1	fine sand	n.d.	n.d.
	212	236	2.7	22.3	fine sand	< 0.1	0.1
	214	178	2.7	20.6	fine sand	< 0.1	0.1
Pr-0909	ML	67	50.3	0.0	very coarse silt	3.8	35.1
	STS	390	3.4	73.7	medium sand	< 0.1	0.4
	BR	88	1.9	5.3	very fine sand	0.1	1.0
	NW	68	44.7	0.0	very coarse silt	1.1	12.2
	KL	117	3.3	5.2	very fine sand	0.2	2.5
	TR	154	4.7	5.4	fine sand	0.3	3.6
	TS	108	3.2	5.1	very fine sand	0.3	1.4
	BOS	148	3.2	5.8	fine sand	0.4	3.0
	FP	122	3.1	5.8	very fine sand	0.2	0.2
	SOS	268	3.3	23.0	medium sand	0.1	0.2
	KO	246	3.6	22.2	medium sand	< 0.1	0.3

Benthic nitrogen dynamics

In fine grained sediments with high organic carbon content (stations ML, NW), nitrate is consumed within the uppermost centimetre, whereas nitrate penetration depth was several centimetres in fine-grained sediments with low organic carbon concentrations (stations BR, KL). The nitrate consumption rates were generally higher during the winter and reached a maximum at station ML (2.8 ± 0.3 mmol N m^{-2} d^{-1}). The highest consumption rate was observed during the summer at station NW (1.1 ± 0.3 mmol N m^{-2} d^{-1}). In both seasons, the nitrate consumption rates dropped below 0.01 mmol N m^{-2} d^{-1} at the northernmost stations (Fig. 3.3).

Pore water ammonium concentrations reached up to 3 mmol l^{-1} (station ML) in organic carbon rich sediments and was always diffusing upwards to be released from sediments into the water column (Fig 3.4). The highest efflux of ammonium was observed at station NW (4.0 ± 0.7 mmol N m^{-2} d^{-1}) in summer, where the bottom water

concentration of ammonium rose above 40 µmol l^{-1}. In sediments with low organic carbon content, ammonium is oxidized to nitrate. Especially in permeable, coarse sediments, nitrification consumed all available ammonium, turning these sediments into ammonium sinks and nitrate sources. This is noticeable at stations STS, 214 (winter) and FP, SOS (summer), where nitrification built up a nitrate peak within the sediment. The resulting effluxes of nitrate never exceeded 100 µmol N m^{-2} d^{-1} (Fig. 3.3).

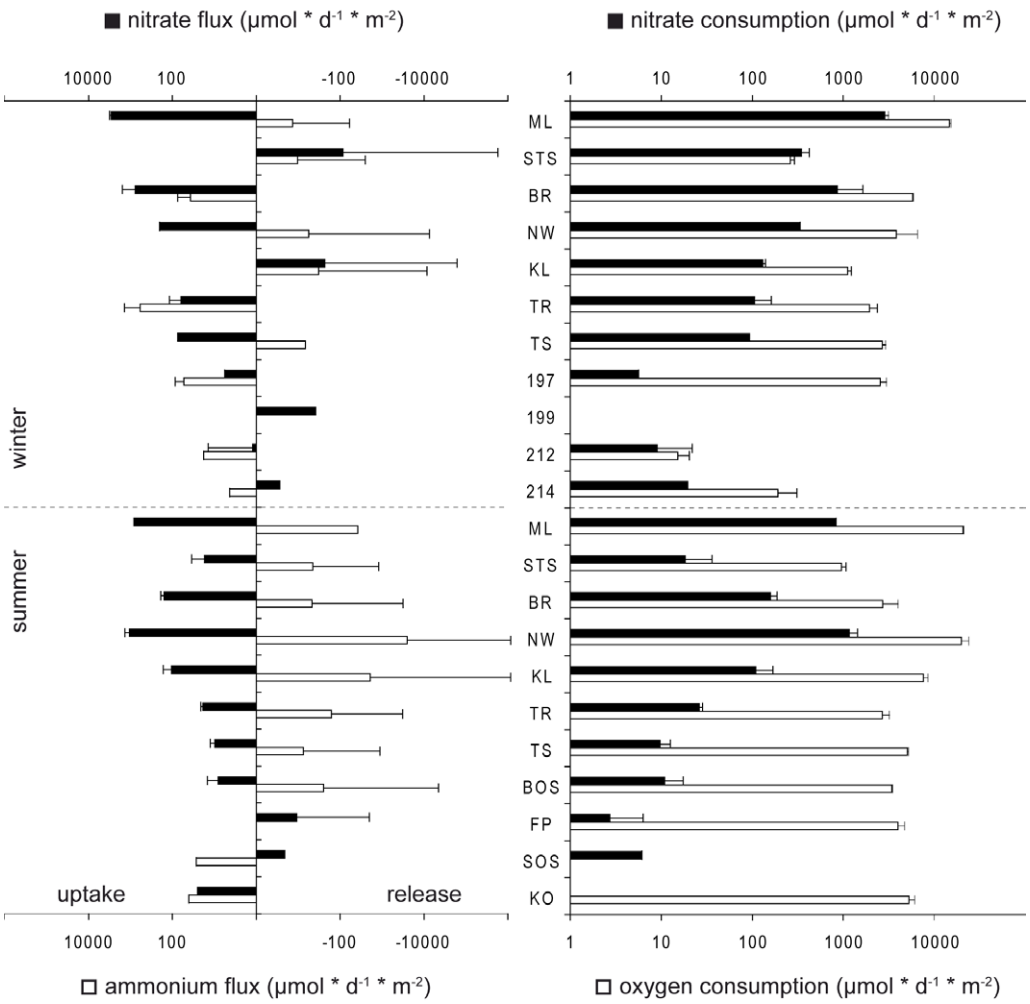

Fig. 3.3: Seasonal and spatial variability of nitrate and ammonium fluxes across the sediment- water interface (left panel) and consumption rates of nitrate and oxygen (right panel). Note logarithmic scale, error bars indicate 1 standard deviation. Rates and fluxes < 1 µmol m^{-2} d^{-1} are not displayed.

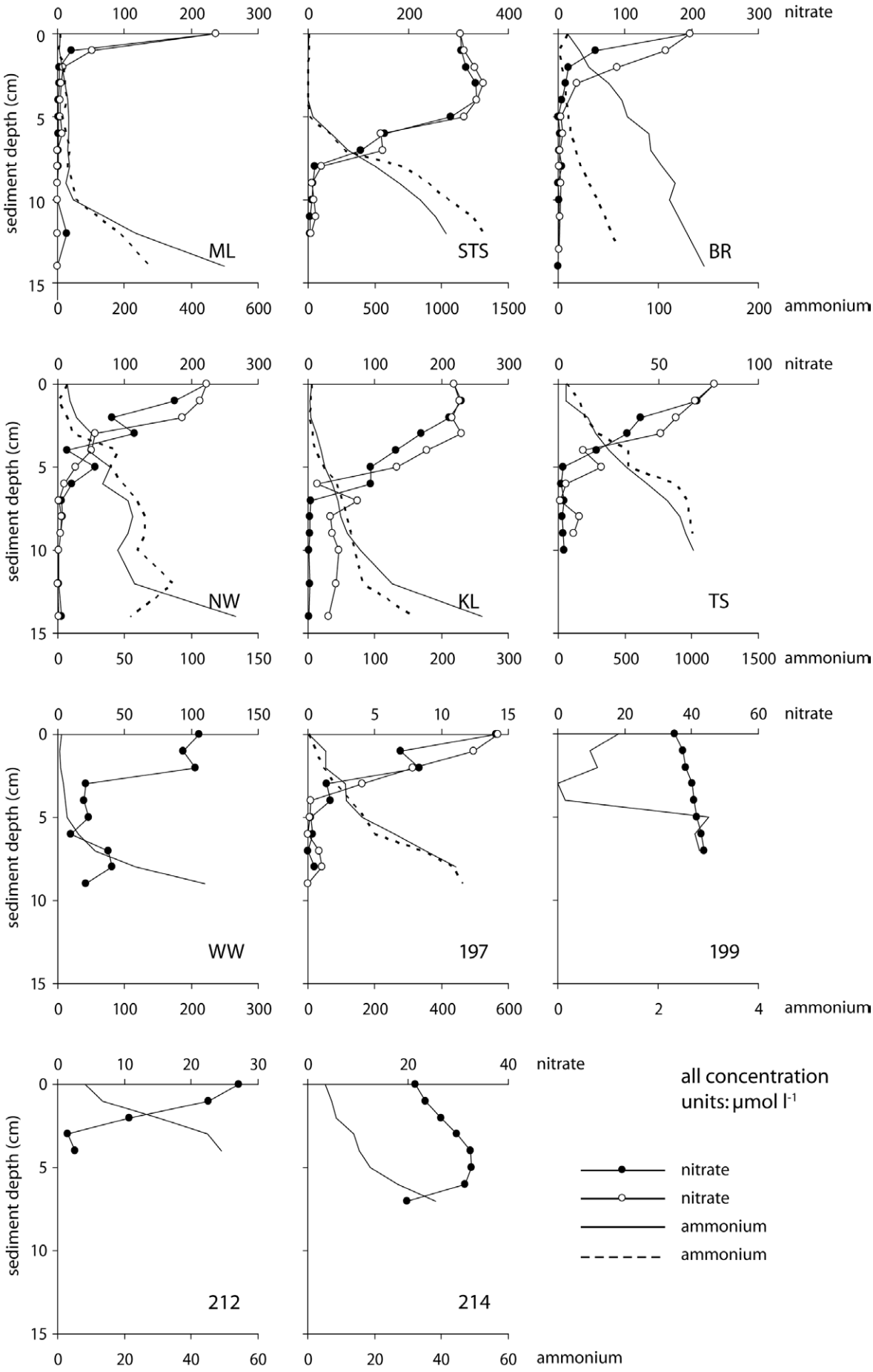

Fig. 3.4a: Pore water concentrations of nitrate and ammonium during winter conditions. All concentration units: µmol l^{-1}.

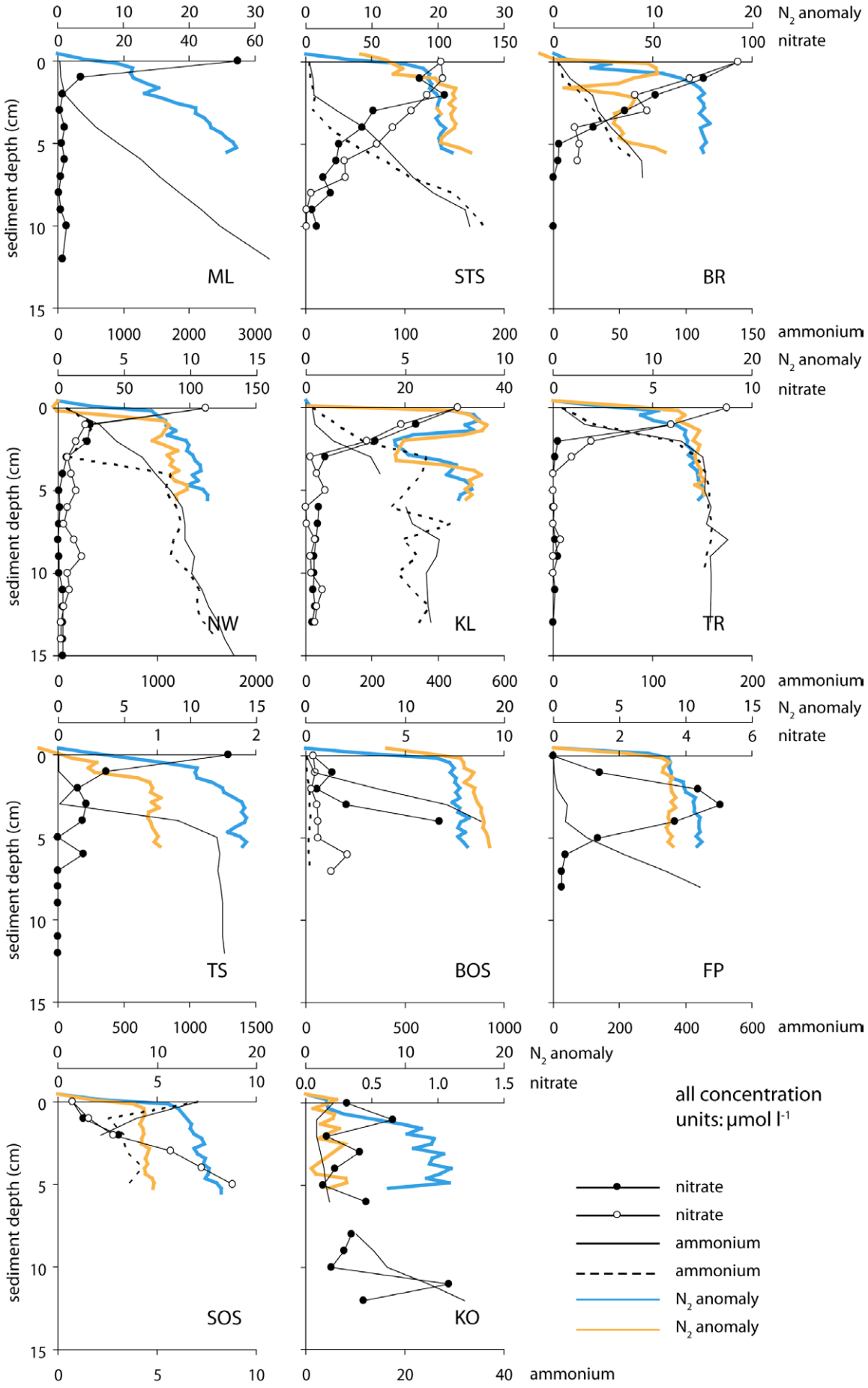

Fig. 3.4b: Pore water concentrations of N_2 anomaly (with respect to air-saturation), nitrate and ammonium during summer conditions. All concentration units: µmol l^{-1}.

Oxygen respiration rates

The sedimentary oxygen consumption rates of the estuarine stations (ML – KL) were one order of magnitude higher than at the Wadden Sea stations (BOS - KO). During the summer campaign, the maximum oxygen consumption rate was observed at stations ML (20.6 ± 0.4 mmol O_2 m^{-2} d^{-1}) and NW (20.0 ± 4.0 mmol O_2 m^{-2} d^{-1}), respectively. During the winter campaign, these rates were lower: ML: 14.7 ± 0.5 mmol O_2 m^{-2} d^{-1}, NW: 3.8 ± 2.7 mmol O_2 m^{-2} d^{-1} (Fig. 3.3).

Correlation analysis

The correlation analysis of potential key variables of nitrate consumption revealed significant correlation of the nitrate consumption rate with the concentrations of TOC in the sediment (Spearman rank correlation coefficient r_s: 0.77, $p < 0.001$) and with nitrate (r_s: 0.81, $p < 0.001$) and oxygen (r_s: 0.58, $p < 0.01$) in the bottom water. A correlation between nitrate consumption and temperature was not evident (r_s: 0.17, $p > 0.4$). See also Tab. 3.3. Elbe fresh water tended having higher oxygen concentrations than saline North Sea water due to salinity-dependent oxygen solubility. Since the Elbe is also the major nitrate source, oxygen concentration is regarded here as covariate of the nitrate concentration, which simply reflects that the concentrations of nitrate and oxygen are ultimately dependent of the mixing ratio of Elbe water and North Sea water.

Tab. 3.3: Spearman correlation coefficients (r_s). Significant results are indicated with * ($p < 0.01$) and ** ($p < 0.001$). N: number of data pairs.

		temperature	$[NO_3^-]$	TOC	$[O_2]$
$[NO_3^-]$	r_s	-0.136			
	p	0.547			
	N	22			
TOC	r_s	0.153	0.568 **		
	p	0.508	0.007		
	N	21	21		
$[O_2]$	r_s	-0.627 **	0.805 **	0.411	
	p	0.002	0.000	0.064	
	N	21	21	21	
NO_3^- flux	r_s	0.169	0.805 **	0.773 **	0.582 **
	p	0.453	0.000	0.000	0.006
	N	22	22	21	21

N_2/Ar measurements

The newly developed needle-type membrane inlet was robust enough to be inserted into firm sediments with sharp-edged shell debris and operated without any failure. The possible spatial resolution was 2 mm, but the profiles were measured in 3 mm intervals as a compromise between resolution and measurement time per profile.

The observed N_2 production rates were generally scaling with the nitrate consumption rates. The coarse grained stations (STS, TS - KO) were found to produce significantly more N_2 than consuming nitrate (Fig 3.5). However, the N_2 production rates generally scale with the expected nitrate consumption rates, which base on the combined parameters c_{NO3} and c_{TOC} (Fig. 3.11). A noticeable exception is station NW, where the nitrate consumption (1171 ± 257 µmol N m^{-2} d^{-1}) significantly exceeded the N_2 production (624 ± 228 µmol N m^{-2} d^{-1}). Measurements of the stable isotope ratio of N_2 in sediment cores of the same station amended with ^{15}N-nitrate and incubated for 3 days (incubation performed by A. Deek, see Deek (2011) for details) show that the labelled $^{29}N_2$ / $^{30}N_2$ was produced in a thin surface layer together with nitrate consumption (Fig. 3.6).

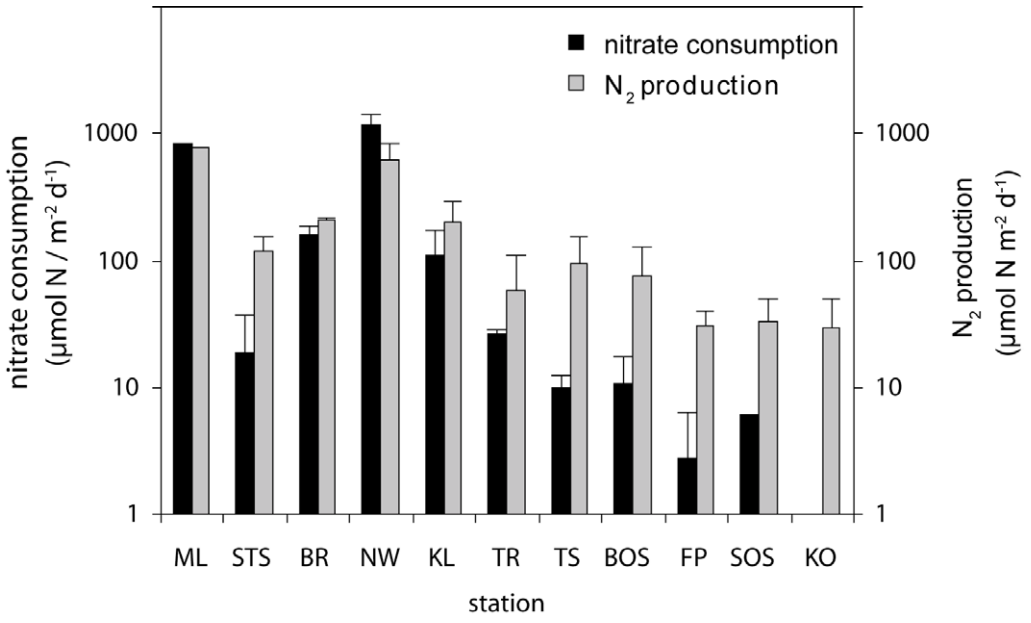

Fig 3.5: Rates of nitrate consumption calculated with nitrate pore-water concentrations and N_2 production calculated with pore-water N2 concentrations measured with needle-type inlet MIMS. Note logarithmic scale.

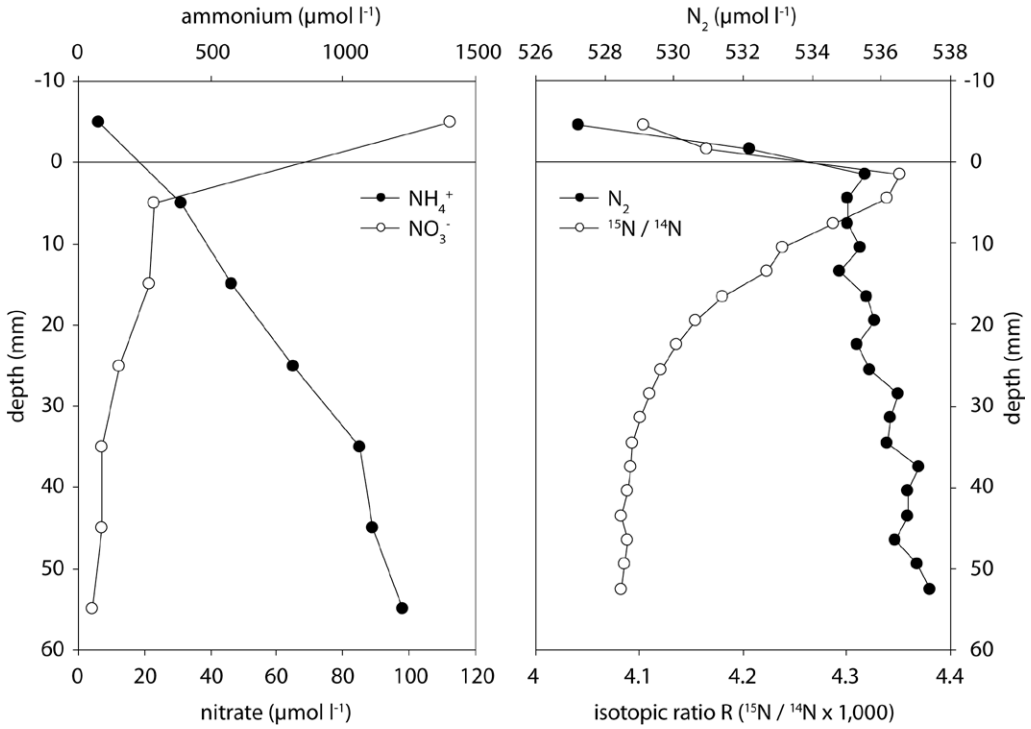

Fig 3.6: Left: Profiles of nitrate and ammonium concentrations in the pore water in cohesive sediment at station NW, Pr-0909. Right: Profiles of N_2 and isotopic ratio ^{15}N / ^{14}N in the pore water of station after 3d incubation with $^{15}NO_3^-$-amendment. Incubated core provided by courtesy of A. Deek, see Deek (2011) for details.

3.4 Discussion

Predominant transport mechanism

The calculation of fluxes and reaction rates on the basis of concentration profiles requires knowledge of the predominant transport mechanisms and their effect on the concentration profiles. Hence, the contribution of potential transport processes to the overall exchange between water column and sediment was assessed, starting with inspection of sediment characteristics.

Molecular diffusion is almost independent of the sediment bedforms and a typical roughness enhances diffusion only slightly by increasing the specific surface area. A second transport mechanism independent of bedforms is the wave-driven shear dispersion (Webster 2003). The intensity of shear dispersion is influenced by the pore width of the sediment and thus by the grain size. Our calculations according to Webster (2003) indicate that shear dispersion is virtually absent in the sampled sediments. A third potential transport mechanism is the transfer of turbulence from the water column into the sediment interstices (Higashino & Stefan 2008). Similar to shear dispersion, the transfer of turbulence is dependent on pore width and thus is negligible in the sampled sediments. A forth and potentially most significant transport is pore water advection induced by wave action (Precht & Huettel 2003) or steady flow (Elliott & Brooks 1997) in interaction with sediment bedforms. However, the intensity of the pore water advection is further governed by the sediment permeability as it determines whether the transport is dominated by either diffusion (low permeability) or advection (high permeability). The threshold between these two transport regimes is at 1×10^{-12} m^2 (Huettel & Rusch 2000, Wilson et al. 2008). In this study, permeabilities have been calculated on the basis of grain size distributions which tends to overestimate the actual permeability by a factor > 2 (Forster et al. 2003). Considering this overestimation, permeabilities of sampled silts and fine sands are below or at the edge of the diffusive-advective transition (Tab. 3.2), and thus we assume diffusive transport. This is supported by the linear concentration gradients just below the surface, which are characteristic for diffusion (Fig 3.4). Only the medium sands have permeabilities well above the threshold and are prone to advective pore water flow caused by interactions of the flow with bedforms like sand ripples. However, even the most permeable station STS clearly exhibits linear concentration gradients during the summer, so we also assume diffusive transport for these stations. This view is supported by Jansen et al. (2005) who compared advective and diffusive fluxes in sandy Wadden Sea sediments. They found no significant effect of advection on fine sands (160 µm grain size) and less than 1.5-fold increased fluxes at medium size sand (300 µm grain size). Huettel et al. (1996) examined similar sand (300 µm grain size) in flume

experiments and reported a twofold increased solute transport into sand with ripples compared to a flat control. Additionally, Lohse et al. (1996) measured oxygen profiles in North Sea sediments and found enhanced transport only in the uppermost few millimeters of the sediment, which is not resolved by the relatively coarse intervals of the pore water sampling with the employed rhizon pore water samplers. Finally, van Raaphorst et al. (1990) have examined pore water concentrations of North Sea sediments and calculated effective diffusion coefficents close or equal to the value of molecular diffusion.

Dependency of nitrate consumption

The correlation analysis (Tab. 3.3) revealed that diffusive nitrate fluxes into the sediment depended primarily on the sediment TOC contents and the nitrate concentrations in the water column, but it is unlikely that TOC and nitrate limit the nitrate flux simultaneously. Instead, a close inspection of the Pr-0909 data suggests that low sediment TOC content limits benthic nitrate uptake at high nitrate concentrations and vice versa. The highest benthic nitrate uptake was observed at station 'NW' where the highest nitrate concentration coincided with the second highest TOC content (Fig. 3.9, asterisk).

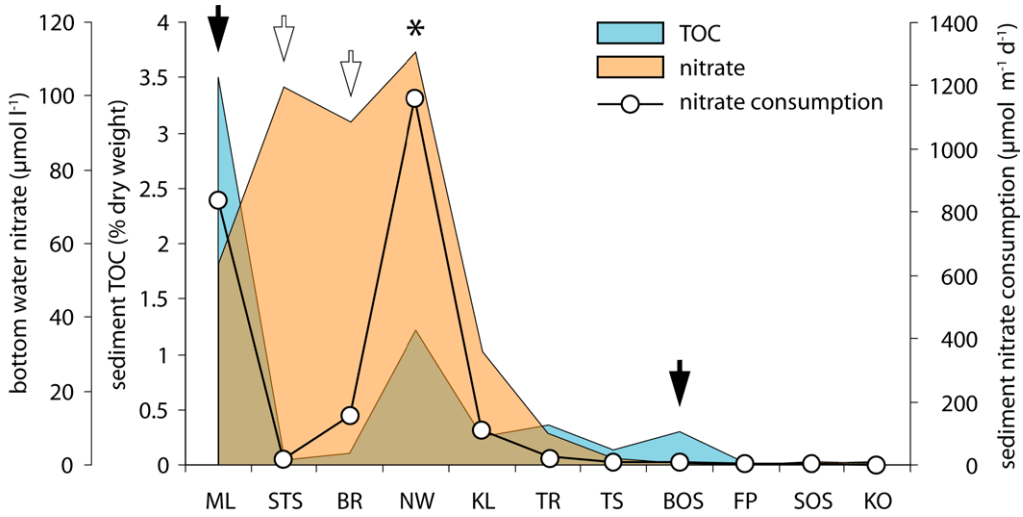

Fig 3.9: Rates of nitrate consumption calculated with nitrate pore-water concentrations along the estuarine salinity gradient during Pr-0909. Black arrows indicate assumed nitrate-limited nitrate consumption, white arrows indicate assumed TOC-limited nitrate consumption. The asterisk marks the highest nitrate consumption rate where highest nitrate concentration conicided with second-highest TOC content.

The above-described dynamic of benthic nitrate uptake resembles second-order kinetic, which is generally described by equation 3.1

$$v = k \times [A] \times [B] \quad (3.1)$$

v: reaction rate
k: rate constant
[A]: concentration of reactant A
[B]: concentration of reactant B

Applied to benthic nitrate consumption rate and logarithmized to account for a wide range of values, equation 3.1 may be written as 3.2

$$\log_{10} NCR = \log_{10} k \times \log_{10} \left(c_{NO3-} \times \frac{l}{\mu mol} \times w_{TOC} \right) \quad (3.2)$$

NCR: nitrate consumption rate
k: rate constant
c_{NO3-}: bottom water nitrate concentration
w_{TOC}: sediment TOC mass fraction

The hypothesis of second-order kinetic of benthic nitrate consumption was verified by plotting nitrate consumption rates versus the product of nitrate and TOC, which yielded a straight line in the log-log plot (Fig 3.10 top) with a Pearson correlation coefficient of $R^2 = 0.83$. The Spearman correlation coefficient of $r_s = 0.95$ is substantially above the Spearman correlation coefficients of nitrate consumption rate and solely nitrate ($r_s = 0.77$) or TOC ($r_s = 0.63$), respectively. Further, the linear regression of the Pr-0909 data also fits the Pr-0309 data, which graphically confirms the absence of noticeable temperature effects. Thus, the numerical product of bottom water nitrate concentration and sediment TOC content appears as a fair estimator of the nitrate consumption rate. This conclusion is supported by the fact that the regression of this study's data also fits the nitrate consumption rates of North Sea sediment obtained by Lohse et al. (1993). Additionally, artificial addition of 100 µmol l^{-1} nitrate during experimental incubation increased nitrate consumption rates, which also match the regression obtained with this study's data (Fig. 3.10 bottom).

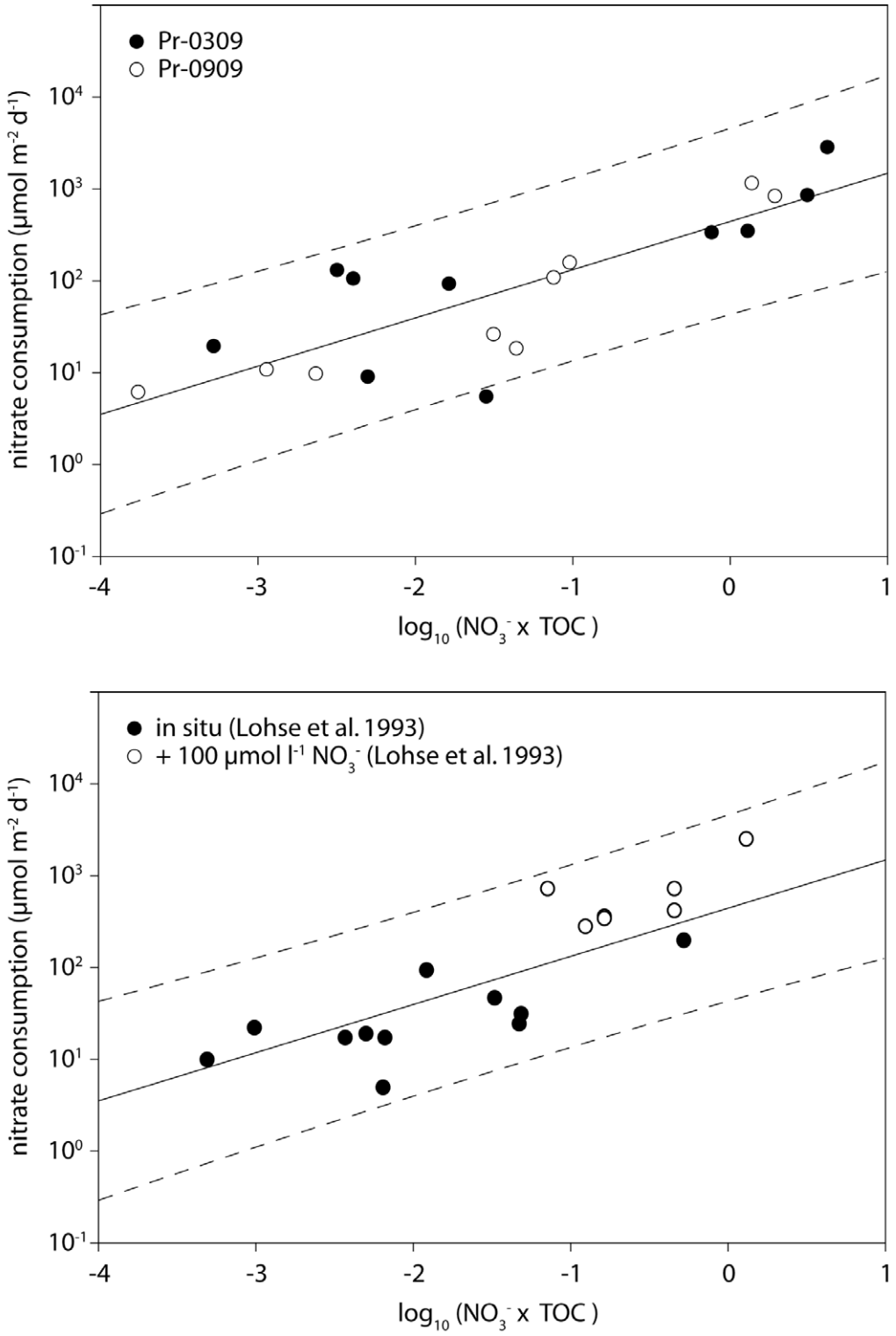

Fig 3.10: Top panel: Rates of nitrate consumption based on nitrate pore-water profiles during Pr-0309 (full circles) and Pr-0909 (open circles). Bottom penal: Rates of nitrate consumption under in situ conditions (full circles) and with addition of 100 µmol l^{-1} nitrate (open circles). In both panales, solid line represents linear regression of Pr-0909 data (R^2 = 0.83), dashed lines indicate prediction interval with 95 % confidence.

In summary, equation 3.3 enables estimating expected nitrate consumption rates on the basis of robust station parameters, namely bottom water nitrate concentration and sediment TOC mass fraction. It should be noted that the bottom water nitrate concentrations have been excluded from the calculations of the nitrate consumption rates, which are thus independent and the correlation between bottom water nitrate concentrations and benthic nitrate consumption rates are not simply an artefact the rate calculations.

$$\log_{10}(NCR) = 0.532 \times \log_{10}\left(c_{NO3-} \times \frac{l}{\mu mol} \times w_{TOC} \right) + 2.618 \quad (3.3)$$

NCR: nitrate consumption rate
c_{NO3-}: bottom water nitrate concentration
w_{TOC}: sediment TOC mass fraction

Assessment of N_2 measurements

Nitrate consumption rates are not necessarily identical with denitrification rates because coupled nitrification-denitrification may substantially contribute to overall N_2 production especially in well oxygenated sediments. Consumed nitrate may also be assimilated into organic matter or preserved within the pool of reactive nitrogen as ammonium by DNRA. During cruise Pr-0909, the N_2 production rates were estimated with three methods, which offer comparing the results. The employed methods were vertical N_2 profiles measured with needle-type membrane inlet (this study), and two isotope-pairing methods employed on sediment cores with flow-through incubation and batch incubation, respectively (Deek 2011). Generally, each method has its specific strengths and drawbacks, which let every method yield representative measurements under specific condition while it may yield wrong estimates under inappropriate conditions. For brief examples, the employed diffusive flux method yields underestimates in the presence of significant pore-water advection, and the flow-through incubation is prone to regime shifts in the course of three days of incubation under artificial conditions. However, a direct comparison of the three methods' results may detect differences and similarities. Since there is no "gold standard" for denitrification measurements, it remains uncertain which of the three employed methods performed best at which station and whether detected differences are result of random errors or inadequate results of one or even all three methods.

Instead, it is proposed here to compare the obtained N_2 production rates on the basis

of observed nitrate consumption rates, because nitrate directly fuels N_2 production in case of direct denitrification. If N_2 production equals twice the nitrate consumption, this suggests a dominance of Anammox, because Anammox consumes nitrate and ammonium in equal rates and only one half of the nitrogen of the produced N_2 is provided by nitrate. In case N_2 production exceeding nitrate consumption more than twice, this points to a significant contribution of coupled nitrification-denitrification to N_2 production, while DNRA may be detected if N_2 production rate substantially falls below nitrate consumption rate. Since also the observed nitrate consumption rates contain random errors, it is further proposed here to employ the fitting equation 3.3 to calculate “expected nitrate consumption rates” and thus to ultimately compare the obtained N_2 production rates on the basis bottom water nitrate concentration and sediment TOC.

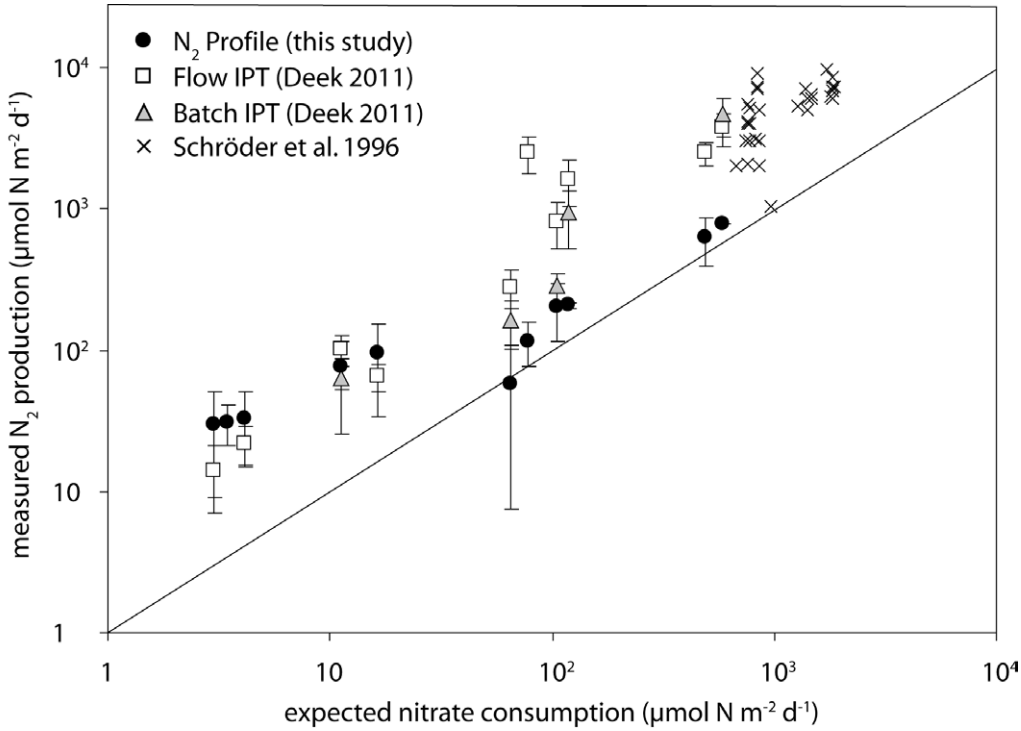

Fig. 3.11: Measured N_2 production vs. expected nitrate consumption rates calculated with equation 3.3. For comparison, denitrification rates of Elbe estuary sediments (crosses, Schröder et al. 1996). Error bars indicate standard deviation as $\log_{10}$ ($\mu \pm \sigma$). The diagonal line represents 1:1 agreement with expected values according to equation 3.3.

The N_2 production rates of all three methods generally scale with the expected rates of nitrate consumption (Fig. 3.11). All three methods consistently found a systematic offset at low expected nitrate consumption rates (< 100 µmol m^{-2} d^{-1}), which applies to stations such as STS, TS, KO with permeable, coarse sediment and low TOC content. In these stations, the turnover zones of nitrate and ammonium are

overlapping (Fig. 3.4), which suggests a coupling between nitrate and ammonium. This coupling could be due to anammox coupled to incomplete denitrification (Kartal et al. 2007) and would yield a two-fold higher efflux of N_2 than denitrification. However, N_2 production exceeds nitrate consumption more than twofold, which is most probably result of coupled nitrification-denitrification within the sediment. This assumption is supported by the results of the batch isotope-pairing incubation, which imply that only 3 % of the water column nitrate contributed to N_2 production at station BOS (S. Meyer, pers. comm.). The nitrate profiles of the stations BOS, FP and SOS (summer, Fig. 3.4b) feature internal nitrate peaks and suggest nitrate production within the sediment.

At higher expected nitrate consumption rates (> 100 µmol m^{-2} d^{-1}), the results of the isotope pairing incubations (Deek 2011) exceed the expected values. This excess could be an effect of the stagnant conditions during incubations, because the turbulence of the supernatant water column is significantly reduced in both methods compared to in situ flow. This declined flow would reduce oxygen supply to the sediment, which in turn enhances denitrification (Schröder et al. 1996). The results of the batch isotope-pairing incubation at station ML suggest that water column nitrate contributed 60 % to N_2 production (S. Meyer, pers. comm.), which implies coupled nitrification-denitrification or dominant anammox. In either case, the produced N_2 should also become detectable in the N_2 profiles, which is not the case. Instead, the results of the N_2 profile method (this study) meet the expected values and thus suggest that denitrification of the water column nitrate is the dominant source of N_2.

This study's estimates of nitrate consumption and N_2 production employ modelling diffusive fluxes on the basis of concentration profiles, and thus might be biased simultaneously. Neglecting pore water advection in permeable sediment by the diffusion model is a potential source of biased results, but might be of minor importance here because the estimates of all three methods agree well at the stations with highest sediment permeability (e.g. BOS, FP, KO). A second possible error source shared by both profiling methods is the limited spatial resolution of the pore water samples and N_2 measurements, respectively. This effect shall be demonstrated with the results at station NW during summer. The calculated N_2 production (624 ± 228 µmol N d^{-1} m^{-2}) explains only half of the nitrate consumption (1159 ± 273 µmol N d^{-1} m^{-2}). Although dissimilatory nitrate reduction to ammonium (DNRA) or nitrate storage within sulphur bacteria would result in nitrate consumption without N_2 production, this apparent discrepancy is best explained with the sampling resolution which is too coarse to capture all internal zonations. This is illustrated by the measurement of the $^{15}N/^{14}N$ ratio of N_2 measured on sediment cores amended

with ^{15}N-nitrate of the same station, which reveals that the nitrate is consumed in a thin layer close to the surface (Fig. 3.8). Such steep concentration gradients of nitrate and N_2 are not sufficiently resolved by the sampling intervals of the pore water samplers and, to a lesser extent, by the needle-type membrane inlet. Reaction rates calculated on these profiles likely underestimated the true reaction rates. In summary, limited spatial resolution offers an alternative explanation for the marked differences between the results of the incubation methods and the profiling method at high N_2 production rates.

Despite the inherent uncertainty of the employed method to estimate expected nitrate consumption rates, the suggested method might enable interpreting historical data. Denitrification rates reported by Schroeder et al. (1996) of Elbe estuary sediments are higher than the rates of this study and the results of Deek (2011), and reach values up to 9.6 mmol N m^{-2} d^{-1} at station ML. This can be attributed to the higher concentrations of nitrate in the water column (up to 450 µmol l^{-1}) and organic carbon in the sediment (up to 8 % dry weight at station ML) during the 1980s, when the sampling was done by Schroeder et al. (1996). These conditions probably have promoted denitrification similarly to the effect of nitrate amendment observed by Lohse et al. (1993) as illustrated in figure 3.10, and the rates of Schroeder et al. (1996) match the regression obtained with this study's measurements.

3.5 Conclusions

The newly developed needle-type membrane inlet for the estimation of N_2 fluxes across the sediment-water interface with a mass spectrometer is a feasible addition to the routine measurement of nitrate fluxes to establish the rates of benthic nitrification and nitrate consumption. The comparison of the nitrate consumption rates of the N_2-profiling method and isotope-pairing incubations, respectively, show a potential underestimation of the true consumption rates by the N_2-profiling method due to its limited spatial resolution. While the spatial resolution of nitrate concentration profiles can be improved by the use of nitrate microsensors (Larsen et al. 1996), it is not that simple for the needle-type membrane inlets. The inlet probes used for MIMS consume the dissolved gases and create a halo of depleted pore-water around the membrane. This halo expands during the dwell time. Since the size of this gas-depleted halo defines the actual spatial resolution, it is necessary to reduce both the membrane dimension and the dwell time to further improve the spatial resolution of needle-type membrane inlets. The profiling methods for nitrate and dinitrogen ultimately become improper in completely anoxic sediments, because denitrification occurs in this case directly at the surface without detectable concentration gradients. The isotope-pairing incubation methods are then clearly superior as they are then insensitive to insufficient simulation of the hydrodynamic conditions.

The empirical site descriptor based on the concentrations of nitrate in the bottom water and organic carbon in the sediment correlates with the diffusive nitrate fluxes into the sediment. It implies that the benthic nitrate consumption is mainly limited by the transport of the nitrate from the bottom water towards the zone of denitrification in the sediment. The dataset of this study is still limited as it does not contain samples from shallow sediments influenced by tide and waves. This shortcoming will be addressed in chapter 4. However, if the correlation of benthic nitrate consumption and the empirical site descriptor is verified by additional data, this site descriptor would offer a convenient method to estimate the benthic nitrate consumption in ecosystem models.

4. Benthic elimination of reactive nitrogen in the German Bight (southern North Sea)

Abstract

The German Bight as a part of the southern North Sea is substantially influenced by the river Elbe that is discharging high loads of anthropogenic nitrate. The effects on the coastal ecosystem comprise plankton blooms, seasonal bottom water anoxia and shifts of the pelagic and benthic communities. Recent counter measures reduced the nitrate load and increased the oxygenation of the Elbe estuary, but have apparently also greatly reduced the estuary's capacity for nitrate removal. The current contribution of the surface sediment to nitrate removal from the Elbe plume was determined with analyses of pore-water and sediment samples. Additionally, profiles of N_2 were measured with membrane inlet mass spectrometry equipped with needle-type membrane inlet. Measurements in sediment of the Elbe estuary, Wadden Sea and adjacent German Bight were fitted to a model of benthic nitrate consumption, and the results suggest that benthic N-elimination is controlled by water column nitrate, oxygen and TOC in the sediment. The effect of temperature was not evident. The fitted model was further employed to estimate the total rates of benthic nitrate consumption and N_2 production. The estimated nitrate consumption constantly removed 1-3 % of the Elbe nitrate discharge. Benthic N_2 production in German Bight was fuelled up to 90 % by coupled nitrification-denitrification, and eliminated 3-7 % of the Elbe nitrate discharge during late winter and 19-43 % during late summer, respectively.

4.1 Introduction

The German Bight is part of the southern North Sea, and is semi-enclosed by an industrialized hinterland. The rivers Elbe, Weser, Ems and Eider discharging into the German Bight drain this intensively used catchment and are significant sources of pollutants such as reactive nitrogen compounds (e.g. Johannsen et al. 2008, Dähnke et al. 2008). The load of reactive nitrogen discharged by the Elbe into the German Bight reached a maximum in the 1980's and various efforts constantly reduced the load since then (Amann et al. 2012). These changes are not reflected in the published results of benthic denitrification measurements (see also tab. 1.1), and attempts estimating the elimination of reactive nitrogen in German Bight sediments (e.g. Pätsch et al. 2008) have no recent data basis.

The present study ventures to combine spot measurements of benthic nitrate consumption and N_2 production with an analytical model to estimate nitrate consumption of the whole study area. This method resembles the study of Deutsch et al. (2010), who extrapolated the benthic N-removal of the Baltic Sea based on TOC-distribution maps. Employing sediment TOC content as predictor founds on regularly observed correlation of nitrate consumption and TOC content (Saunders & Kalff 2001, Tomaszek & Czerwieniec 2003, Deutsch et al. 2010). However, other studies reported correlation of benthic nitrate consumption with nitrate concentration (Nielsen et al 1995, Trimmer et al. 1998, Lohse et al. 1993), oxygen (Rysgaard et al. 1994, Veraart et al. 2011) and temperature, respectively (Saunders & Kalff 2001, Tomaszek & Czerwieniec 2003, Veraart et al. 2011). It becomes obvious that denitrification is controlled by several factors. Hence, the present study attempts combining these potential predictors to estimate the nitrate consumption in North Sea sediment. The underlying model views benthic nitrate consumption with a transport-centred perspective.

Molecular diffusion was chosen here as starting point because this transport mechanism is ubiquitous and transports solutes wherever transport gradients exist. This mechanism has the least transport capacity compared to e.g. advection (Precht & Huettel 2003, Cook et al. 2006) or shear dispersion (Webster & Taylor 1992). Hence, molecular diffusion sets the baseline for nitrate transport into the sediment. For simplicity, the following scenario presumes a flat sediment surface and molecular diffusion as sole transport mechanism while excluding pore water advection and bioturbation, which will be addressed in the discussion section. Extreme conditions such as complete absence of nitrate and oxygen are also excluded. The sediment is assumed being homogeneous with respect to reactivity, which implies quasi zero-order kinetic of oxygen consumption (Stolper et al. 2010) and nitrate consumption

(Nielsen et al. 1990), respectively. Oxygen is preferably consumed to nitrate (Brandes et al. 2007) and inhibits denitrification at concentrations down to at least 90 µmol l^{-1} (Gao et al. 2010). Thus, no nitrate consumption occurs in the uppermost, oxygenated sediment layer. In this context, the diffusive boundary layer covering the sediment may be regarded as part of the diffusion-controlled sediment layer that separates turbulent water column and nitrate consumption zone within the sediment. Below the oxygenated layer, nitrate consumption depletes the pore water nitrate and creates a nitrate concentration gradient from the bottom water through the oxygenated layer toward the nitrate consumption zone. Consequently, nitrate from the water column diffuses along this gradient into the sediment. Under steady state conditions, the diffusive nitrate uptake (DNU) equals the diffusive flux (J) through the oxygenated sediment layer, which can be described with Fick's first law (Fick 1855)

(4.1) $$DNU = J = D_{eff} \times \frac{\Delta c_{nit}}{\Delta z}$$

DNU: diffusive nitrate uptake
J: diffusive nitrate flux
D_{eff}: effective diffusivity
Δc_{nit}: nitrate concentration difference
Δz: diffusion length

Since nitrate diffusing into the sediment is completely consumed, the concentration gradient is correlated with the nitrate concentration in the water column, so equation 4.1 may be generalized to term 4.2. See also figure 4.1.

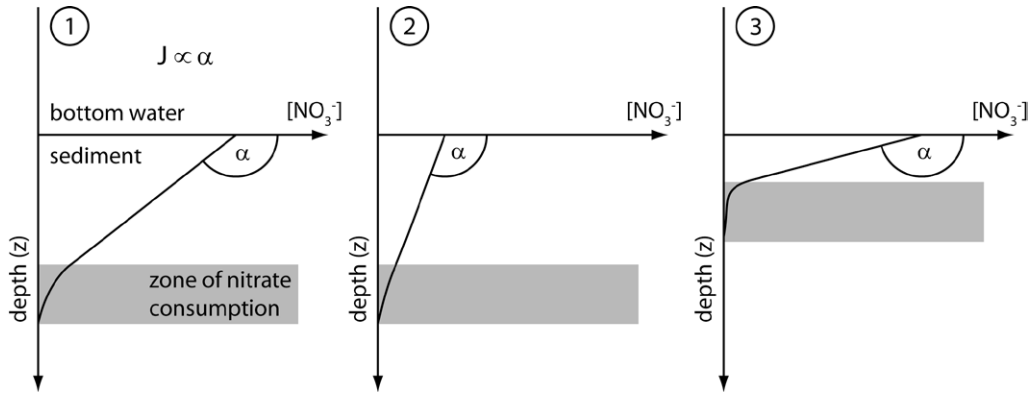

Fig. 4.1: Idealized concentration profiles of nitrate across the sediment-water interface (1). The diffusive flux (J) is proportional to the steepness of the concentration gradient (α) in the oxygenated, uppermost sediment and thus dependent on the depth of the nitrate consumption zone and the bottom water concentration of nitrate. As for example, a low nitrate concentration in the bottom water reduces the nitrate flux (2), whereas a shallow nitrate consumption zone increases the nitrate flux (3). Internal nitrate production by nitrification is neglected. Not drawn to scale.

(4.2) $$DNU \propto \frac{\Delta c_{nit}}{\Delta z}$$

DNU: diffusive nitrate uptake
Δc_{nit}: nitrate concentration difference
Δz: diffusion length

If regarding the presumptions of the diffusion scenario, then equation 4.1 is analogue to equation 5 of Meysman et al. (2010) and describes the relation of diffusive oxygen uptake (DOU) and oxygen penetration depth (OPD) in equation 4.3

(4.3) $$OPD = 2\phi D \times \frac{c_{oxy}}{DOU}$$

OPD: oxygen penetration depth
Φ: porosity
D: diffusivity
c_{oxy}: bottom water oxygen concentration
DOU: diffusive oxygen uptake

which again may be generalized to term 4.4

(4.4) $$OPD \propto \frac{c_{oxy}}{DOU}$$

OPD: oxygen penetration depth
c_{oxy}: bottom water oxygen concentration
DOU: diffusive oxygen uptake

Further, Seiter et al. (2005) showed that DOU scales with sediments TOC content (term 4.5), though TOC is not an ideal proxy of reactivity of the organic matter. However, microbial degradation is not the sole link between DOU and TOC because organic matter generally increases porosity, which increases diffusivities within the sediment. This implies that even refractory organic matter may enhance DOU by increasing the sediment porosity.

(4.5) $$DOU \propto TOC$$

DOU: diffusive oxygen uptake
TOC: total organic carbon content

If defining that the oxygen penetration depth is the sediment depth where oxgen concentration is sufficiently low for loosening inhibition of denitrification, then Δz (equ. 4.2) equals OPD. Finally, terms 4.2, 4.4, and 4.5 can be combined to

(4.6) $$DNU \propto \frac{c_{nit}}{c_{oxy}} \times TOC$$

DNU: diffusive nitrate uptake
c_{nit}: bottom water nitrate concentration
c_{oxyt}: bottom water oxygen concentration
TOC: total organic carbon content

By using logarithms, term 4.6 can be formed into a linear model that can be fitted to observational data employing multiple linear regression of the generic form

(4.7) $$Y = b_1 x_1 + b_2 x_2 + ... + b$$

Y: model estimate
b b_1 b_2 :fitting parameters
x x_1 x_2: measured data

The final model is

$$\log_{10}(DNU) = b_{nit} \log_{10}(c_{nit}) + b_{TOC} \log_{10}(w_{TOC}) + b_{oxy} \log_{10}(c_{oxy}) + b \quad (4.8)$$

DNU: diffusive nitrate uptake
c_{nit}: bottom water nitrate concentration
c_{oxy}: bottom water oxygen concentration
w_{TOC}: organic carbon mass fraction
b_{nit}, b_{TOC}, b_{oxy}, b: fitting parameters

The fitted model can be employed subsequently for the estimation of benthic nitrate uptake on the basis of distribution maps of nitrate, oxygen and TOC. Analogously, the same method may be used for the estimation of N_2 production rates because nitrate from the water column fuels denitrification. However, alternative N_2 sources such as coupled nitrification-denitrification and anammox are less dependent on water column nitrate, and the resulting model may weight parameters differently.

4.2 Material and Methods

Study site

The sampling campaigns in Elbe estuary, German Bight and North-Frisian Wadden Sea were carried out between March 2009 and February 2010 with the RV *Ludwig Prandtl* and RV *Heincke*, respectively. The sampled stations are depicted in figure 4.2, the geographic positions are listed in annex, table 7.1. Temperature, salinity and oxygen saturation of the bottom water were measured with an OTS 1500 multiprobe (Meerestechnik-Elektronik) during the cruises Pr-0309 and Pr-0909, and with a SBE911plus (Seabird) during the cruises He-304 and He-318. Based on own observations and long-term trajectories (Breton & Salomon 1995), we conclude that the Elbe plume is not crossing the 7.5° E meridian, thus the study area covers 11,700 km^2 and comprises the inner German Bight east of 7.5° E and south of 55° N, outer Elbe estuary, and tidal flats of the Wadden Sea along the coast. The Wadden Sea comprises 3,300 km^2 of sheltered flats exposed at Mean Lower Low Water and interspersed tidal creeks.

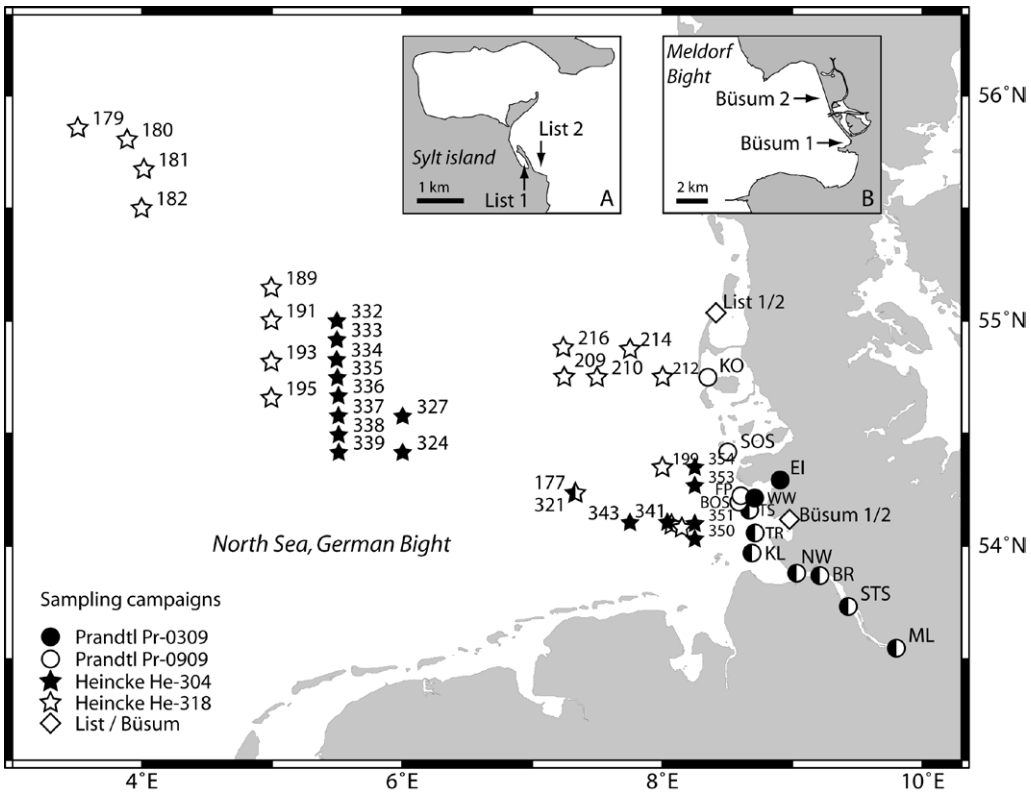

Fig. 4.2: Overview of the sampled stations in Elbe Estuary, German Bight and North Frisian Wadden Sea. Insert A shows the positions of the Wadden Sea stations List 1 and List 2 in the List-Rømø tidal bassin. Insert B shows the positions of the Wadden Sea stations Büsum 1 and Büsum 2 in the Meldorf Bight.

Sediment cores were retrieved with a multicorer equipped with acrylic glass (PMMA) tubes (60 cm long and 10 cm wide). The intertidal stations List and Büsum within the Wadden Sea were sampled at rising tide by manually pushing the acrylic glass tubes into the sediment. A subset of these tubes was prepared for pore water sampling by drilling holes in a 1 cm interval and sealing them with a septum prior to deployment. Directly after retrieval, the supernatant of the pore water cores was carefully removed and the pore water was extracted with rhizon core solution samplers (Rhizosphere Research) connected to disposable syringes (see Meijboom and van Nordwijk 1992 and Seeberg-Elverfeldt et al. 2005 for details). The first few hundred microliters of pore water were discarded to prevent oxygenation of the pore water by removing air bubbles. The samples were then transferred to evacuated Exetainers (Labco) and stored frozen until nutrient analysis. The sediment cores used for O_2 and N_2 profiling were capped with rubber stoppers without any headspace and kept cool until the analysis. Lastly, one core of each station was sliced in 1 cm intervals and stored frozen until analysis of the sediment characteristics.

Tab 4.1: Overview of sampling campaigns in the Elbe estuary, German Bight and North-Frisian (NF) Wadden Sea.

cruise	vessel	date (month / year)	area
Pr-0309	RV L. Prandtl	03 / 2009	Elbe estuary, NF Wadden Sea
He-304	RV Heincke	05 / 2009	German Bight
Pr-0909	RV L. Prandtl	09 / 2009	Elbe estuary, NF Wadden Sea
He-318	RV Heincke	02 / 2010	German Bight, Dogger Bank
List	-	12 / 2008 - 04 / 2010	NF Wadden Sea
Büsum	-	12 / 2008 - 04 / 2010	NF Wadden Sea

Sediment characteristics

The frozen sediment slices were freeze-dried, and the resulting weight loss was used to calculate the water content. The water content was used to calculate the volumetric porosity based on the assumed mean grain density of 2.65 g cm^{-3}. A subsample of the dry residues was then sieved through mesh sizes of 1000 µm, 500 µm, 250 µm, 125 µm, and 63 µm to establish the grain size distributions using Gradistat (Blott & Pye 2001). Permeabilities were calculated on the basis of these grain size distributions using the formula of Beyer (1964). Further subsamples of the dry sediment samples were used to determine the concentrations of total nitrogen and organic carbon with an Elemental Analyzer (Thermo Flash EA) calibrated against acetanilide.

Oxygen measurements

Immediately after arrival at the temperature-controlled laboratory kept at in-situ temperature, several oxygen profiles were measured across the sediment-water interface with needle-type microoptodes (Oxy50, Presens) connected to a Microx TX3 (Presens). After decapping, temperature and oxygen saturation were measured in the bulk supernatant and compared to the values measured in-situ with the multiprobe to assess the alterations during the transport. The supernatant was then adjusted to 10 cm height and aerated with an air pump until steady state prior to the profiling. During the profiling, the sensor was positioned with an autonomous micromanipulator (Pyroscience). The sensor readings in the aerated supernatant (100 % air saturation) and down in the anoxic sediment (0 % air saturation) were used to calibrate the optodes for each profile individually to account for the constant abrasion of the sensor tip. The oxygen measurements were conducted directly onboard during cruises He-304 and He-318. During the remaining campaigns, the oxygen measurements were conducted in nearby land-based laboratories in List (Wadden Sea station, Alfred-Wegener-Institute), Büsum (FTZ Research and Technology Center) and Hamburg (University of Hamburg).

N_2/Ar Profiles

The pore water concentrations of dissolved dinitrogen have been profiled with a needle-type membrane inlet for membrane inlet mass spectrometry developed here. This probe was manufactured from stainless steel capillaries and carried a short silicone tube (Dow Corning) as membrane (see chapter two for details). The probe was connected to the mass spectrometer via a 1/16” stainless steel transfer tube with an inline cold trap. The trap was cooled with a mixture of 85 g $MgCl_2$ and 100 g crushed ice to approximately -30 °C, mainly to block fluid water in case of a membrane failure. The resulting gas stream was analysed with a quadrupole mass spectrometer (GAM 200, InProcess Instruments). N_2 was measured according to the N_2/Ar method (Kana et al. 1994) at m/z 28 and argon as a reference at m/z 40. The profiles were obtained by positioning the probe in 3 mm intervals with an autonomous micromanipulator (Pyroscience), holding each position for 5 minutes to allow stabilisation of the N_2/Ar ratio. After this time, the values of 10 consecutive measurement cycles have been averaged. Each profile was calibrated individually with argon as reference for the correction of the dinitrogen signal. These calculations base on the equilibrium solubilities of N_2 and Ar provided by Hamme & Emerson (2004). The measurements were conducted onboard during He-304 and He-318, and otherwise in nearby land-based laboratories in List, Büsum and Hamburg.

Pore water nutrient analysis

The pore water samples were kept frozen in septum capped Exetainers (Labco). After fast thawing in an water bath at room temperature, the samples were acidified with 6 µmol l^{-1} hydrochloric acid (1 % v/v final concentration) to stabilize any gaseous ammonia as ammonium. Aliquots were then taken with syringes through the septum and analyzed with a nutrient autoanalyzer (AA3, Seal Analytical) with methods according to Grasshoff et al. (1983).

Calculations

Reaction rates and diffusive fluxes of nitrate and oxygen across the sediment-water interface were calculated on the basis of the concentration profiles and sediment porosities using the algorithm of Berg et al. (1998), assuming steady state profiles. The local effective diffusion coefficients have been corrected for porosity and temperature. The bottom water concentrations have been excluded from the calculations, since the modelled flux over the water-sediment interface and thus the total reaction rate is very sensitive to errors in the bottom water concentration and the porosity of the top layer.

The obtained rates of nitrate consumption and N_2 production were fitted to the linear model (equ. 4.8) by multiple linear regression, using the software SPSS. The fitted model was further employed to estimate the total nitrate production and N_2-production of the sediment within the study area. The estimates base on distribution maps of nitrate, oxygen and TOC established with this study's data and additional monitoring data of the same period collected by Federal Maritime and Hydrographic Agency (BSH), State Agency for Agriculture, Environment and Rural Areas of Schleswig-Holstein (LLUR) and Marine Environmental Data Base (MUDAB).

Collection of published data

The validity of the model described above was additionally tested by collecting published data on benthic nitrate consumption and N_2-production and fitting the linear model (equ. 4.7) to this data. Datasets were rejected if values of TOC, nitrate or oxygen were incomplete. If oxygen values were missing but salinity and temperature were given, oxygen concentration was assumed being air-saturated and calculated according Garcia & Gordon (1992). Results from slurry incubations were rejected due to conflicts with the assumed limited transport of nitrate from the bottom water toward the denitrification zone.

Tab. 4.2: Sources of published data. Abbreviations: AIT: acetylene inhibition technique, BC: benthic flux chamber, CFI: core flux incubation, IL: isotopic labeling, IPT: isotope pairing technique, PPM: pore-water profile modeling.

reference	method	study area
Capone et al. 1992	AIT	Great Barrier Reef
Deek et al. 2011	CFI, IPT	Wadden Sea
Deutsch et al. 2010	IPT	Baltic Sea
Devol 1991	BC	eastern North Pacific
Devol et al. 1997	BC	Arctic Ocean
Dong et al. 2000	IPT	Colne Estuary
Enoksson et al. 1990	AIT	Kattegat
Gihring et al. 2010a	BC, IPT	Gulf of Mexico
Gihring et al. 2010b	CFI, IPT	Arctic Ocean
Glud et al. 1998	IPT, PPM	Arctic Ocean
Jenkis & Kemp 1984	IL	Chesapeake Bay
Jensen et al. 1992	IPT	Wadden Sea
Kieskamp et al. 1991	AIT	Wadden Sea
Koop et al. 1990	CFI	Baltic Sea
Kristensen et al. 1998	IPT	Phuket Mangroves
Laursen & Seitzinger 2002	BC	Mid-Atlantic Bight
Lohse et al. 1993	AIT, CFI	southern North Sea
Lohse et al. 1996	AIT, IPT	southern North Sea
Nielsen & Glud 1996	BC, IPT	Kattegat
Patel et al. 2008	CFI	Ago Bay
Rysgaard-Petersen et al. 1998	CFI, IPT	Søbygaard Sø
Schröder et al. 1996 (*)	BC	Elbe Estuary
Seizinger et al. 1993	AIT, CFI, IPT	Vilhelmsborg Sø
Sundbäck et al. 2000	CFI, IPT	Kattegat
Stockenberg & Johnstone 1997	AIT	Baltic Sea
Tomaszek & Czerwieniec 2003	BC	Reservoirs
Trimmer et al. 2000 (**)	IPT	Thames Estuary
Vance-Harris & Ingall 2005	IL	Georgia shelf, Atlantic
van Raaphorst et al. 1990	CFI	North Sea
Wang et al. 2003	IPT	St. Lawrence Estuary
Zimmerman & Benner 1994	CFI	Galveston Bay

Additional water column data was retrieved from monitoring databases of ARGE Elbe (*) and Environment Agency, UK (**).

4.3 Results

Distribution of sediment TOC in the German Bight

The results of the sediment analyses reveal a marked linear correlation (R^2 = 0.84) between the TOC mass fraction and the mass fraction of fines < 63 µm grain size (Fig. 4.3). Further, a dataset of 9948 grain size analyses (MUDAB database) from Wadden Sea and North Sea sediments was used to map the distribution of fines (Fig. 4.4). This map is consistent with the sediment map developed by Figge (1981) and allows deduction of TOC distribution within the study area by using the correlation shown in figure 4.4.

The majority of sediments consist of well-sorted sand with low content of fines and TOC, which is the result of the constant deposition and re-suspension of the unconsolidated beds. The fines and thus the POC are concentrated in areas with reduced flow velocity, which permits the sedimentations of fine and light-weight particles with low sinking velocity. Such areas with elevated concentrations of fines and TOC are the shallow margins of the back-barrier tidal flats along the coast and the 'Helgoland mud area' with its depocenter at 54° 5'N, 8° 5'E (Hebbeln et al. 2003). This mud aggregation area is congruent with the eddy 'E1' (Fig 4.4, right panel), which was proposed by Hertwick (1983).

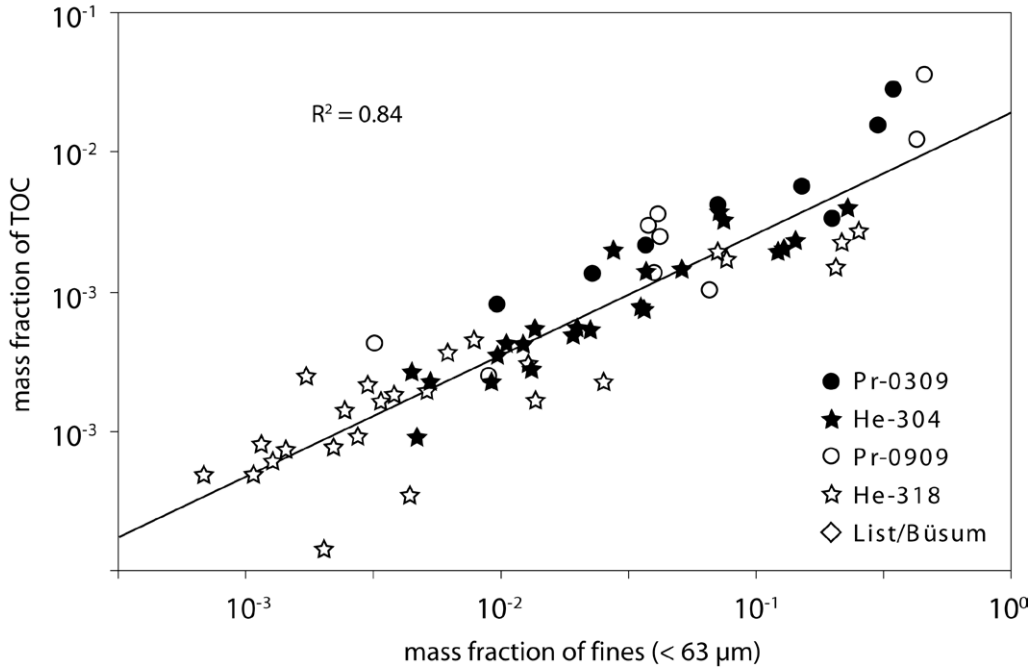

Fig. 4.3: Mass fractions of TOC and fines (< 63 µm) of dried sediment samples from the German Bight and North-Frisian Wadden Sea. Data from cruises Pr-0309, Pr-0909, He-304 and He-318.

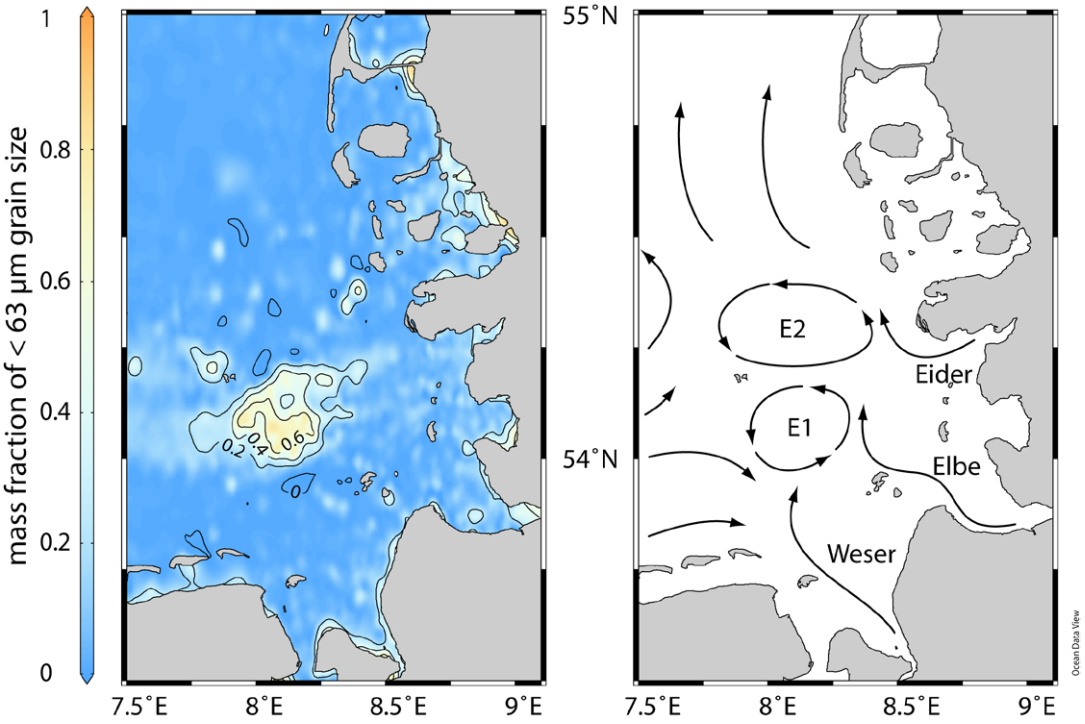

Fig. 4.4: Distribution of fines (< 63 µm) of dried sediment samples from the German Bight and North-Frisian Wadden Sea (left panel), data taken from MUDAB database. Directions of residual currents (right panel), drawn after Hertwick (1983).

Distribution of nitrate in the Elbe plume and North-Frisian Wadden Sea

The nutrient analyses of water column samples were used to map the distribution of nitrate in the study area. During the winter conditions (February, March), the nitrate distribution was clearly determined by the mixing of Elbe water with high nitrate concentration and North Sea water with low nitrate concentrations (Fig. 4.5, left panel). The nitrate concentration in the North-Frisian Wadden Sea was 30-50 µmol l^{-1}. During summer conditions (August, September), nitrate concentrations were lower and intensive nitrate consumption is detectable at salinities above 28 PSU (Fig. 4.5, arrow). The nitrate concentrations in the northern part of the North-Frisian Wadden Sea are below 5 µmol l^{-1} or even below detection limit (Fig. 4.6, right panel). The mouth of the small river Eider (54° 16'N, 8° 51'E, black asterisk) represents a distinctive nitrate source during winter, which is virtually absent during summer.

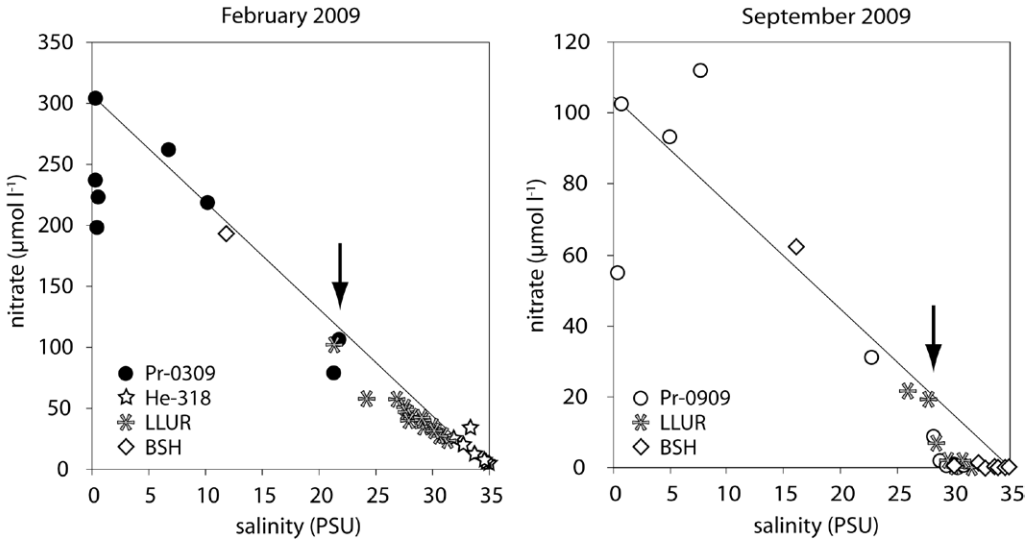

Fig. 4.5: Measured nitrate concentrations in the Elbe plume and adjacent North-Frisian Wadden Sea during winter 2009 (left panel) and summer 2009 (right panel). Data from cruises Pr-0309, Pr-0909, He-318 and from the monitoring programs of ‚Landesamt für Landwirtschaft, Umwelt und ländliche Räume Schleswig-Holstein' (LLUR) and ‚Bundesanstalt für Seeschifffahrt und Hydrographie' (BSH). The arrows indicate the transition from conservative mixing to consumption.

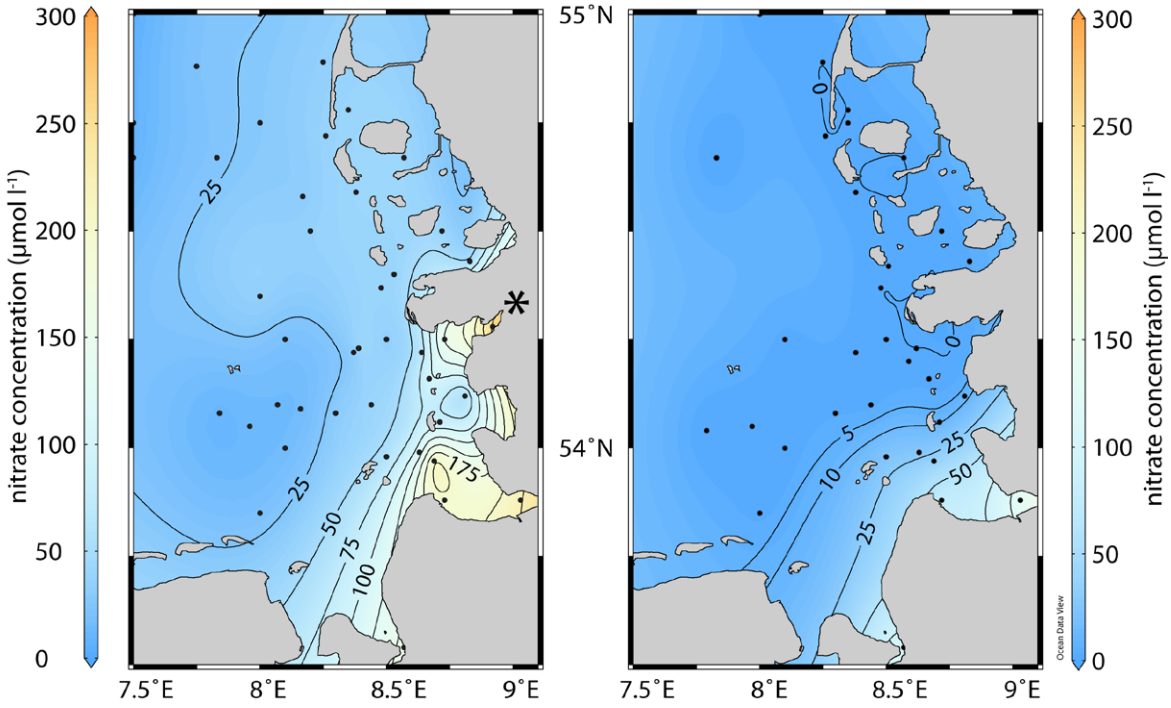

Fig. 4.6: Map of nitrate distribution in the Elbe plume and adjacent North-Frisian Wadden Sea during winter 2009 (left panel) and summer 2009 (right panel). Data from cruises Pr-0309, Pr-0909, He-318 and from the monitoring programs of ‚Landesamt für Landwirtschaft, Umwelt und ländliche Räume Schleswig-Holstein' (LLUR) and ‚Bundesanstalt für Seeschifffahrt und Hydrographie' (BSH).

Model fitting

The linear model (equ. 4.8) was fitted to the established rates of diffusive nitrate utilization and N_2 release using multiple linear regression. This study's data of observed diffusive nitrogen uptake was used for fitting model 'DNU1', collected published data of nitrate consumption (tab. 4.2) was used for model 'DNU2'. Likewise, this study's data on N_2 production were used for model 'DNR3' and the collection of published data for model 'DNR4', respectively. The resulting fitting parameters are summarized in table 4.3. In figure 4.7, estimates based on the fitted models are plotted against measured rates of nitrate consumption.

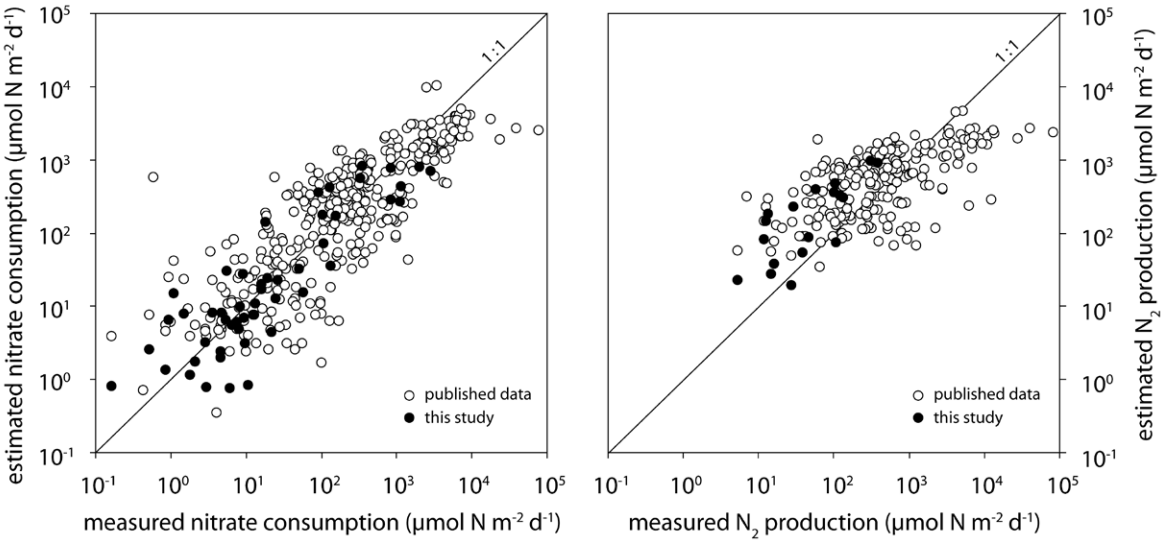

Fig. 4.7: Estimates of bentic nitrate consumption and N_2 production vs. measured rates of this study (full circles) and published data (open circles). The diagonal line indicate 1:1 agreement.

Tab. 4.3: Summarized fitting parameters (b, b_{nit} , b_{TOC}, b_{oxy}) and probability values (p) of multiple-regression fitting of equation 4.7 to observed rates of nitrate consumption and N_2 production. Data sources: this study and published data listed in table 4.2.

model	coefficients								data
	b_{nit}	p	b_{TOC}	p	b_{oxy}	p	b	p	source
DNU 1	1.027	< 0.01	0.307	< 0.01	-0.264	0.08	1.154	< 0.01	this study
DNU 2	0.832	< 0.01	0.418	< 0.01	-0.091	0.42	1.397	< 0.01	published
DNR 3	0.445	< 0.01	0.252	< 0.01	0.010	0.94	2.023	< 0.01	this study
DNR 4	0.426	< 0.01	0.181	< 0.01	-0.114	0.35	2.504	< 0.01	published

The bottom water nitrate concentration appeared as most important factor in all four models, followed by the sediment TOC content. The impact of bottom water oxygen

concentration had the expected tendency, but was not statistically significant in any model. Excluding datasets with calculated oxygen concentrations assuming air saturation (see methods, data collection) did not improve the model fit. The residuals of all four models did not correlate with temperature.

Based on the four fitted models, all datasets could be plotted against a simplified scale based on nitrate concentration and TOC content (Fig. 4.8).

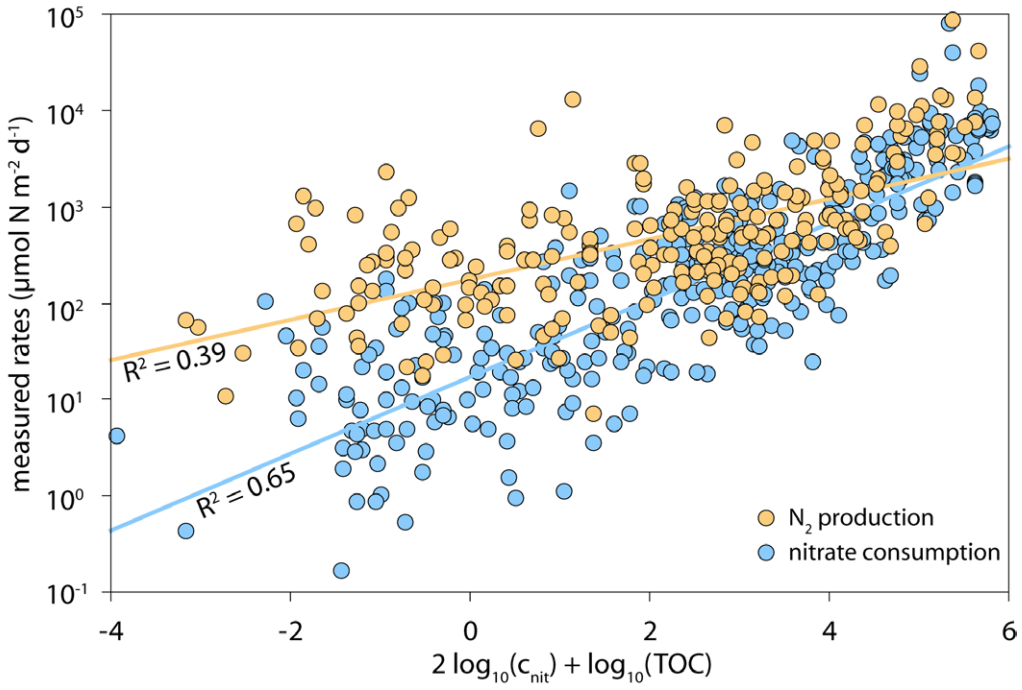

Fig. 4.8: Measured rates of nitrate consumption and N_2 production vs. a model-derieved scale. Data from this study‘s measurements and published results (Tab. 4.2).

Estimated denitrification in German Bight sediments

The distribution maps of nitrate, oxygen and TOC were merged to estimate the nitrate consumption and N_2 production employing the four fitted models (Tab. 4.3). The results are illustrated in figures 4.9 & 4.10 and summarized in table 4.4. Water column nitrate fuelled consumption of 1.34 to 1.69 x 10^5 mol N d^{-1} in march and 0.62 to 0.82 x 10^5 mol N d^{-1} in September, respectively. Compared to the daily nitrate load of river Elbe of 234 x 10^5 mol N d^{-1} (ARGE Elbe) during March, sediments of the study area consumed approximately 1 % of the Elbe nitrate load. In late summer during September, the Elbe nitrate load substantially

decreased to 31 x 10^5 mol N d^{-1} (ARGE Elbe), and the studied sediment consumed 0.62 to 0.82 x 10^5 mol N d^{-1} or 2 to 3 % of the Elbe nitrate load. The observed N_2 production rates were generally higher than nitrate consumption. The benthic N_2 production eliminated 10.1 to 22.3 x 10^5 mol N d^{-1} of reactive nitrogen during March and 6.0 to 13.3 x 10^5 mol N d^{-1} during September, respectively. These rates equal 3 to 7 % of the Elbe nitrate load in March and 19 to 43 % in September.

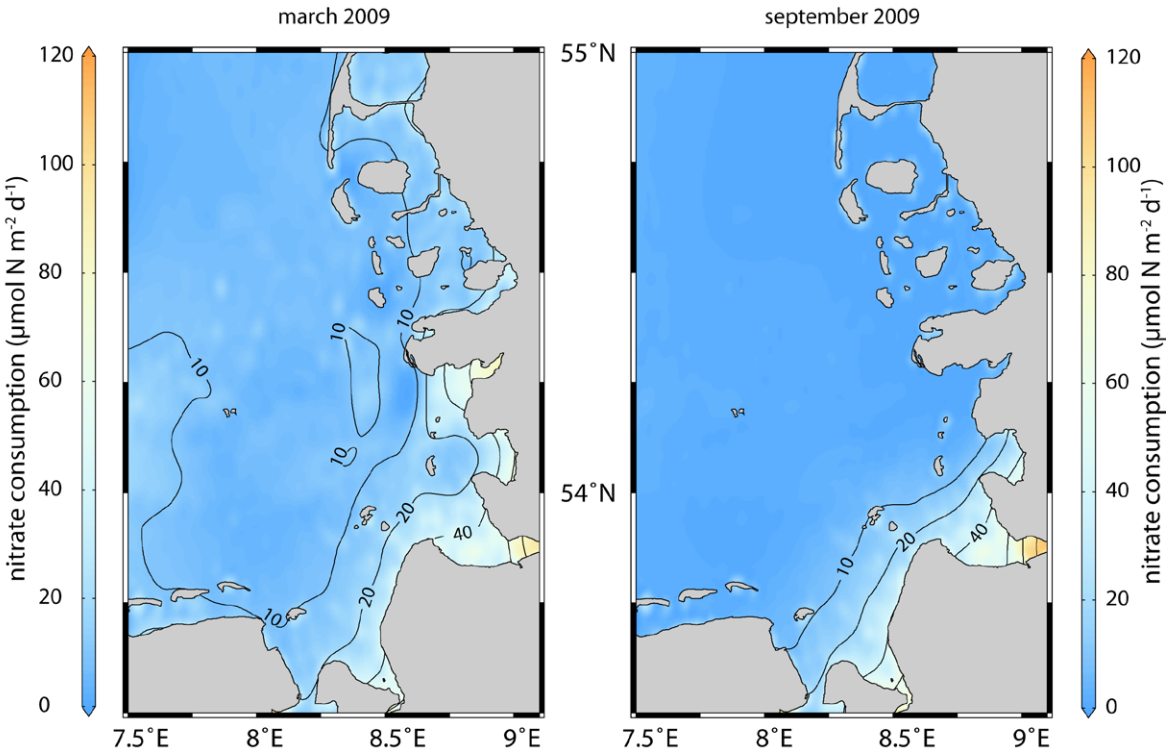

Fig. 4.9: Map of estimated diffusive nitrate uptake based on this study‘s data and model DNU 1 (Tab. 4.3).

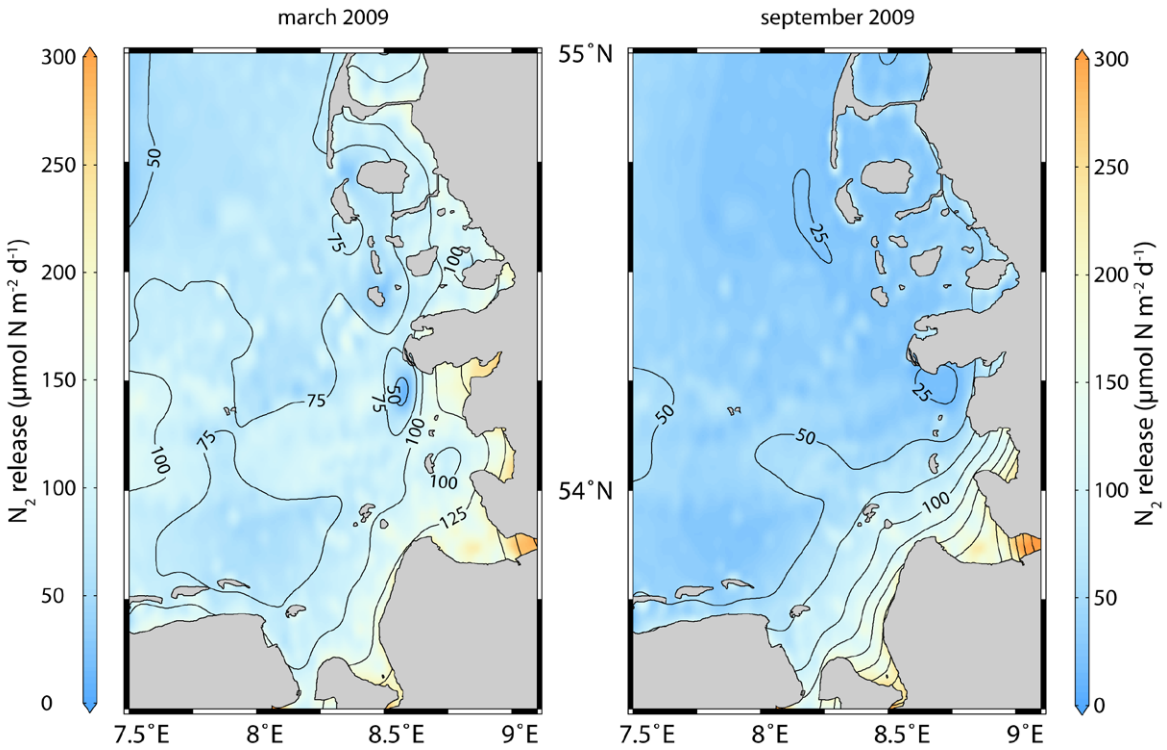

Fig. 4.10: Map of estimated diffusive N_2 release based on this study's data and model DNR 3 (Tab. 4.3).

Tab 4.4: Summarized estimates of benthic nitrate consumption and N_2 production based on this study's data and published results.

month	model	area	mean rate (µmol N m^{-2} d^{-1})	total turnover (10^5 mol N d^{-1})	fraction of Elbe nitrate load
March	DNU 1	whole study area	12	1.3	< 0.01
	DNU 1	Wadden Sea	26	0.9	< 0.01
	DNU 2	whole study area	15	1.7	0.01
	DNU 2	Wadden Sea	22	0.7	< 0.01
	DNR 3	whole study area	87	10.1	0.03
	DNR 3	Wadden Sea	121	3.9	0.01
	DNR 4	whole study area	191	22.3	0.07
	DNR 4	Wadden Sea	255	8.3	0.03
September	DNU 1	whole study area	5	0.6	0.02
	DNU 1	Wadden Sea	14	0.5	0.01
	DNU 2	whole study area	7	0.8	0.03
	DNU 2	Wadden Sea	16	0.5	0.02
	DNR 3	whole study area	51	6.0	0.19
	DNR 3	Wadden Sea	80	2.6	0.08
	DNR 4	whole study area	114	13.3	0.43
	DNR 4	Wadden Sea	170	5.5	0.18

4.4 Discussion

Factors controlling benthic N-turnover

Nitrate appeared as dominant factor of benthic nitrate consumption in the German Bight (tab. 4.3, b_{nit} values), which is in agreement with results of Lohse et al. (1993) and Deek et al. (2011). The sediment TOC content was identified as second most important factor, which was also suggested by Deek et al. (2011). According to the model derivation, nitrate consumption was expected being inversely correlated with oxygen concentration. The model fit yielded this inverse correlation, though the result using this study's data is significant only on the 10 % level and is not significant in the collection of published results. The poor correlation of oxygen concentration and measured nitrate consumption may be accounted to the fact that such measurements often involve confined incubations, which are prone to altered flow conditions and insufficient oxygen supply and hence overestimated results. Surprisingly, temperature had no evident impact on nitrate consumption, which supports the results of Deek et al. (2011) but contrasts results of e.g. Gihring et al. (2010a) or Veraat et al. (2011). It is conceivable that the dominance of factors such as nitrate or TOC disguise the effect of temperature. However, Veraat et al. (2011) concluded that temperature affects nitrate consumption via altered oxygen dynamic, and as shown above, the impact of oxygen itself is poorly reflected by the obtained nitrate consumption measurements. Hence, the applied methods may be inappropriate to observe the effect of temperature.

Analogously to nitrate consumption rates, equation 4.7 was fitted to observed N_2 production rates and yielded similar models. The impact of water column nitrate on N_2 production was substantially lower than on nitrate consumption, suggesting that denitrification of water column nitrate was not the sole source of N_2. Instead, N_2 production systematically exceeds nitrate consumption in sediments under low nitrate/TOC conditions (Fig. 4.8) by one order of magnitude. This cannot be explained simply with anammox because the resulting N_2 production exceeds nitrate consumption only twofold (Kartal et al. 2007). The best explanation of the N_2 excess is coupled nitrification-denitrification, which oxidizes ammonium produced during degradation of organic matter and subsequent denitrification of this internally produced nitrate. Low TOC content permits deep oxygen penetration and concomitantly substantial ammonium nitrification. N_2 produced by subsequent denitrification can easily exceed N_2 produced by denitrification of water column nitrate al low concentration (Fig 4.8). Analogously, high TOC contents result in low oxygen penetration and thus low nitrification intensity. Denitrification based on this low nitrification intensity is less significant than denitrification fuelled directly by bottom water nitrate.

The fate of Elbe nitrogen load

Denitrification directly fuelled by water column nitrate is intimately linked with nitrate concentration. Consequently, nitrate consumption is restricted to the estuaries in late summer (September) and expands farther toward open North Sea during late winter (March). The fraction of the Elbe nitrate load that was eliminated by direct denitrification was generally below 4 % in all estimates, and this low efficiency corresponds with the observed conservative mixing of riverine nitrate (Fig. 4.5) and agrees with the conclusions of Dähnke et al. (2008). Despite low nitrate consumption rates, observed rates of N_2 production were one order of magnitude higher than the nitrate consumption rates.

This high apparent excess of N_2 production can be attributed to coupled nitrification-denitrification within the sediment. The collection of published data further suggests that this is common in low TOC sediments exposed to low nitrate bottom water. However, the source of the ammonium to be nitrified in low-TOC low-nitrate sediment is decomposition of organic matter and hence ultimately primary production. Joint & Pomroy (1993) observed high rates of primary production in the German Bight throughout the year, and established rates of approximately 300 mg C m^{-2} d^{-1} in February and 1,200 mg C m^{-2} d^{-1} in September. Applying the Redfield ratio of C : N = 6.6 : 1, the depth-integrated nitrogen assimilation rates are 3.8 mmol N m^{-2} d^{-1} in February and 15 mmol N m^{-2} d^{-1} in September, respectively. These rates of nitrate assimilation are sufficient to provide the observed rates of coupled nitrification-denitrification upon decomposition of this primary production in the sediment. Supporting this conclusion, Sundbäck & Miles (2000) reported that microbial nitrate assimilation is the dominant nitrate sink in shallow bays of Kattegat and Skagerrak. These results further support the approach of Seitzinger & Giblin (1996), which links benthic denitrification with primary production.

This study's estimates base on diffusion as sole transport process, though this is the least efficient one. Hence, the estimates presented here represent a baseline, and phenomena such as bioirrigation and pore-water advection potentially enhance the solute transport from the bottom water into the sediment interstices and fuelling higher rates of nitrification and denitrification. The marked scatter of denitrification and N_2 production observed under similar conditions may be attributed to different intensities of bioirrigation and pore-water advection. However, it's a misconception that high filtration rates generally result in high denitrification rates. The results of Cardenas et al. (2008) suggest instead that increasing filtration enhances denitrification until it approaches a maximum at moderate filtration rates. If filtration increases beyond this point, denitrification decreases substantially whereas

oxygen consumption continuously increases (Fig 4.11). The initial increase in denitrification expresses loosened limitation by the intensified downward transport of nitrate. Low denitrification rates at intensive filtration are result of high oxygen concentrations within the percolated sediment volume, and nitrate passes partly unaffected through the sediment. This suppressive effect of intensive percolation on denitrification is further enhanced by the migration of bedforms, which reduces the residence time of pore-water (Elliott & Brooks 1997) and creates a 'redox seal' that efficiently suppresses denitrification (Precht et al. 2004). First observations of the hydrodynamic conditions in Wadden Sea reported an average significant wave height of 24 ± 14 cm (Hörnum station, COSYNA database, HZG Geesthacht) and tidal flow velocities in the range of 20-80 cm s^{-1} (Albers & von Lieberman 2007). The combined hydrodynamic forces of wave action and tide substantially exceed flume conditions of the study of Precht & Huettel (2003), which yielded filtration rates up to 590 l m^{-2} d^{-1} in similar sediment. The even higher hydrodynamic forces in the Wadden Sea may result in very high filtration rates as the results of de Beer et al. (2005) suggest, which would imply very low nitrate consumption (Fig. 4.11).

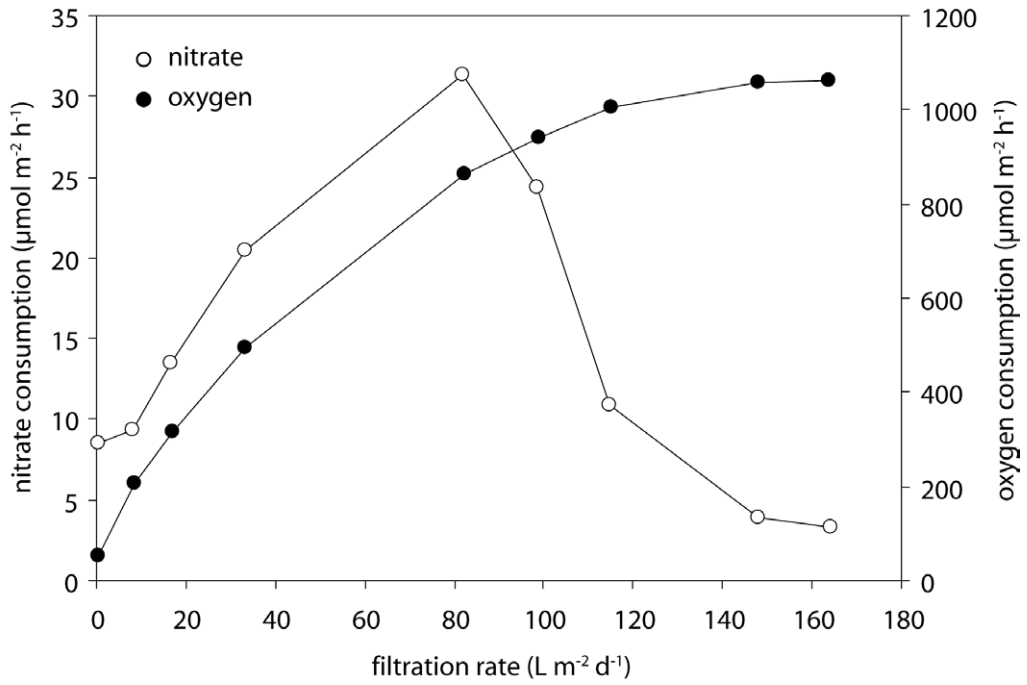

Fig. 4.11: Effect of sediment filtration rate on oxygen and nitrate consumption. Drawn after Cardenas et al. (2008).

The role of the Wadden Sea

A secondary motivation for the present study was to elucidate the role of the sheltered Wadden Sea sediment. The majority of this sediment is permeable sand and thus potentially enables pore water advection. As described above, it is an important characteristic of intensive filtration that percolating pore-water may re-emerge too soon for complete nitrate consumption. Viewed in this light, incubations with strictly downward percolation (de Beer et al. 2005, Gihring et al. 2010a) appear prone to overestimate nitrate consumption rates because this percolation mode does not permit nitrate escaping from the sediment. Hence, the results of Gihring et al. (2010a) and Gao et al. (2010) should be considered cautiously for the estimation of nitrate consumption. The study of Deek et al. (2011) examined Wadden Sea sediment with flow-through incubations of whole sediment cores and the obtained denitrification rates were systematically higher than the results of the present study. The incubation of a comparatively large sediment surface potentially permitted activity of pumping macrozoobenthos and may account for the increased denitrification rates. But the sediment oxygen demand during incubations was very high with respect to the oxygen resupply rate by water exchange, which led to decreased oxygen concentration in the core supernatant (Ankele 2010) and probably to overestimated denitrification rates.

Despite uncertain results caused by employment of imperfect methods, it becomes apparent that the rates of nitrate consumption and N_2 production are significantly higher in the Wadden Sea than in sediment of the open North Sea (Tab 4.4). The Wadden Sea comprises one fourth of the studied area but accounts for approximately half of the N-turnover. This study's results suggest that the dominance of Wadden Sea sediment is caused by higher TOC content and higher nitrate concentrations in the vicinity of estuaries. The promoting effects of TOC and nitrate on nitrate consumption are most probably also present in permeable sediment, because TOC and mineral fines settle preferable at the shallow, sheltered margins of the Wadden Sea (4.4), and both fractions reduce the sediment permeability by clogging the pore throats. Reduced permeability results in lower filtration rates and longer residence time of pore-water. Hence, TOC and fines oppose the impact of high flow velocity and bedform migration and thus may locally hamper the formation of a 'redox seal' (Precht et al. 2004) resulting in higher nitrate consumption rates.

A lost nitrate sink

The presence of oxygen generally suppresses denitrification. This may result in virtually complete suppression of denitrification in permeable sediment intensively percolated with high oxygen bottom water. In these cases, most of the nitrate entering the sediment is passing through unaffected. Ammonification may even contribute additional nitrate and turn intensively percolated sediment into a nitrate source.

If the bottom water entering the sediment is low in oxygen, then denitrification commences soon and nitrate is consumed along the majority of flow paths, resulting in efficient nitrate removal. In such cases, intensively percolated sediment is a far more efficient nitrate sink than well-oxygenated permeable sediment or diffusion controlled cohesive mud. Recent results of Johnson et al. (2011) employing the eddy-correlation technique indicate substantial nitrate removal in permeable sediment at reduced oxygen concentration in the water column (100 µmol l^{-1}), which indeed exceeded nitrate consumption of cohesive sediment. This promoting effect of low oxygen bottom water on nitrate consumption helps to explain the high denitrification rates observed in the Elbe estuary in the 1980s by Schroeder et al. (1996). In the 1980s, the river Elbe had high nitrate concentrations, low oxygen concentrations, and the bottom water frequently became anoxic. (ARGE 2007, Amann et al. 2012). Consequently, the Elbe estuary was a significant nitrate sink in this period (Dähnke et al. 2008). Successful implementation of water protection policies improved the oxygen supply and events of oxygen depletion became rare during the last decade (ARGE 2007). Apparently, the Elbe estuary concomitantly lost a significant nitrate sink, and now appears nonreactive in recent studies with respect to nitrate (Dähnke et al. 2008, this study Fig. 4.5). Results of this study and Deek et al. (2011) suggest that cohesive sediment is now the major benthic nitrate sink. However, intensive hydraulic engineering substantially reduced the extent of shallow, muddy marsh sediment as discussed in Dähnke et al. (2008).

4.5 Conclusions

The present study derived a simple prediction model for benthic nitrate consumption and N_2 release based on diffusive fluxes, which was successfully fitted to a set of own measurements of German Bight sediment and a collection of published data, respectively. The statistics suggest that benthic N-elimination is mainly driven by water column nitrate concentration and sediment TOC content, whereas the expected impact of oxygen and temperature was not evident.

The fitted prediction model in conjunction with distribution maps of nitrate, TOC and oxygen were subsequently employed for estimates of the total nitrate removal and N_2 production of German Bight sediment. The estimated nitrate consumption constantly removed 1-3 % of the Elbe nitrate discharge. Benthic N_2 production was found fuelled up to 90 % by coupled nitrification-denitrification, and eliminated 3-7 % of the Elbe nitrate discharge during late winter and 19-43 % during late summer, respectively.

5. Benthic remineralisation rates of the shelf and slope sediments off Nambia.

Abstract

The Benguela Upwelling System off Namibia (Southern Africa) is among the most productive marine ecosystems, and the primary production is mainly fuelled by the upwelling of nutrient-rich deep-water. Deposition of organic matter from the surface water onto the broad continental shelf enable intensive interaction between bottom water and sediment, which gradually modifies the upwelling water by consumption of oxygen and nitrate, and by release of ammonium and phosphate. As a potential consequence, primary production and benthic remineralisation are mutually modulated. This study aimed to investigate this interplay at 36 stations along the Namibian coast, comprising stations with 30 – 3,000 m water depth. Profiles of nutrients were established by sampling the pore-water. Profiles of oxygen and N_2 were measured with microoptodes and membrane inlet mass spectrometry with needle-type membrane inlet, respectively. The results show that the efflux of phosphate and ammonium from the sediment was exponentially increasing with increasing temperature. High oxygen concentrations (> 250 µmol l^{-1}) restricted the efflux of ammonium by nitrification at high water depths, and low oxygen concentrations led to excessive phosphate mobilisation at low water depths. Denitrification fuelled by water column nitrate was generally found nitrate limited and was most intensive where nitrate-rich SACW reached the sediment. The production of N_2 was mainly a result of coupled nitrification-denitrification and was found correlating well with the total oxygen flux into the sediment. As a consequence, the water column N:P ratio is reduced by denitrification at oxygen concentrations above 50 µmol l^{-1}. Additional mobilisation of sediment-bound phosphate at oxygen concentrations below 50 µmol l^{-1} is further reducing the N:P ratio of the upwelling bottom water.

5.1 Introduction

The Benguela Current, unlike other eastern boundary currents, flows over a broad continental shelf. The 100 m isobath is about 50 km offshore at 23 °S, which enables intensive interplay of sediment and bottom water. The Benguela Current is the dominant surface current along the Namibian coast and represents the eastern part of the South Atlantic subtropical gyre (Peterson & Stramma 1991). It starts as equatorward current off Cape of Good Hope and follows the South African coast. It receives water masses mainly from the cold South Atlantic Current, but also from the warm Agulhas Current. This relatively fresh and oxygenated water is named Eastern South Atlantic Central Water (ESACW) (Mohrholz et al. 2001). At around 27 °S, the Benguela Current broadens and most of the current bends westward to become part of the South Equatorial Current. One branch continues following the coast northwards until it joins the Angola Current at the Angola-Benguela Frontal Zone (ABFZ) at around 17 °S, and both currents are deflected westward to form the southern limb of the Angola Gyre (Stramma & England 1999).

Compared to ESACW water, Angola Current water is characterised by low oxygen concentration and higher nutrient concentrations as well as higher temperature and salinity, respectively. This water mass is South Atlantic Central Water (SACW) (Poole & Tomczak 1999, Mohrholz et al. 2001). It has a slightly higher density than the Benguela ESACW, and a branch of the Angola Gyre is injected under the lighter ESACW into the Benguela system. This water is flowing southwards along the shelf edge as poleward undercurrent as south as 27 °S, where it is deflected westwards (Stramma & England 1999). Both water masses, SACW and ESACW, mix with each other during their way over the shelf, and the local concentrations of oxygen and nutrients depend on the mixing ratio of SACW and ESACW (Mohrholz 2008).

The hydrodynamic setting is perturbed by wind-driven coastal upwelling. Easterly trade winds blow parallel to the coast and displace the surface water westward by Ekman transport (Ekman 1905, Mohrholz et al. 2008). As a consequence, the deeper return flow transports water coastward onto the shelf and into the upper water column, which has a reduced oxygen concentration and increased nutrient concentrations. If bottom water modified by processes at the sediment-water interface contributes to the upwelling water, recycled nutrients reach the upper water column and fuel intensive primary production in the magnitude of up to 600 mg C m^{-3} d^{-1} (Silió-Calzada et al. 2008). This intensive production is the basis of dense populations of grazing animals and their predators. But despite grazing, vast quantities of the primary production are deposited onto the broad continental shelf, where organic matter accumulates as mud belts (Inthorn et al. 2006).

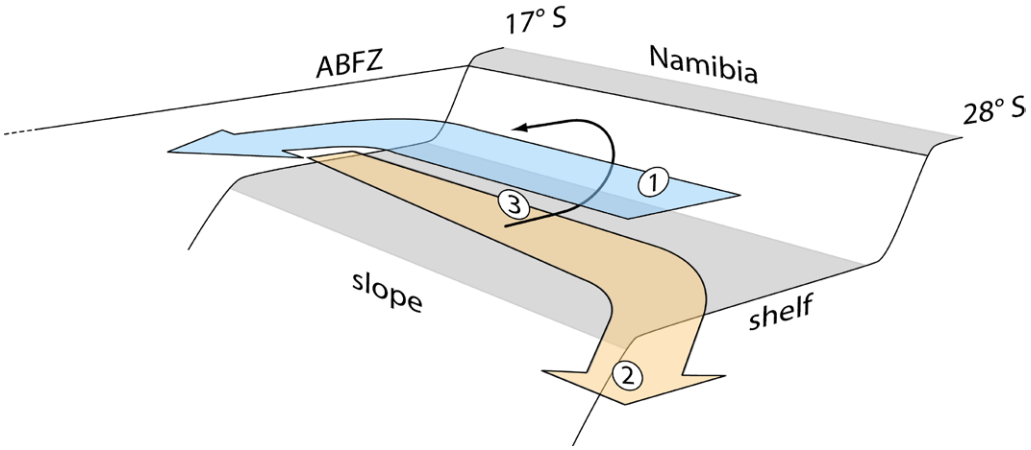

Fig. 5.1: Conceptual illustration of the interaction of ESACW and SACW via coastal upwelling. The coastal branch of the Benguela Current (1) with ESACW is flowing northward along on the Namibian coast and is deflected westward at the Angola-Benguela Frontal Zone (ABFZ). The poleward undercurrent (2) transports SACW southward and is deflected westward at approximately 27° S. Wind-driven coastal upwelling (3) displaces the ESACW at the surface and SACW flows towards the coast. Figure based on Petersen & Stramma (1991) and Brange & Pillar (1992).

The inner mud belt accumulates in relatively shallow water in depths between 100 – 200 m. Processes at the sediment-water interface imprint characteristic changes of nutrient ratios, which may reach into the surface water via coastal upwelling, where quantity and ratio of nutrients control growth of primary producers (Dutkiewicz et al. 2012). Specifically, oxygen depletion causes intensive elimination of reactive nitrogen (Lavik et al. 2005), which reduces the N : P ratio of dissolved nutrients, whereas phosphate sequestration increases the N : P ratio (Goldhammer et al. 2010). Further, the inner mud belt of the Namibian shelf is seasonally exposed to relatively warm bottom water (SACW), which permits intensive microbial activity and results in high rates of nutrient turnover. A frequent consequence of high remineralisation rates is the successive consumption of available electron acceptors and thus the depletion of oxygen, nitrate and sulphate, accompanied by accumulation of reaction products such as carbon dioxide, dinitrogen, hydrogen sulphide and methane in surface sediment and bottom water. If the concentrations of gaseous products exceed solubility, then ebullition forms bubbles within the sediment. Occasionally, such gas accumulations erupt into the water column and may cause mass extinctions if the erupting gas contains hydrogen sulphide (Emeis et al. 2004).

A better understanding of the processes at the sediment-water interface and their impact on the Benguela ecosystem is of significant economical interest because the Benguela provides enormous stocks of exploited fish species such as sardines and hake. However, populations of economically exploited species collapsed during the

last decades and the causes are not well understood (Sumaila & Stephanus 2006, Bundy et al. 2009). The anticipated climate change is believed to affect the meteorological forcing of upwelling (Harley et al. 2006). This study aims to improve insight into the interplay of water column and surface sediment, and may ultimately contribute to sustainable management of the natural resources of the Benguela Current System.

5.2 Material and Methods

Study site and sampling

The samples were retrieved during the cruise MSM 17/3 of the RV Maria S. Merian along the Namibian continental shelf in February 2011, which is the season with low upwelling intensity (Shannon 1985) and low primary production rates (Silió-Calzada et al. 2008). The working area comprised continental shelf and slope between Lüderitz (26°40'S) and the Kunene mouth (17°15'S). The sampled stations are depicted in figure 5.2 and their positions are tabulated in table 7.2 in the annex section.

Undisturbed sediment cores were retrieved with a multicorer (Oktopus Kiel) equipped with acrylic tubes (PMMA) with an inner diameter of 10 cm and a length of 60 cm. Concentration profiles of dissolved gases across the water-sediment interface were measured on board directly after the retrieval of the sediments cores. Pore water was sampled with rhizon core solution samplers (Rhizosphere Research) using core liners prepared with sealed sampling ports. The rhizon samplers were conditioned in deionized water and connected to sterile, disposable syringes. The first few hundred microliters of the sampled pore water were discarded for flushing and removing any air bubbles. Pore water aliquots for nutrients analysis and ^{15}N measurements of the DIN were transferred to evacuated Exetainers (Labco) and stored at -20°C. Additional cores were sliced in 1 cm intervals and stored at -20°C for CHN analysis and measurement of water content and grain size distribution.

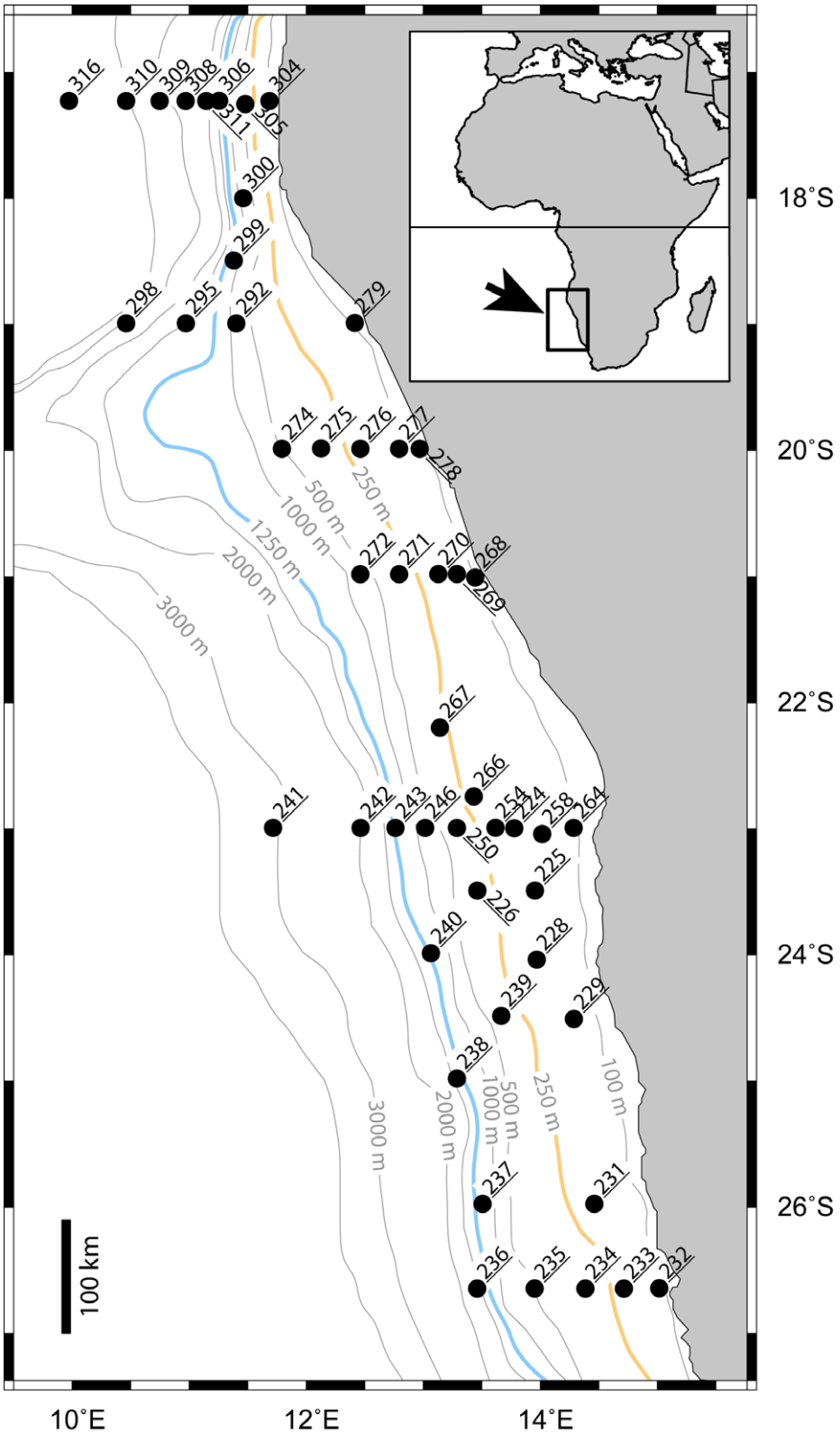

Fig. 5.2: Sampled stations during the cruise MSM 17/3 of the RV Maria S. Merian along the continental shelf and slope off the Namibian coast. The line with orange hue indicates transition between shelf and upper slope at the 250 m isobath, the line with blue hue indicates transition between upper slope and lower slope at 1250 m, respectively. Insert shows the working area (arrow) at the coast of southern Africa.

Sediment characteristics

The frozen sediment slices were freeze-dried, and the resulting weight loss was used to calculate the water content. The volumetric porosity was calculated then from the water content, assuming a mean grain density of 2.65 g cm^{-3}. A subsample of the dry residues was used to determine the concentrations of total nitrogen and organic carbon with an Elemental Analyzer (Carlo Erba NA 1500) calibrated against acetanilide.

Measurement of dissolved gases

The oxygen concentration profiles were measured within minutes after the retrieval of the sediment cores. Multiple profiles across the sediment-water interface were measured with an autonomous micromanipulator (Pyro Science) and needle-type microoptodes (Presens, Oxy50) connected to a Microx TX3 (Presens). The supernatant was then adjusted to 10 cm height prior to the profiling. The sensor was calibrated for each profile individually to account for the constant abrasion of the sensor tip. The sensor readings in the anoxic sediment (0 % oxygen saturation) and in air-equilibrated standard (100 % oxygen saturation) were used for a two-point calibration. Concentration profiles of dissolved N_2 and Ar were measured simultaneously with a quadrupole mass spectrometer (InProcess Instruments, GAM 200) equipped with a needle-type membrane inlet and a second micromanipulator (Pyro Science). Argon was measured as m/z 40 and used according to Kana et al. (1994) as reference for N_2 (m/z 28). The concentrations of Ar and N_2 were calibrated with a three-point calibration with air-equilibrated temperature-salinity standards (Kana et al. 1994). Both setups were placed in temperature controlled laboratories to prevent instabilities and biased reaction rates within the sediment cores due to warming.

Isotope Pairing Incubations

Rates of nitrate consumption were additionally determined with the Isotope Pairing Technique (Nielsen 1992, Risgaard-Petersen et al. 2003). Using acrylic push cores with 3.5 cm diameter, undisturbed subsamples were taken directly from the retrieved multicores. The subcores were distributed to four groups with different tracer concentrations and at least three parallels. It was ensured that the parallel subcores were sampled from different multicores to reduce the probability of biased results caused by heterogenity among the multicores. Subcores were amended with $Na^{15}NO_3$ in the final concentrations 0 / 70 / 140 / 210 µmol l^{-1}, and closed with rubber stoppers. During the incubation, the subcores were stored in darkness and in-situ temperature. Externally driven, oscillating paddles were used to stirr the water

column during the incubation. After approximately 12 h incubation, the subcores were homogenized to slurries. Samples were transfered to gastight Exetainers (Labco), and were fixed with saturated $ZnCl_2$ solution. The concentrations of $^{28}N_2$, $^{29}N_2$, and $^{30}N_2$ were determined as m/z 28, m/z 29, and m/z 30 with a GAM-200 QMS (InProcess Instruments) equipped with a flow-through membrane inlet (manufactured at Helmholtz Zentrum Geesthacht). The isotopic ratios were calibrated against atmospheric N_2 by measuring air-equilibrated thermo-saline standards.

Pore water nutrient analysis

The pore water samples were kept frozen in septum capped Exetainers (Labco). After fast thawing in an water bath at room temperature, the samples were acidified with 6 M hydrochloric acid (1 % v/v final concentration) to stabilize any gaseous ammonia as ammonium. Aliquots were then taken with syringes through the septum and analyzed with a nutrient autoanalyzer (AA3, Seal Analytical) with methods according to Grasshoff et al. (1983).

Calculations

Reaction rates and diffusive fluxes across the sediment-water interface were calculated on the basis of Fick's 1st law (Fick 1855), employing the algorithm of Berg et al. (1998) to concentration profiles. The local effective diffusion coefficients have been corrected for porosity and temperature. The bottom water concentrations have been excluded from the calculations, since the modelled flux over the water-sediment interface and thus the total reaction rate is very sensitive to errors in the bottom water concentration and the porosity of the top layer. Isosurface maps were generated with the software Ocean Data View (Schlitzer 2011). Results were analysed with the software SPSS. For correlation analysis, Spearman's correlation of rank-transformed values was preferred to Pearson's correlation of untransformed values because Spearman's correlation is not presupposing linearity and is less sensitive to outliers (Gideon & Hollister 1987). The Spearman correlation coefficent r_s is analogous to Pearson's correlation coefficient R^2.

Measured bottom water nutrient concentrations were compared with hypothetical concentrations, which base on the assumption that apparent oxygen utilization (AOU) is a valid proxy of remineralization. Hypothetical bottom water concentrations of phosphate, ammonium and nitrate were estimated on the basis of the ratios O_2 : N : P = 172 : 17 : 1 established by Takahashi et al. (1985). The O_2 : N : P ratio of Takahashi et al. (1985) was preferred to Redfield's ratio (Redfield et al. 1963) because the oxygen value in the 'Redfield Ratio' was computed and not observed (Takahashi et al. 1985). Phosphate concentration was estimated assuming that

1 mol O_2 is consumed for the remineralisation of 1 mol organic carbon, which further releases phosphate in the ratio P : O_2 = 1 : 172.

(5.1) $$c = c_0 + \left(\frac{1}{172} \times AOU \right)$$

c: expected phosphate concentration
c_0: initial phosphate concentration
AOU: apparent oxygen utilisation

Likewise, the expected ammonium and nitrate concentrations were estimated with equations 5.2 and 5.3. Equation 5.2 assumes the case that all nitrogen is released as ammonium and excludes nitrification. Equation 5.3 assumes complete nitrification subsequently to ammonification, and includes additional 1.5 mol O_2 for nitrification of the initially produced ammonium.

(5.2) $$c = c_0 + \left(\frac{17}{172} \times AOU \right)$$

c: expected ammonium concentration
c_0: initial ammonium concentration
AOU: apparent oxygen utilisation

(5.3) $$c = c_0 + \left(\frac{17 \times AOU}{172 + 17 \times 1.5} \right)$$

c: expected nitrate concentration
c_0: initial nitrate concentration
AOU: apparent oxygen utilisation

The apparent nitrogen deficit N* was calculated employing the ratio N : P = 16 (Deutsch et al. 2001, Tyrell & Lucas 2002) with equation 5.4, and additionally based on AOU with equation 5.5, respectively. Positive N* indicate loss of reactive nitrogen.

(5.4) $$N^* = \left(16 \times c_{pho}\right) - c_{DIN}$$

N*: apparent nitrogen deficit
c_{pho}: phosphate concentration
c_{DIN}: dissolved inorganic nitrogen concentration

(5.5) $$N^* = c_0 + \left(\frac{17}{172} \times AOU \right) - c_{DIN}$$

N*: apparent nitrogen deficit
c_0: initial DIN concentration
c_{DIN}: DIN concentration

5.3 Results

Definitions of bottom water types

Salinity and temperature of bottom water samples (Mohrholz, in preparation) were used to identify the origin of the bottom water. Antarctic Intermediate Water (AAIW) was identified according to Stramma & England (1999) at T-S Point 4.6 °C, 34.3 PSU (Fig. 5.3). North Atlantic Deep Water (NADW) was assigned to the T-S point 3.9 °C, 34.9 PSU. Likewise, the South Atlantic Central Water (SACW) was identified along the T-S curve between 4.5 °C, 34.3 PSU and 20 °C, 36 PSU (Poole & Tomczak 1999, Mohrholz et al. 2008). NADW-type bottom water had the highest oxygen concentration of up to 250 µmol l^{-1} and nitrate concentrations as low as 20 µmol l^{-1}. AAIW-type bottom water had the highest observed nitrate concentrations of up to 87 µmol l^{-1} (station 234) and average oxygen concentrations of 100 µmol l^{-1}. SACW-type bottom water had the lowest oxygen concentrations as low as 0 µmol l^{-1} and nitrate concentrations as low as 10 µmol l^{-1}. The highest bottom water temperature of 18 °C was observed at the shallow station 268 (23 m), where modified surface water (SW) reached the bottom.

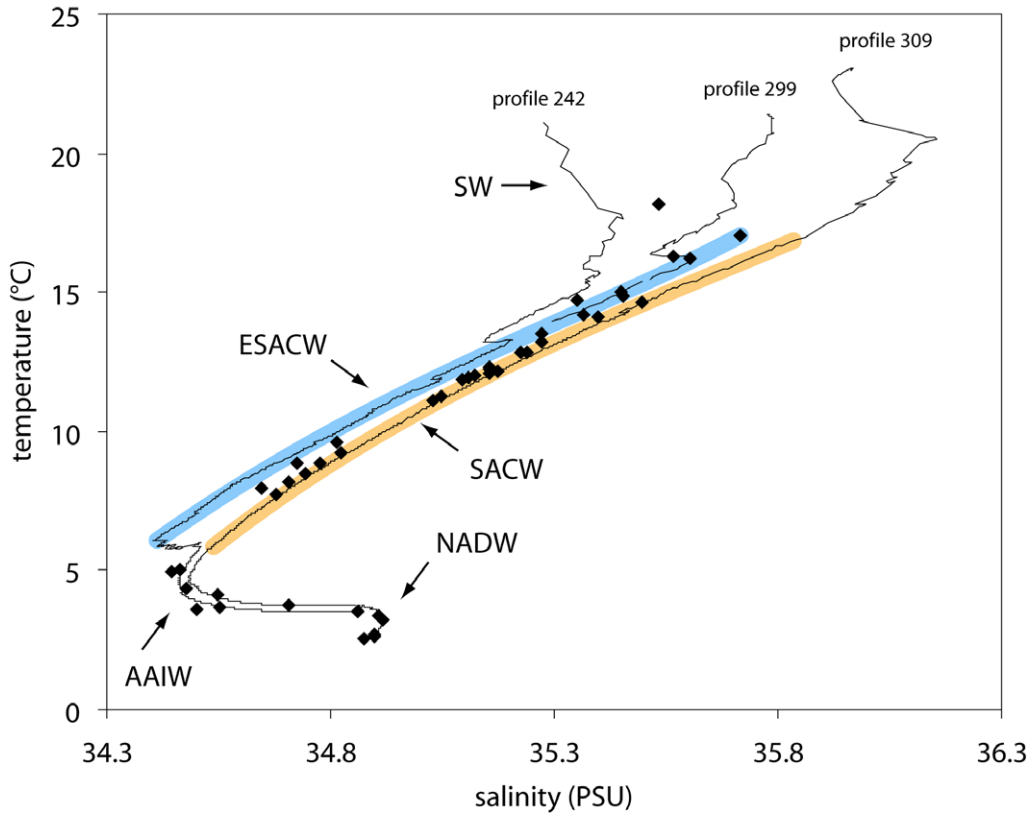

Fig. 5.3: Definitions of the water masses. The thin lines represent T-S profiles of individual CTD casts, filled diamonds represent all bottom water samples. SW: surface water, ESACW: Eastern South Atlantic Central Water, SACW: South Atlantic Central Water, AAIW: Antarctic Intermediate Water, NADW: North Atlantic Deep Water.

Sediment properties

Surface sediment generally had high porosity with a mean of 0.86 ± 0.1. The TOC concentrations were between 0.3 % dry weight (station 268) and 9.6 % dry weight (station 269). The highest TOC concentrations in the range 6 – 10 % dry weight were found on the inner shelf parallel to the coast in a depth of 100-250 m in the area between 19 °S and 24 °S. In the area at 26.5 °S (Lüderitz), a local TOC maximum was found in 250-500 m depth. Multiple mudbelts parallel to the coast, however, have not been observed (Fig. 5.4, left). The molar C:N ratio of the surface sediment's TOC and Ntot ranged from 6.9 (station 233) to 11.4 (station 299). The C:N ratio was lowest on the shelf along the coast and highest on the upper continental slope in depths between 250 and 1000 m (Fig. 5.4, right).

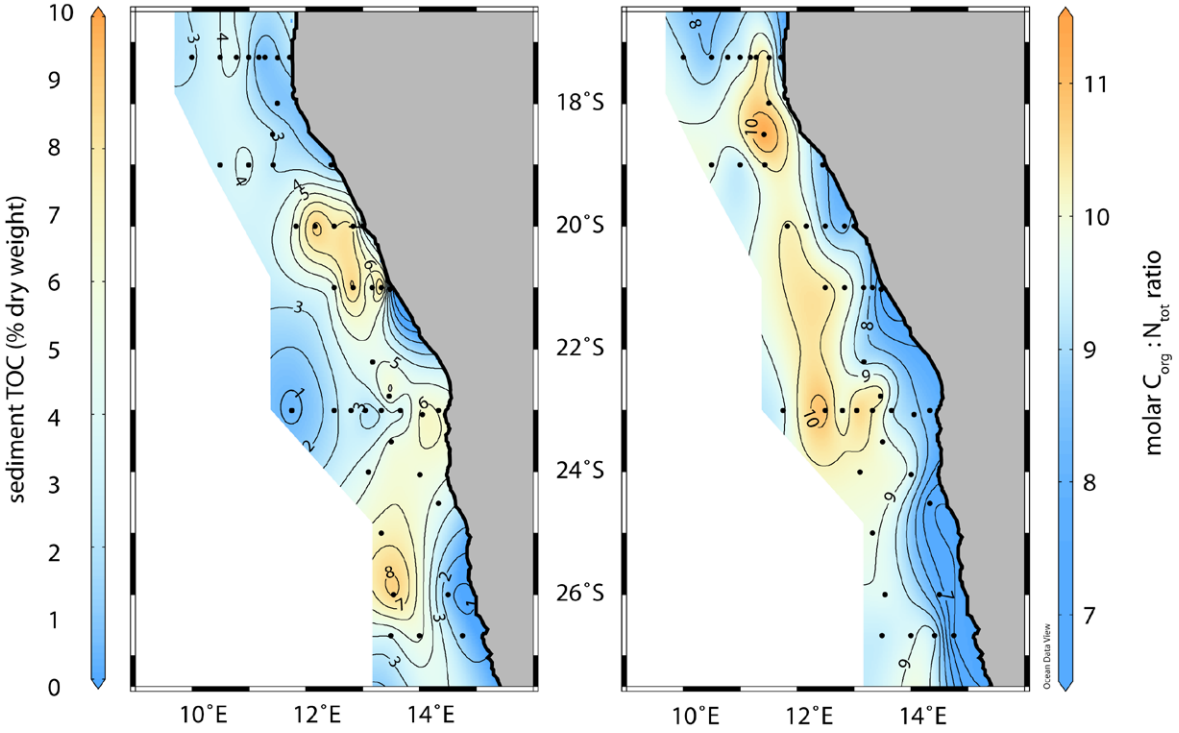

Fig. 5.4: Concentration of TOC in the surface sediment (left), and molar ratio of C_{org} : N_{tot} (right).

Oxygen at the sediment-water interface

Bottom water oxygen concentrations depended on the origin of the respective water mass. The bottom water in depths >1,000 m is dominated by NADW and had the highest oxygen concentrations of up to 238 µmol l^{-1} (station 308). The shallow SACW-dominated stations on the shelf generally had low oxygen concentration below 60 µmol l^{-1}. The bottom water oxygen was below detection limit at 19 °S

(Rocky Point), and the area between 23.5 °S (Walvis Bay) and 26.5 °S (Lüderitz). An exception of the general inverse proportionality of bottom depth and bottom water oxygen concentration was observed at station 268 (23 m), where mixing with well-oxygenated surface water led to a bottom water oxygen concentration of 98 µmol l^{-1}.

Diffusive oxygen uptake correlated significantly with bottom water oxygen concentration (r_s = 0.48, $p < 0.01$). Oxygen uptake reached 3.5 ± 1.2 mmol m^{-2} d^{-1} at 168 µmol O_2 l^{-1} and was as low as 0.3 ± 0.4 mmol m^{-2} d^{-1} at 2 µmol l^{-1} oxygen (Fig. 5.5). Consequently, mapped oxygen consumption rates had a pattern similar to the distribution of oxygen in the bottom water (Fig. 5.6). Additionally, oxygen consumption rates were proportional to the sediment TOC concentration while oxygen concentration was above 50 µmol l^{-1}, but consumption rates decreased sharply toward 0 mmol m^{-2} d^{-1} (e.g. station 226, 231) concentrations below 50 µmol l^{-1}. Diffusive oxygen consumption and bottom water temperature had no significant correlation (r_s = -0.25, $p > 0.18$).

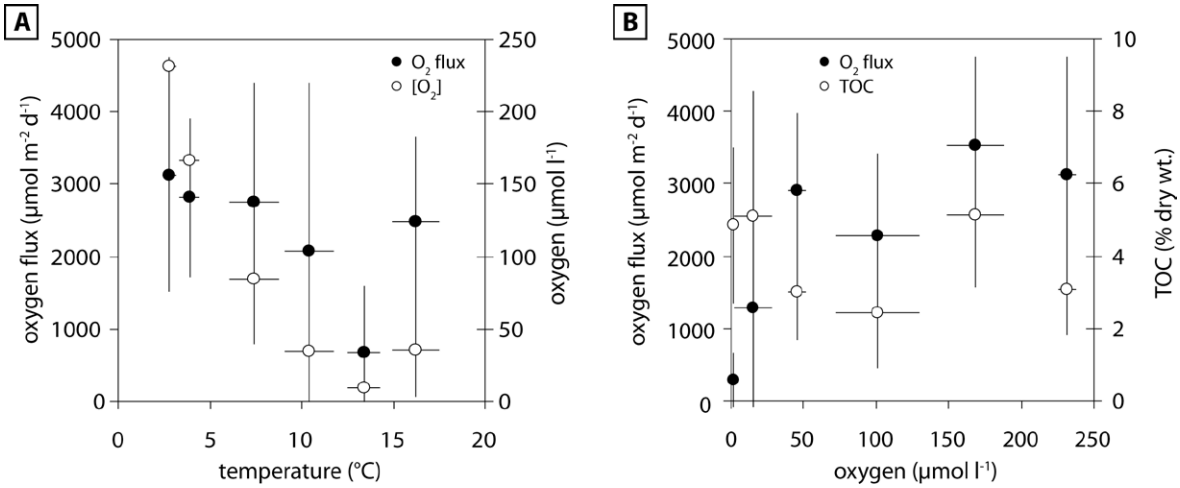

Fig. 5.5: Mean concentrations and benthic consumption rates of oxygen (n=6) as functions of temperature (A), and mean oxygen consumption and mean sediment TOC content (n=6) as functions of the oxygen concentration (B). Errorbars indicate 1 standard deviation.

Tab. 5.1: Spearman correlation coefficients (r_s) of oxygen flux into sediment and various parameters. Significant results are indicated with ** ($p < 0.001$).

		temperature	TOC	C_{org} : N_{tot}	$[O_2]$	$[NO_3^-]$
O_2 flux	r_s	-0.249	0.291	0.336	0.478 **	0.322
	p	0.185	0.119	0.070	0.007	0.083
	N	30	30	30	30	30

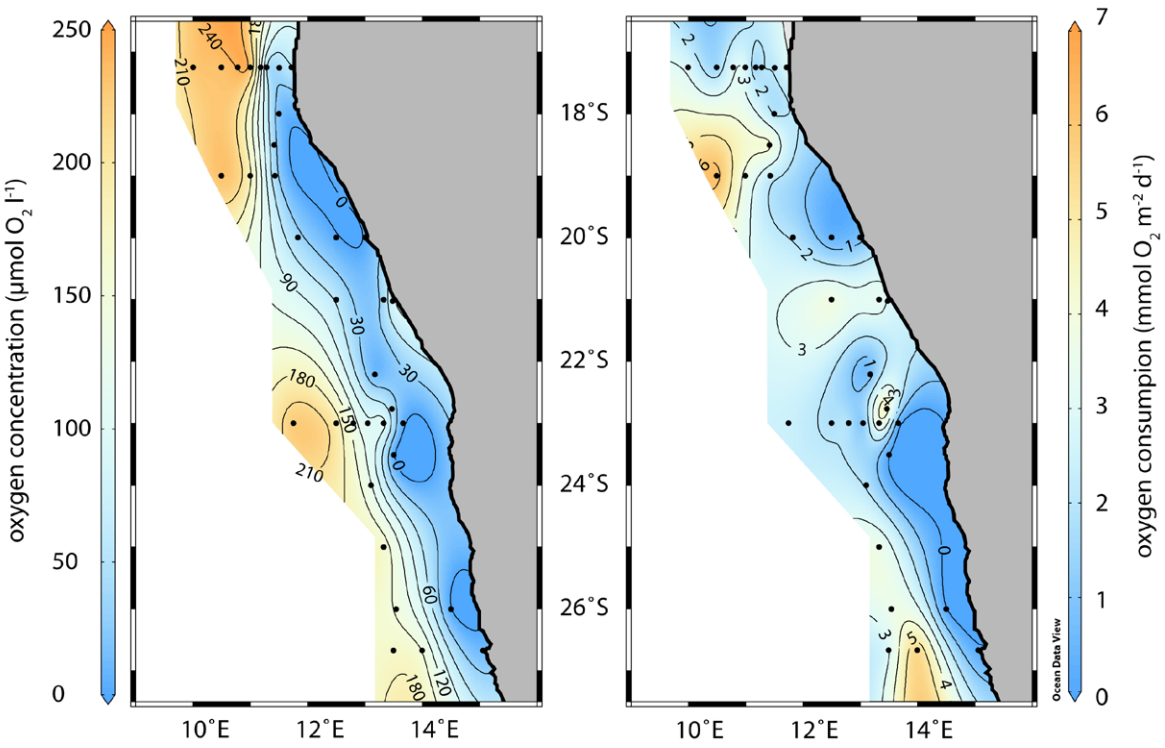

Fig. 5.6: Concentration of dissolved oxygen in the bottom water (left), and benthic oxygen consumption rate (right).

Nutrient stoichiometry

The apparent oxygen utilisation (AOU) was employed to estimate expected nutrient concentrations in the bottom water. Estimates with equations 5.1 – 5.3 assume that the observed oxygen deficit was caused by remineralisation of organic matter. Phosphate concentrations observed at 1 cm above the sediment were in good agreement with AOU-based estimates while the temperature was below 10 °C. Warm and oxygen-depleted bottom water had phosphate concentrations substantially above the estimates (Fig. 5.7 a). Ammonium concentrations had a different pattern. Ammonium was generally below 5 µmol l^{-1} and had no correlation with the AOU at temperatures below 10 °C. Similarly to phosphate, observed ammonium was high in warm and oxygen-depleted water but never exceeded the AOU-based estimates (Fig. 5.7 b). Nitrate concentrations in the bottom water were generally below the AOU-based estimates. Stations with temperature below 10 °C had an offset of less than 10 µmol l^{-1}, and stations with temperature above 10 °C had offsets of up to 25 µmol l^{-1} (Fig 5.7 c).

The apparent nitrogen deficit N* was calculated as difference between expected DIN concentration and observed DIN. The expected DIN concentration based on

phosphate (equ. 5.4) resulted in N* values between 5 µmol N l^{-1} in cold oxygen-rich water and 250 µmol N l^{-1} in warm oxygen-depleted water (Fig. 5.7 d). Calculated N* values based on AOU and using equation 5.5 were similar to phosphate-based N* estimates while temperature was below 11 °C and oxygen above 50 µmol O_2 l^{-1}. In oxygen-depleted, warm water, N* values were significantly below phosphate-based estimates.

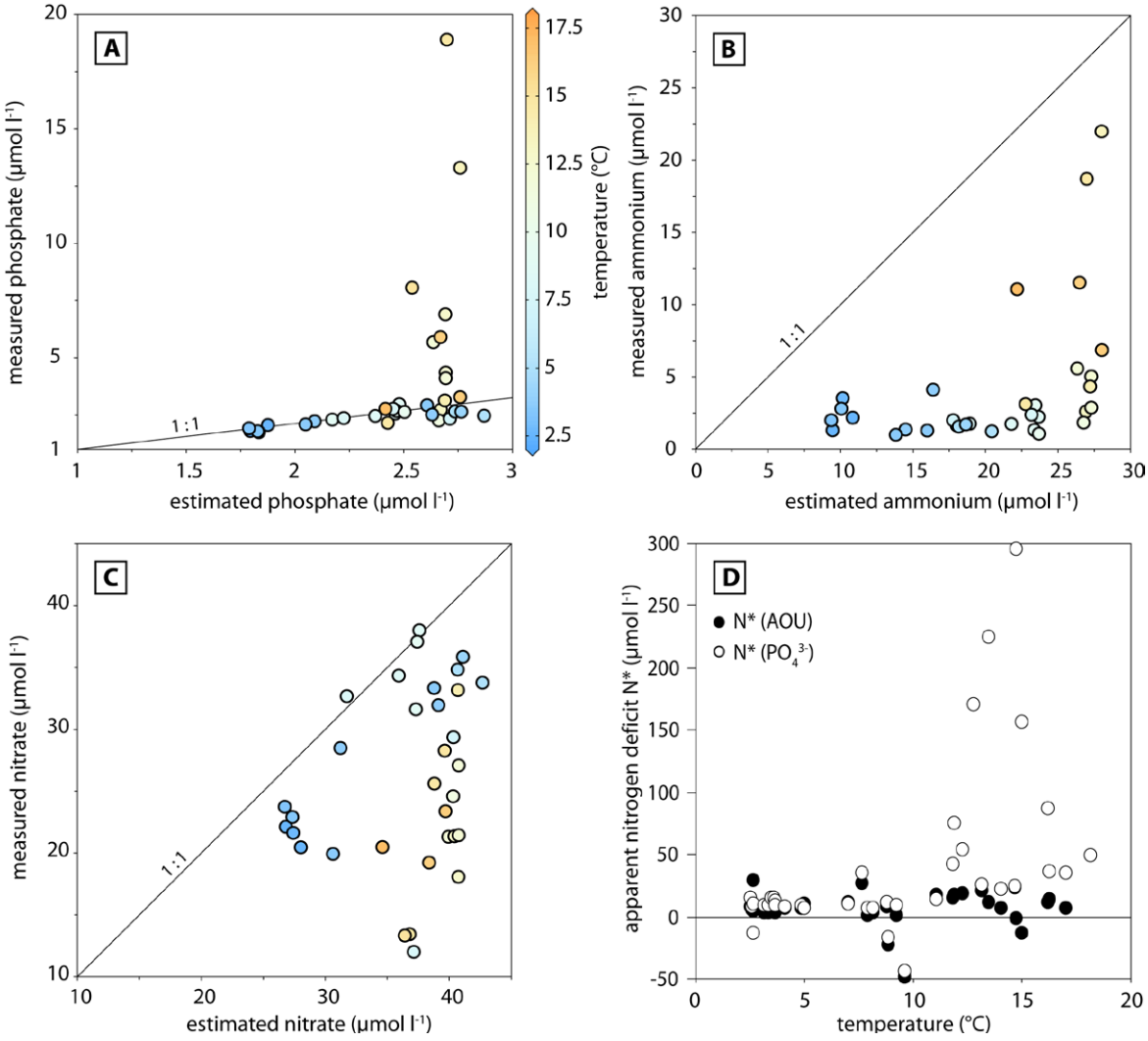

Fig. 5.7: Bottom water nutrient stoichiometry. A: Measured bottom water phosphate concentrations vs. AOU-based phosphate estimates. B: Measured bottom water ammonium concentrations vs. AOU-based ammonium estimates. C: Measured bottom water nitrate concentrations vs. AOU-based nitrate estimates. Diagonal lines represent 1 : 1 agreement. D: Apparent nitrogen deficit N* based on AOU (closed circles, calculated with equ. 5.4) and phosphate concentration (open circles, calculated with equ. 5.5).

Nutrients at the sediment-water interface

Nutrient fluxes across the sediment-water interface were estimated on the basis of vertical pore-water concentration profiles. Phosphate fluxes were always directed into the water column and were lowest in the deepest stations (station 241: -1 µmol m^{-2} d^{-1}). The rates of phosphate release and the resulting phosphate concentration in the bottom water generally increased with increasing temperature (r_s = -0.45, p 0.005), peaked at station 229 (820 µmol PO_4^{3-} m^{-2} d^{-1}), and decreased again at temperatures > 15 °C (Fig. 5.8 b). Similar to phosphate, ammonium concentrations and fluxes were low at deep stations (station 211: -1 µmol NH_4^+ m^{-2} d^{-1}). The concentrations and rates of ammonium release increased with increasing temperature (r_s = -0.62, p < 0.001), peaked at station 224 (8,750 µmol NH_4^+ m^{-2} d^{-1}), and decreased at temperatures > 15 °C (Fig. 5.8 a). The pore water concentrations increased with decreasing depth (Fig. 5.13). In contrast to temperature, the TOC concentration had no clear correlation with the fluxes of phosphate (r_s = -0.19, p = 0.26), or ammonium (r_s = -0.19, p = 0.27). The concentrations and fluxes of phosphate and ammonium are mapped in figures 5.10 and 5.12.

The highest nitrate concentrations in the bottom water were observed at stations on the upper slope, which were influenced by the nitrate-rich AAIW in a depth between 250 m and 500 m. The mean nitrate concentration was 35 µmol l^{-1} and peaked at station 234 with a concentration of 87 µmol l^{-1}. Diffusive nitrate fluxes correlated with bottom water nitrate concentration (r_s = 0.33, p = 0.06), and highest nitrate consumption rates (Fig 5.8 c, positive fluxes) of up to 700 µmol m^{-2} d^{-1} were observed concomitant with highest nitrate concentrations at the upper slope. Concentration and consumption rate of nitrate decreased with decreasing temperature (r_s = -0.56, p < 0.001) and increasing bottom depth, and nitrate fluxes ultimately changed direction at the deepest stations (241, 310, 316). There, nitrate was released into the water column with a mean rate of -90 µmol NO_3^- m^{-2} d^{-1}. Further, nitrate consumption rates increased with decreasing oxygen concentration (r_s = 0.53, p = 0.001). In contrast to oxygen, nitrate was not depleted at any sampled station. Nitrite was virtually absent in the bottom water at most stations, though the sediment of all deep stations had internal nitrite maxima of up to 4 µmol l^{-1} (station 272). The sediment released nitrite with rates of up to 10 µmol m^{-2} d^{-1} (Fig 5.8 d, negative fluxes). The nitrite concentrations were increased up to 1 µmol l^{-1} in anoxic bottom water of the shelf at 19 °S and 24 °S. The sediment at these stations consumed nitrite from the water column with rates of up to 18.5 µmol m^{-2} d^{-1} at station 225 (Fig. 5.8 d, positive fluxes). The concentrations and fluxes of nitrate and nitrite are mapped in figures 5.9 and 5.11.

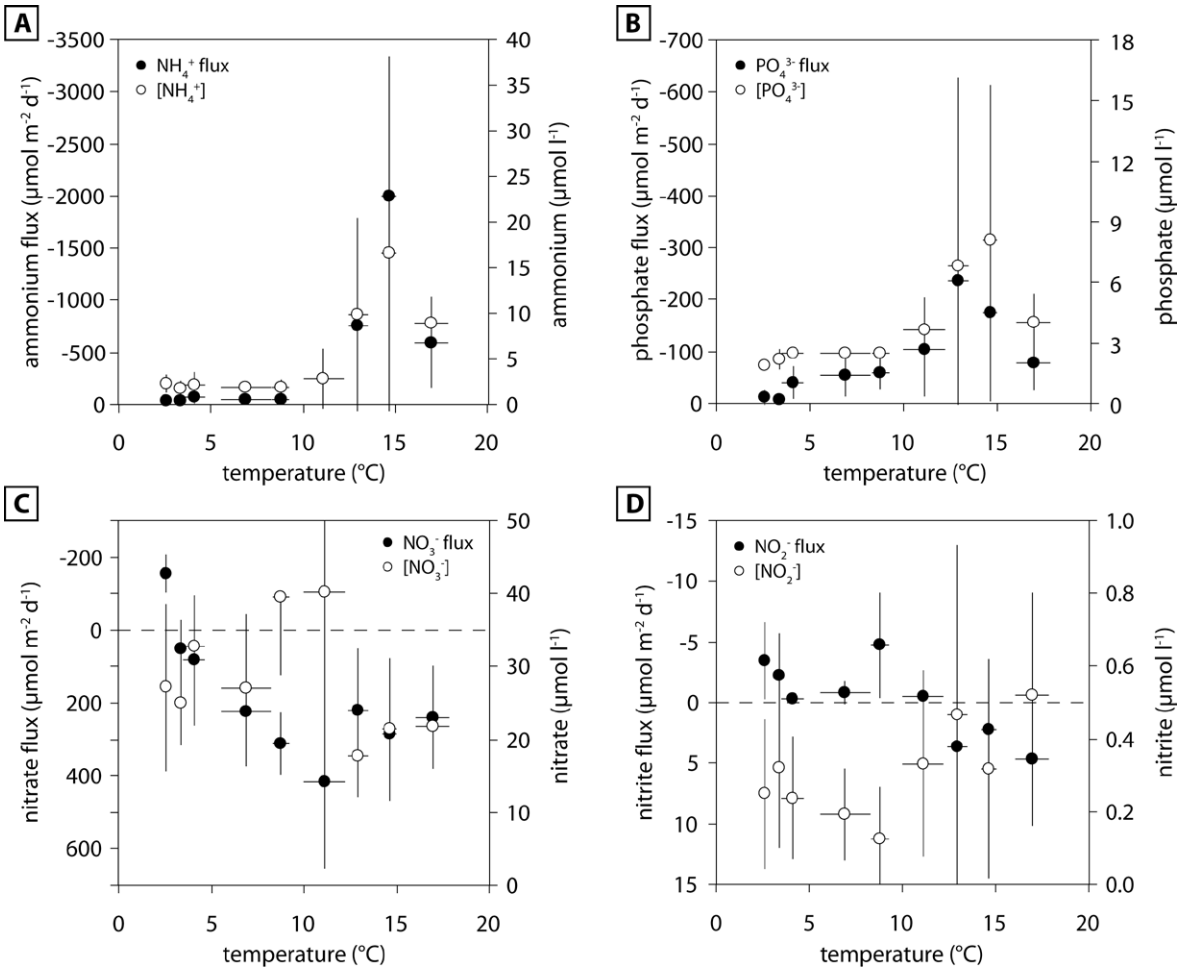

Fig. 5.8: Mean bottom water concentrations and fluxes (n=4) of ammonium (A), phosphate (B), nitrate (C), and nitrite (D). Negative fluxes indicate release from the sediment into the water column, positive fluxes indicate uptake from the water column. Errorbars indicate 1 standard deviation.

Tab. 5.2: Spearman correlation coefficients (r_s). Significant results are indicated with * ($p < 0.01$) and ** ($p < 0.001$), N denotes number of analyzed data sets.

		temperature	TOC	C_{org} : N_{tot}	$[O_2]$	$[NO_3^-]$
PO_4^{3-} flux	r_s	-0.451 **	0.193	0.279	0.353 *	0.025
	p	0.005	0.261	0.099	0.032	0.884
	N	36	36	36	36	36
NH_4^+ flux	r_s	-0.615 **	-0.191	0.551 **	0.430 **	0.342 *
	p	< 0.001	0.265	< 0.001	0.008	0.041
	N	36	36	36	36	36
NO_3^- flux	r_s	0.560 **	0.175	0.140	-0.526 **	0.328
	p	< 0.001	0.330	0.439	0.001	0.062
	N	36	36	36	36	36

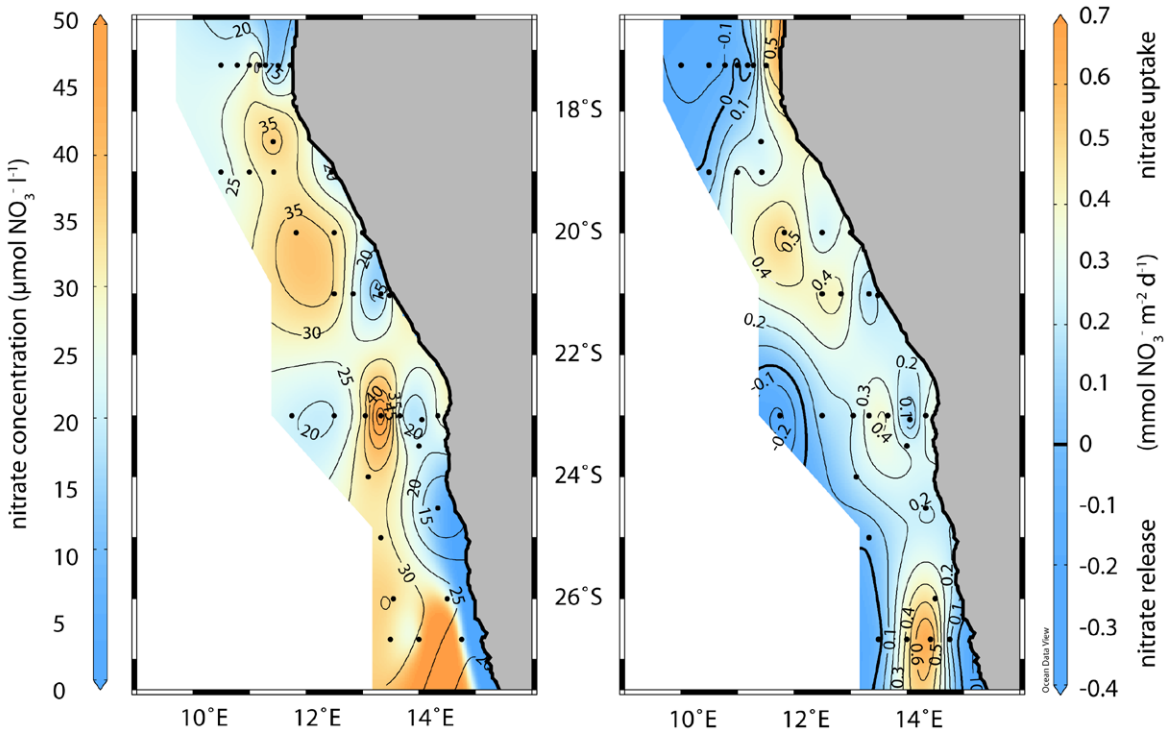

Fig. 5.9: Concentration of nitrate in the bottom water (left), and nitrate flux across the sediment-water interface (right). Positive fluxes denote nitrate consumption, negative fluxes denote nitrate export into the water column.

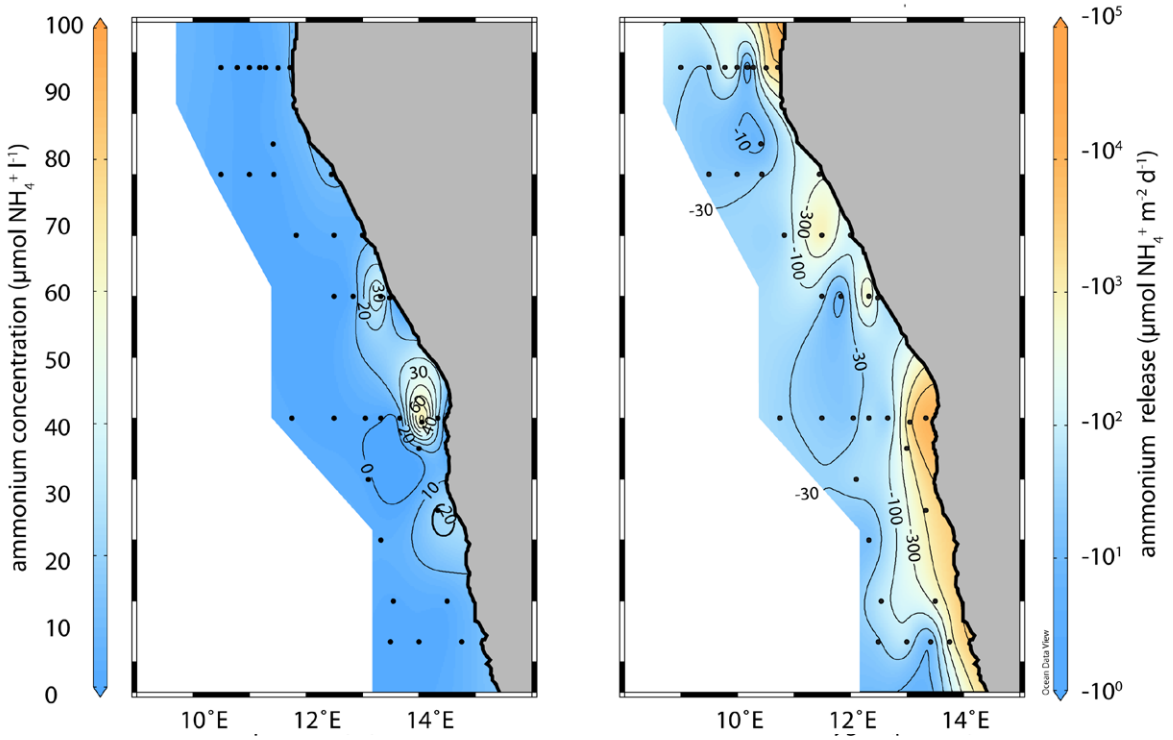

Fig. 5.10: Concentration of ammonium in the bottom water (left), and ammonium flux across the sediment-water interface (right).

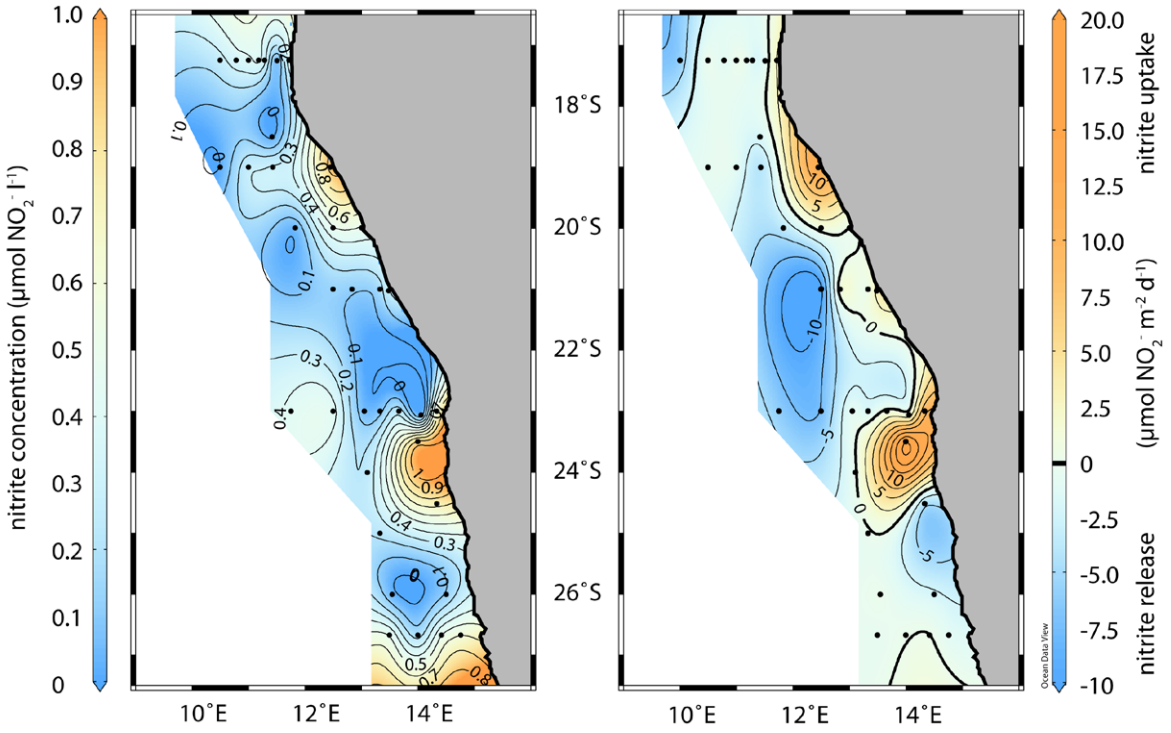

Fig. 5.11: Concentration of nitrite in the bottom water (left), and nitrite flux across the sediment-water interface (right). Negative fluxes denote nitrite export into the water column.

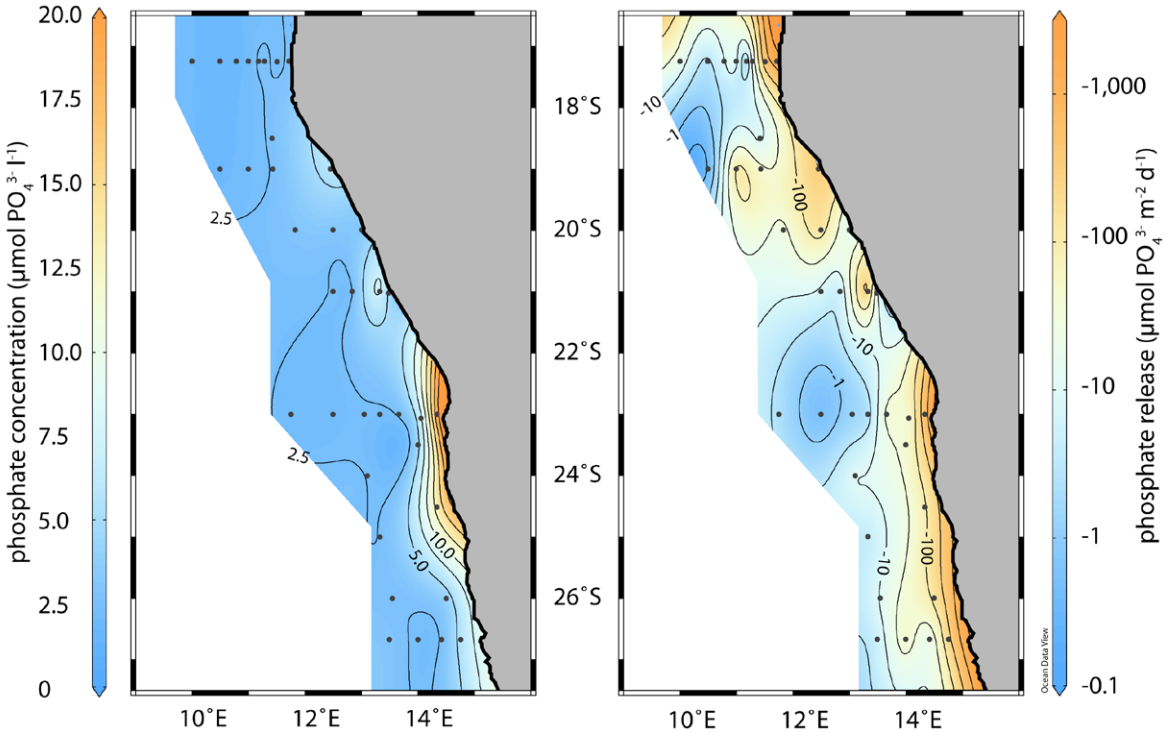

Fig. 5.12: Concentration of phosphate in the bottom water (left), and phosphate flux across the sediment-water interface (right). Negative fluxes denote phosphate export into the water column.

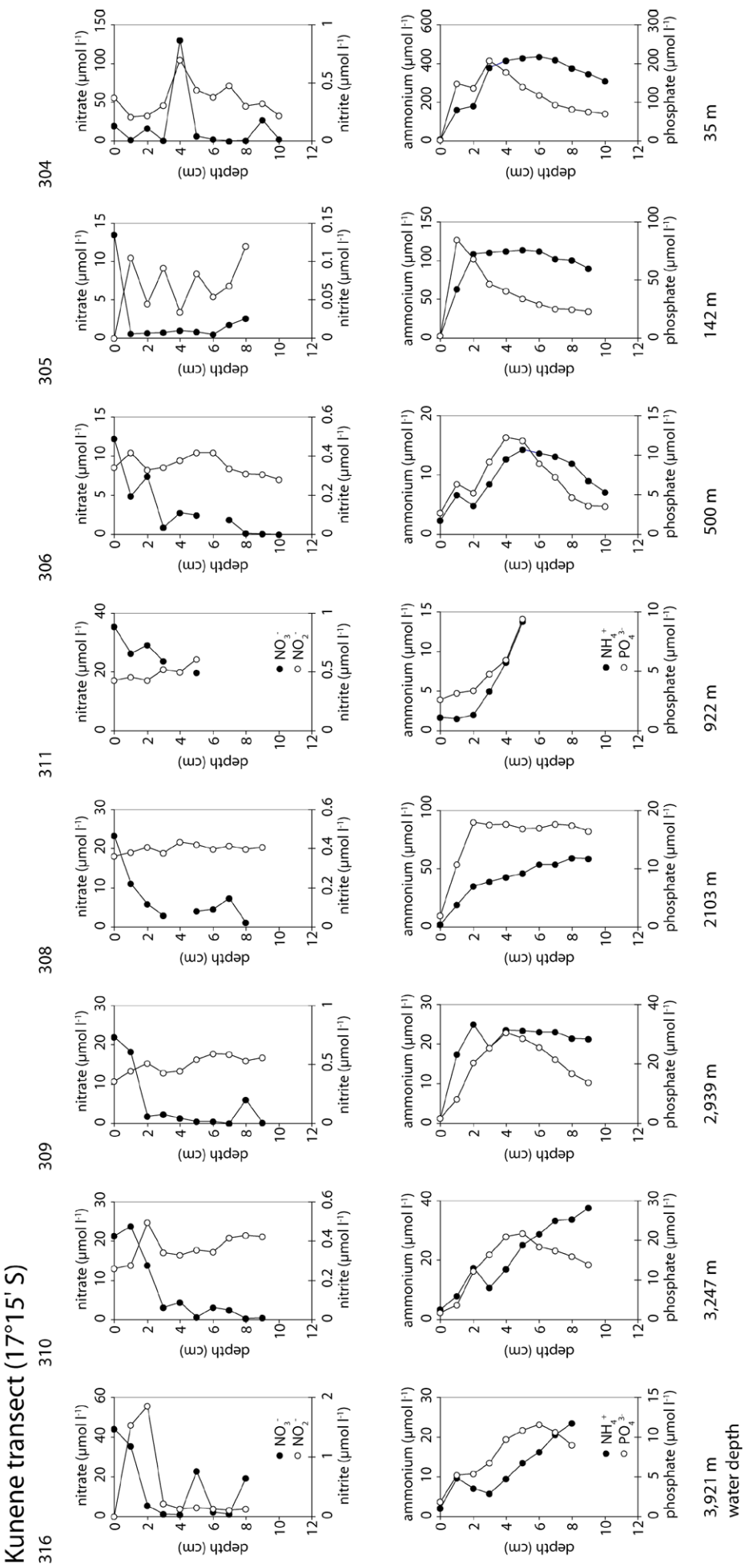

Fig. 5.13: Pore water concentration profiles of nitrate and nitrite (upper row), and ammonium and phosphate (lower row). Note different scales.

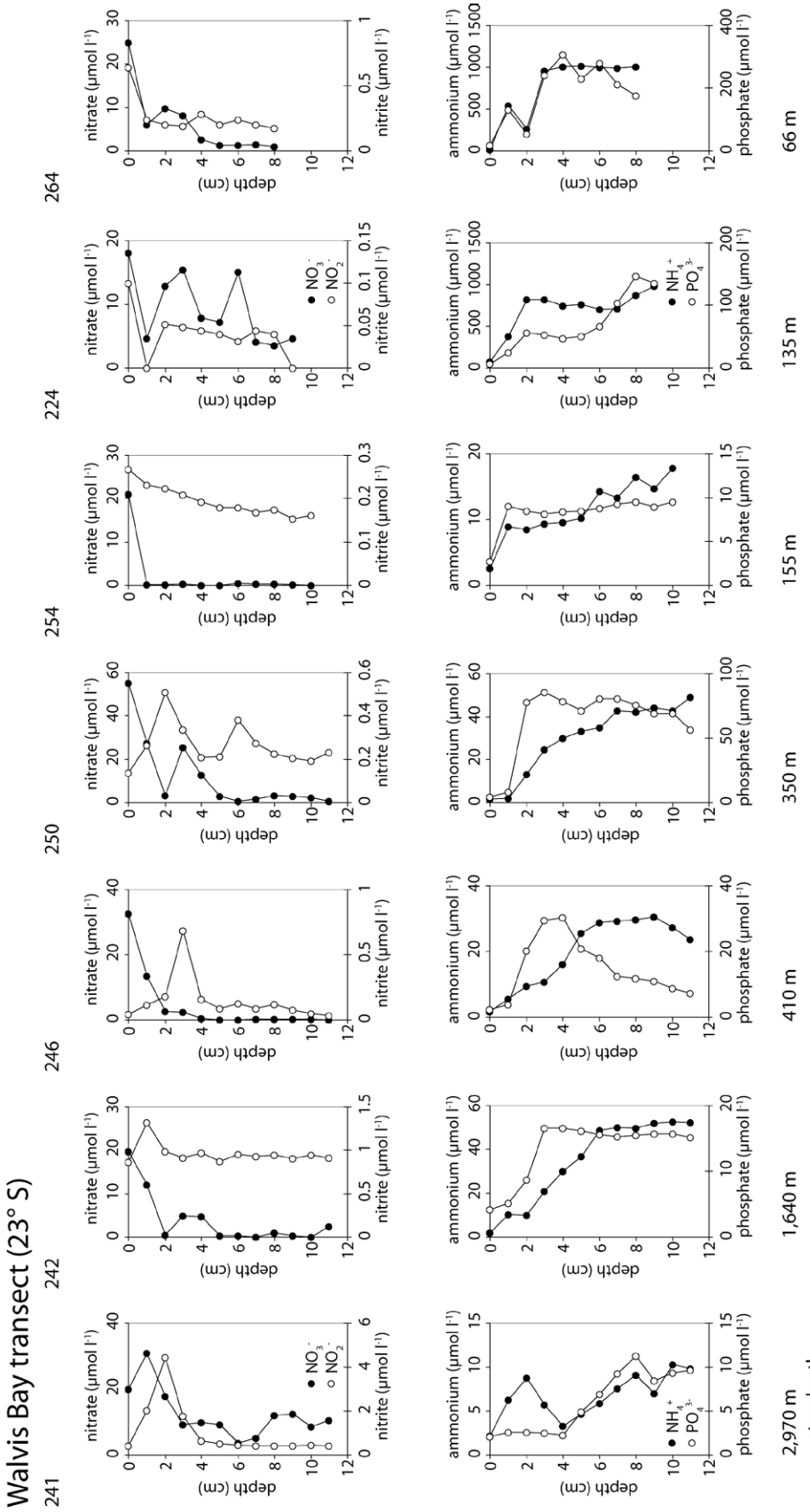

Fig. 5.14: Pore water concentration profiles of nitrate and nitrite (upper row), and ammonium and phosphate (lower row). Note different scales.

Elimination of reactive nitrogen

The rates of N_2 production indicate the elimination of reactive nitrogen via denitrification or anammox. The potential production of N_2 within the sediment was measured by isotope pairing incubations using ^{15}N-nitrate as tracer. The results range from 0.5 mmol N_2 m^{-2} d^{-1} (station 233) to 3.9 mmol N_2 m^{-2} d^{-1} (station 292), and are tabulated in table 5.3 and plotted in figure 5.17. The measured N_2 profiles were used to calculate the N_2 fluxes across the sediment-water interface. The obtained results span from -61 µmol N_2 m^{-2} d^{-1} (N_2 release, station 295) to -1,274 µmol N_2 m^{-2} d^{-1} (N_2 release, station 271), results are mapped in figure 5.15. The mean N_2 fluxes decreased with increasing temperature (r_s = 0.52, p = 0.015) and were further inversely correlated with the bottom water oxygen concentration (r_s = -0.50, p = 0.022). The results of the isotope pairing incubation agreed with the results of the N_2 flux calculations (figure 5.16.).

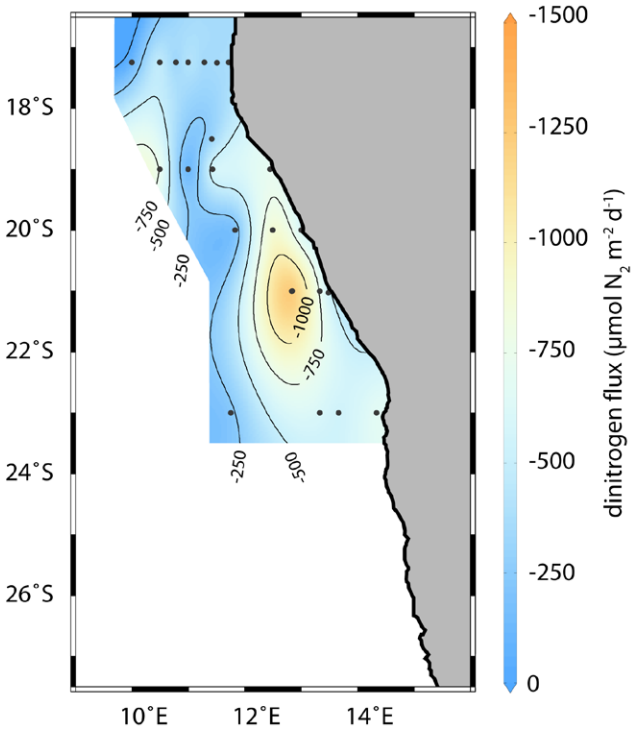

Fig. 5.15: N_2 fluxes across the sediment-water interface.

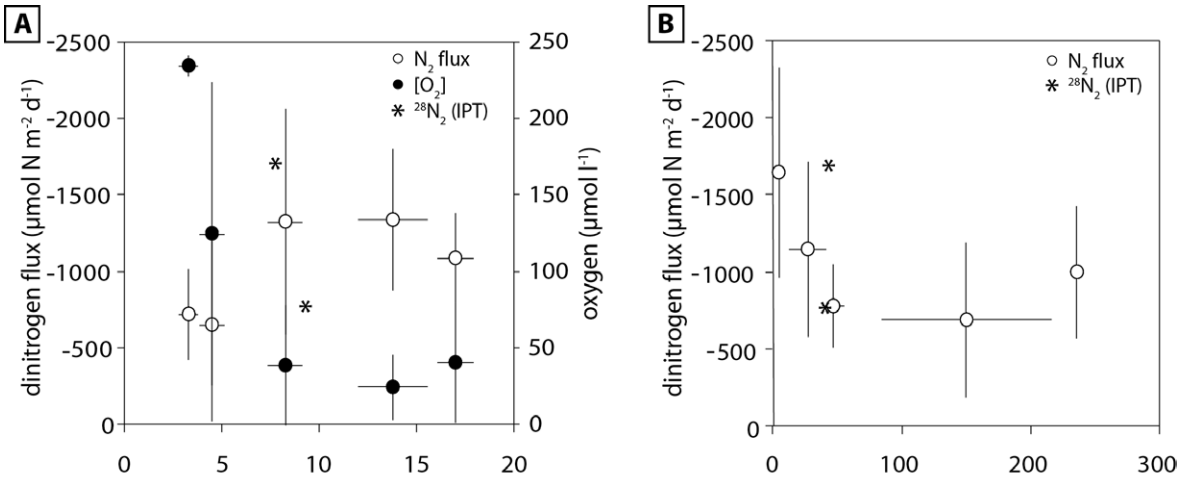

Fig. 5.16: Mean fluxes (n=4) of N_2 across the sediment-water interface vs. temperature (left panel) and bottom water oxygen concentration (right panel). The results of the isotope pairing incubation (IPT, asterisks) at stations 292, 299, and 306 were included for comparison. The IPT results of stations 233 and 236 were omitted because these stations were far outside of the area with N_2 profile measurements. Negative fluxes denote release of N_2, error bars indicate 1 standard deviation of means.

Tab. 5.3: Results of isotope pairing incubations.

station	temperature (°C)	$[NO_3^-]$ (µmol l^{-1})	$^{28}N_2$ production (mmol m^{-2} d^{-1})	comment
233	8.8	31.6	3.9	
236	7.7	12.0	1.9	
268	18.2	24.3		failed
277	14.8	28.3		failed
292	11.9	21.3	0.5	
299	9.2	37.1	0.6	
306	3.6	33.4	1.0	

Tab. 5.4: Spearman correlation coefficients (r_s). Significant results are indicated with * ($p < 0.01$) and ** ($p < 0.001$).

		temperature	TOC	C_{org} : N_{tot}	$[O_2]$	$[NO_3^-]$
N_2 flux	r_s	0.521 *	0.135	-0.153	-0.497 *	-0.149
	p	0.015	0.559	0.507	0.022	0.518
	N	21	21	21	21	21

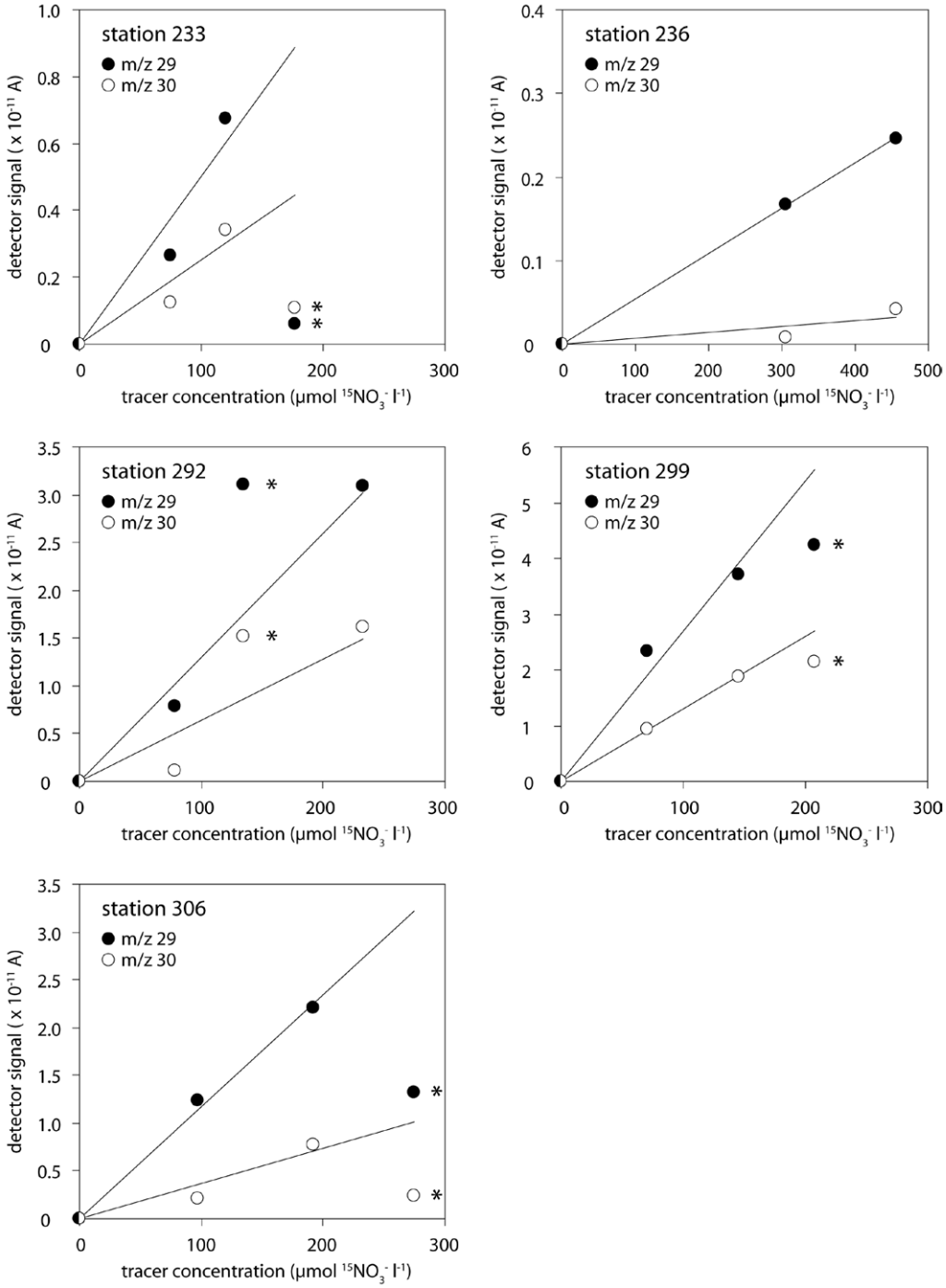

Fig. 5.17: Results of the $^{29}N_2$ and $^{30}N_2$ measurements of the isotope pairing incubations. Note different scales. Incubations marked with an asterisk were regarded as outliers and excluded from calculations.

5.4 Discussion

The sediment as source and sink of nutrients

The observed TOC distribution with an extended mud belt on the inner shelf between 19 °S and 24 °S and a deeper depocenter at 27 °S agrees with the general TOC distributions reported by e.g. Mollenhauer et al. (2002) or Inthorn et al. (2006). Multiple, continuous belts as described in Bremner & Willis (1993) and van der Plas et al. (2007) have not been observed, which can be attributed to the low spatial resolution of the present study. TOC concentrations and C_{org}:N_{tot} ratios of the present study agree with the results of Inthorn et al. (2006) and van der Plas et al. (2007).

Degradation of organic matter releases the main elements phosphorus and nitrogen primarily as phosphate and ammonium. The remineralisation rate driven by poikilothermal bacteria and invertebrates should be positively correlated with the water temperature (e.g. Kristensen et al. 1992). As expected, the temperature had a significant impact on the diffusive fluxes of phosphate (Spearman r_s: -0.45, $p = 0.005$) and ammonium (r_s: -0.62, $p < 0.001$), and the fluxes of both compounds increased exponentially with temperature (Fig. 5.8 c, d). Zabel et al. (1998) found phosphate fluxes in deep sea sediments of the Cape Basin, which are in good agreement with the results of the present study. The results of Zabel et al. (1998) further show that phosphate fluxes increased with decreasing water depth. Temperature and water depth are inversely correlated, hence phosphate fluxes increased in pace with temperature, which is in agreement with results of Kamp-Nielsen (1975). However, the highest fluxes of ammonium and phosphate were observed in sediment of the inner mud belt at bottom water temperatures of 14 °C, whereas coastal sediment in water temperatures above 15 °C had significantly lower efflux of ammonium and phosphate, respectively. These coastal stations with a mean TOC content of 2.0 ± 1.4 % had significantly less organic matter than sediments of the inner mud belt, which had 6.1 ± 3.2 % TOC. This indicates that remineralisation is constrained by organic matter availability in coastal sediment, although a correlation of TOC with phosphate flux ($r_s = 0.19$, $p = 0.26$) and ammonium flux ($r_s = 0.19$, $p = 0.27$) is not statistically significant. The fact that organic matter is the source of released ammonium and phosphate is reflected in the correlation of ammonium efflux with C_{org}:N_{tot} ratio ($r_s = -0.55$, $p < 0.001$), implying that fresh organic matter with low C:N ratio releases more ammonium than refractory organic matter with high C:N ratio.

The ratio of produced ammonium and phosphate (6.0 ± 6.7) is below the average N : P ratio of primary producers (N : P ≈ 16, Redfield et al. 1963), which constitute the majority of sedimented organic matter. Although organic-bound nitrogen and

phosphorous are not necessarily remineralized and released in equal ratios, this deviation is worth closer examination. The highest phosphate fluxes were observed in stations along the inner mud belt (Fig. 5.8, 5.12) and agree with results of Schulz & Schulz 2005, Goldhammer et al. 2010, Goldhammer et al. 2011, which attribute intensive phosphate release to activity of abundant *Thiomargarita* sulphur bacteria. Pulses of phosphate mobilisation triggered by episodic oxygen depletion were further shown to temporally increase pore-water phosphate concentrations sufficiently to cause precipitation of phosphate minerals such as carbonate apatite (Goldhammer et al. 2010). Precipitated phosphate accumulates in the mud belt, which ultimately turns the sediment into a phosphate sink. The ratio of released ammonium and phosphate is further shifted by nitrification in the presence of oxygen, which may be detected by internal concentration maxima of nitrate and nitrite (Figs. 5.13, 5.14). This recycled nitrate fuels concomitant denitrification and results in nitrate export by deep sediment with temperature < 3 °C (Fig. 5.8) and high N_2 production. Thus, N_2 production scales in pace with bottom water oxygen concentration and less with nitrate concentration (Tab. 5.17). The sediment is generally a sink for reactive nitrogen although recycled nitrate is released at high oxygen concentration while ammonium is released at low oxygen concentration.

The N_2 production rates as a proxy for the elimination of reactive nitrogen via denitrification or anammox had a high direct correlation with the oxygen concentration (r_s: 0.50, $p = 0.022$) and a high inverse correlation with the ammonium efflux (r_s: -0.61, $p < 0.01$) which shows coupled nitrification-denitrification within the sediment. Nitrification appears efficient enough in deep and cold sediments to cause net release of nitrate from the sediment into the water column and suppression of ammonium release. Interestingly, Tyrell and Lucas (2002) observed the highest nitrate deficit in the water column at 12-13 °C water temperature, which agrees well with this study's result that nitrate consumption rates were highest at 11 °C (Fig. 5.8). Consequently, the highest nitrate deficit in terms of deviation from the redfield-ratio based remineralisation trajectory was observed at 13 °C (station 229, 1 µmol l^{-1} O_2, 9 µmol l^{-1} NO_3^-).

Bottom water nutrient stoichiometry

The interval 0 – 1 cm of obtained pore-water profiles was excluded from analysis because concentration and diffusivity changed substantially within this sampling interval, which resulted in biased and erroneous results of the employed implementation of the model of Berg et al. (1998). Thus, pore-water analysis missed the uppermost sediment layer where potential interaction of upward-diffusing remineralisation products and down-ward diffusing oxygen was probably most intense. However,

the bottom water sampled at 1 cm above the sediment surface reflects the net effects of solute fluxes across the sediment water interface as expressed with equations 5.1 – 5.3. Applying these equations to bottom water samples showed that phosphate accumulates in the bottom water in pace with oxygen consumption at oxygen concentrations > 40 µmol l^{-1} (Fig. 5.7), which implies that these sediments released the majority of organic-bound phosphate back into the water column. An apparent phosphate excess was observed in the bottom water of the mud belt with 12 – 15 °C and < 40 µmol O_2 l^{-1}, which corresponds with high phosphate fluxes into the water column (5.8 fluxes), which were ascribed to the activity of *Thiomargarita* sulphur bacteria (Schulz & Schulz 2005, Goldhammer et al. 2010, Goldhammer et al. 2011). Since these bacteria store phosphate while oxygen is available, it is probable that these organisms scavange additional phosphate from the water column to refill internal phosphate storage subsequent to resuspension (Schulz & Jørgenson 2001). Hence, a fraction of the phosphate released by *Thiomargarita* may have been remineralized originally in distant regions and transported onto the Namibian Shelf via regional-scale currents, rendering *Thiomargarita* a biological phosphate pump that aggregates phosphate within the surface sediment.

In contrast to phosphate, bottom water ammonium concentration was independent from apparent oxygen utilisation (AOU) at temperatures < 10 °C (Fig 5.7), while nitrate concentrations increased with increasing AOU, which indicates efficient benthic nitrification. This is supported by the observation of nitrite production at temperatures < 10 °C (Fig 5.8). At higher temperatures and lower oxygen concentrations, the ammonium-nitrate balance was shifted toward ammonium. Nitrification was displaced from the sediment into the water column as indicated by reversed direction of nitrite fluxes and the fact that nitrate was always > 10 µmol l^{-1} even at oxygen below detection limit. The nitrite source in the water column was also observed by Füssel et al. (2011), who measured high rates of nitrite oxidation in the Namibian oxygen minimum zone even at apparent anoxia and stated that the low rates of ammonium oxidation were insufficient to provide the necessary nitrite. Further, Kalvelage et al. (2011) observed high rates of nitrate reduction in the Namibian oxygen minimum zone and suggested that the produced nitrite is an intermediate product of nitrate reduction coupled to anammox. Competing re-oxidation of reduced nitrite would explain why nitrate was not fully consumed during the sampling of the present study.

The balance between nitrification and coupled denitrification further appears temperature dependent because the deviation of observed and estimated nitrate concentration increased with increasing temperature (Fig. 5.7). Stations with higher temperature had significant nitrate loss at moderate AOU, whereas stations with

lower temperature had nitrate concentrations close to the estimates even at higher AOU. The results of Veraart et al. (2011) offer an explanation for the temperature dependent balance of nitrification and denitrification. Veraart et al (2011) found that microbial oxygen consumption and thus the availability of oxygen within the sediment is temperature dependent, which ultimately controls oxygen dependent processes such as nitrification and denitrification. In the present study, nitrite fluxes as proxy of nitrification and denitrification suggest that internal nitrification apparently ceased at temperatures above 11 °C (Fig. 5.8 d).

N : P imbalance

Heterotrophic denitrification is constantly eliminating reactive bioavailable nitrogen while remineralized phosphate is released into the bottom water. Both processes accelerate with increasing temperature, thus progressively reducing the bottom water N : P ratio. This N : P imbalance with respect to the theoretical Redfield-ratio is further pronounced in oxygen-depleted water by mobilization of intracellular polyphosphate by *Thiomaragrita* and the dissolution of iron-bound phosphate. The latter additionally adds dissolved iron to the bottom water, which should set the stage for biological nitrogen fixation if the modified bottom water with low N:P ratio and iron amendment reaches the water surface via upwelling. In fact, Sohm et al. (2011) found nitrogen fixation in recently upwelled water along the northern Benguela. However, overall nitrogen fixation rates were low and presumably limited by the availability of dissolved iron, which may indicate that the amended iron and phosphate precipitate back onto the sediment once the water is re-oxidized.

Upwelling events regularly trigger intensive plankton blooming of non-diazotrophic primary producers. Since nitrogen-fixating primary producers have lower growth rates and higher iron demands than competing non-diazotrophs, available iron is probably scavenged from surface water before significant nitrogen fixation occurs (Dutkiewicz et al. 2012). Hence, the *Thiomargarita*-induced phosphate excess with respect to reactive nitrogen is not compensated by nitrogen fixation but exported from the Benguela as the surface water is displaced westwards. However, Goldhammer et al. (2010) showed that *Thiomargarita* significantly accelerate the sequestration of phosphate, which antagonizes reduced N:P ratios caused by the elimination of reactive nitrogen. Whether or not phosphate released by *Thiomaragrita* actually affects the N : P ratio in the surface water might be controlled by upwelling intensity and initial depth of the upwelling water. If the phosphate-enriched bottom water is not upwelling, then resuspended *Thiomargarita* may re-absorb the abundant phosphate

and contribute to the phosphate trapping effect of the broad shelf as proposed by Tyrell & Lucas (2002). Moreover, phosphate mobilization in oxygen-depleted bottom water biases phosphate-based estimation of N* and result in overestimated nitrogen loss, whereas N* estimates based on oxygen concentration appeared less sensitive to phosphate mobilization (Fig. 5.7 d). Interestingly, both N* estimators detected apparent N excess (negative N* values) at stations 234 & 250, which might indicate erroneous ammonium measurement or a benthic ammonium source independent from phosphate and oxygen.

Limitations of the diffusion model

The utilization of concentration profiles for the estimation of diffusive fluxes poses the question whether or not diffusion is the dominant transport mechanism, because alternative transport processes such as advection potentially exceed diffusive transport by orders of magnitude (e.g. Precht & Huettel 2003). The sampled sediment of the present study generally had high porosity of 0.86 ± 0.1, which consisted of diatom ooze on the continental shelf and gradually changed to calcareous ooze as bottom depth increased. Such cohesive sediment hampers advective movement of pore-water, rendering diffusion the dominant transport mechanism within the bulk sediment. However, Fossing et al. (2000) estimated sulphate reduction rates of Namibian continental slope sediment and concluded that bioirrigation of surface sediment contributed significantly to depth-integrated areal reaction rates. This finding is supported by the results of Glud et al. (1994) which demonstrated for Namibian shelf sediments that in-situ oxygen profiles underestimated the total oxygen uptake measured in benthic chambers. They further showed that ex-situ incubation of retrieved sediment cores led to increased oxygen consumption and thus an overestimation of the in situ oxygen consumption. Glud et al. (1994) ascribed the increased oxygen consumption of retrieved sediment cores to temperature changes during the recovery or decompression, which might have led to lysis of sensitive organisms and thus to an increased availability of labile organic compounds. This artificially increased availability of organic compounds might have also altered the activity of heterotrophic bacteria such as sulphate reducing bacteria, which would have resulted in increased sulphate reduction rates. Hence, estimation of bioirrigation coefficients based on the comparison of incubation results with concentration profiles as described in Fossing et al. (2000) might result in overestimated bioirrigation coefficients.

Despite the uncertain impact of bioirrigation on solute transport, Glud et al. (1994) concluded on the basis of pH profiles that the decompression during the recovery of sediment cores had only a minor effect on the profiles of pore water solutes, and we are confident that the obtained concentration profiles are representative for the diffusive fluxes. The calculated diffusive fluxes therefore represent a baseline of the bulk sediment, and interference by animals and sediment re-deposition might result in spatially or temporally altered solute fluxes. Lastly, undirected diffusion-like transport affects all solutes simultaneously, which should leave the flux ratios unaffected and thus permits valid conclusions.

Conclusions

The remineralisation of organic matter appeared primarily temperature dependent with respect to production of ammonium and phosphate. Although oxygen respiration and denitrification are basically temperature dependent (Veraart et al. 2011), these catabolic pathways were limited by the availability of oxygen and nitrate, respectively. Hence, the highest overall rate of remineralisation would be expected at the optimum of temperature and oxygen / nitrate concentration. With respect to the C_{org}:N_{tot} ratio of the bulk sediment as a proxy for the remineralisation progress, this optimum is probably at the shelf break and upper slope in a depth of 480 ± 120 m and a water temperature of 7.4 ± 1.3 °C (Fig. 5.4), where high C_{org}:N_{tot} ratio suggests pronounced degradation. Factors such as TOC and oxygen concentration contribute additional variation of nutrient fluxes: Oxygen-depletion triggers intensive phosphate mobilization and ammonioum release in mud belt sediments, low TOC constrains remineralisation in coastal sediment.

The phosphate mobilization of sediment overlaid by anoxic bottom water should further taken into account if the apparent nitrogen deficit is calculated on the basis of the phosphate concentration (Deutsch et al. 2001, Tyrell & Lucas 2002). The results of the present study indicate that phosphate is mobilised if the bottom water oxygen concentrations fall below 50 µmol l^{-1}, which biases the calculated nitrogen deficit. Instead, the oxygen concentration should be considered as a reference for the calculation of the hypothetical stoichiometric nitrogen deficit in isolated hypoxic bottom water.

6. Conclusion and future work

Needle-type membrane inlet mass spectrometry as routine method

The needle-type membrane inlet developed for the present study was successfully employed during several campaigns to measure N_2 profiles across the sediment-water interface. The sampled stations comprise sandy and muddy sediment between the intertidal (chapter 3 & 4) and the deep sea (chapter 5). The simplicity of the MIMS setup enabled operation in remote laboratories and on research vessels. Operation even in rough sea was unproblematic aboard larger research vessels such as “Africana” and “Maria S. Merian”, but measurements failed on the medium-sized vessel “Heincke” during a storm due to unstable pressure within the vacuum line. This sensitivity to movements is probably caused by the turbomolecular pump installed in the employed GAM-200 mass spectrometer, which has magnetic bearings. If the movement of the pump’s rotor exceeds the tolerance of the magnetic bearing, the rotor is decelerated substantially by contact with a solid safety bearing, which is reducing the rotor’s speed and thus reducing the pumping rate. The result is an unstable pressure within the vacuum system, which hampers useful measurements.

It turned out during first routine measurements that epoxy resin is an unfavourable construction material, and inlets containing this material failed after a few hours of operation. In contrast, all-metal inlets (chapter 2) withstood several weeks of continuous operation. The shielded membrane tip developed here was robust enough for safe employment in firm, sandy sediment without noticeable wear of the membrane. The collision of the inlet with embedded stones or shells occasionally buckled the inlet tip, but never resulted in leaks or the intrusion of pore-water into the vacuum line. The risk of fatal water intrusion after an inlet failure is further reduced by a cryo-trap, which was installed inline between membrane and mass spectrometer and stops liquid water by freezing it to solid ice. However, even during normal operation, water vapour is the major contribution to the permeate. The water vapour is partially freezing-out in the cryo-trap, which constantly reduces the free cross-section of the vacuum line. This reduction changes the overall conductivity of the vacuum line, changes the pressure gradient across the membrane, and ultimately shifts the membrane selectivity (chapter 2). The result is a gradual drift of the N_2/Ar baseline and needs additional calibration in long-term measurements. The improved reliability of the shielded membrane probe permits operation without inline cryo-trap to avoid clogging and the resulting drift of the N_2/Ar signal ratio.

The obtained results were in good agreement with concomitantly performed isotope pairing incubations of the short-term batch type, but disagreed with some of the core incubations of the flow-through type (chapter 3). It is discussed in chapters 3 & 4 that "bottle effects" caused by insufficient oxygen supply during incubation may account to this discrepancy between N_2 profiling and flow-through incubation.

Factors controlling benthic nitrate consumption

The benthic nitrate consumption was dependent on the bottom water nitrate concentrations in the North Sea (chapters 3 & 4) and the Benguela Upwelling System (chapter 5). Nitrate consumption in North Sea sediment was dependent on the sediment TOC but independent of temperature and oxygen concentration (chapters 3 & 4). In contrast, TOC had no clear effect in Benguela sediment, whereas oxygen and temperature correlated significant with nitrate consumption. Similarly to nitrate consumption, N_2 fluxes from sediment into water column as a result of elimination of reactive nitrogen were dependent on bottom water nitrate and TOC in North Sea sediment (chapters 3 & 4) and on temperature and oxygen in Beguela sediment (chapter 5), respectively.

These conflictive correlations may express fundamental differences between coastal North Sea and Benguela. However, spatial heterogeneity and additional but neglected factors such as macrozoobenthos activity and sediment reactivity may add random noise or bias to the measured rates of nitrate consumption and N_2 production. If the effect of a factor with low variance within an individual dataset is lower than the random noise of the observed reaction rates, then statistical analysis may fail to detect this effect. With this in mind, the apparent conflictive correlation analyses of North Sea and Benguela measurements may be resolved: Nitrate consumption and N_2 production of both North Sea and Benguela correlated with the factors that had substantial variation during sampling, whereas factors with low variance had less correlation. Specifically, oxygen and temperature had little variance during North Sea sampling (chapters 3 & 4), and nitrate and TOC had only minor variation in Benguela sediment (chapter 5), and none of these had significant correlation with N-turnover. However, plotted against the simplified estimator $2\log_{10}(c_{nit}) + \log_{10}(TOC)$ (chapter 4), the assembled rates of nitrate consumption and N_2 production line up in good correlation with the estimator (Fig. 6.1) and are in agreement with the collection of published data (Fig. 4.8). This ultimately suggests that random scatter indeed disguised impact of low-variance factors on N-turnover measurements.

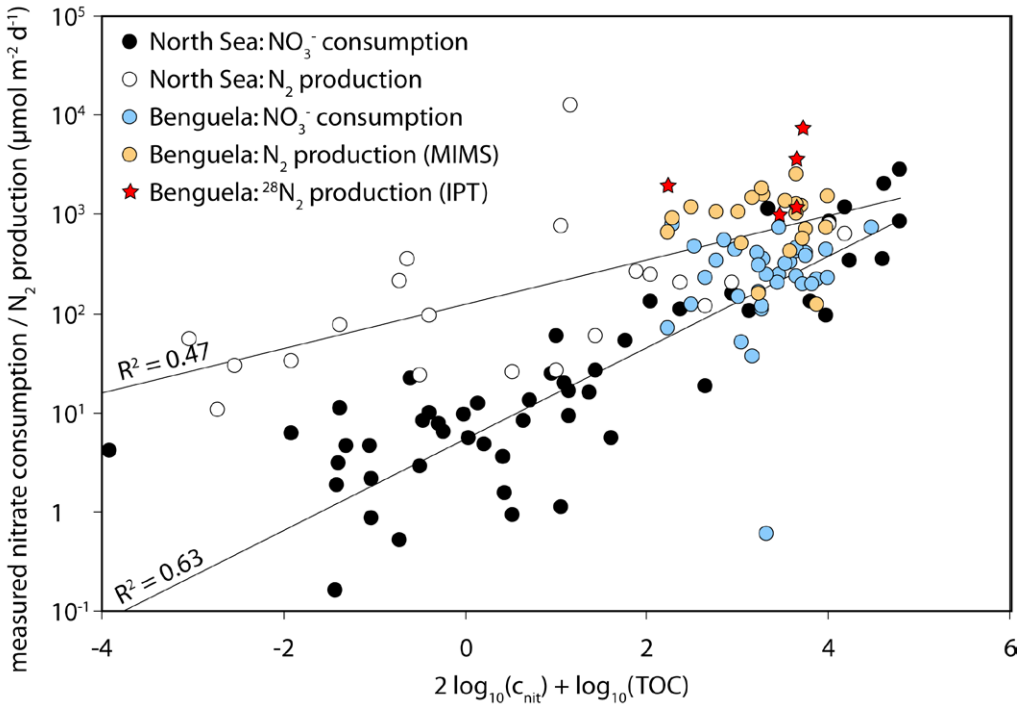

Fig. 6.1: Measured nitrate consumption and N_2 production vs. simplified estimator (chapter 4). Data from North Sea (Pr-0309, Pr-0909, He-304, He-318, Sylt / Büsum monitoring, chapters 3 & 4) and from Benguela Current System (MSM 17/3, chapter 5), respectively. Solid lines represent linear regresion of either combined N_2 productions or nitrate consumptions.

Furthermore, measured nitrate consumption rates of this study and published results (tab. 4.2) correlated well with the transport-centered regression model developed in chapter 4 (Figs. 4.8, 6.1), which seems to indicate that benthic nitrate consumption is ultimately controlled by the intensities of the downward fluxes of oxygen and nitrogen. The assembled data further indicates that sediment in high-oxygen-low-nitrate condition produces substantially more N_2 than is supported by nitrate influx, which suggests internal N-turnover by e.g. coupled nitrification-denitrification. Ammonification mobilizes nitrogen from organic matter and results of chapter 5 (tab. 5.2) indicate that ammonification intensity is dependent on the bulk C_{org}:N_{tot} ratio. Since ammonium is the substrate of coupled nitrificatrion-denitrification, it is to be expected that coupled nitrification-denitrification and hence, total N_2 production is dependent on reactivity proxies derived from bulk C_{org}:N_{tot} ratio or amino acid spectrums (Jennerjahn & Ittekkot 1997, Gaye-Haake et al. 2005). However, reactivity is not implemented in the transport-centered regression model and consequently, assembled N_2 production correlated generally less with the model-derived estimator (Figs. 4.8 & 6.1).

The fate of the Elbe nitrate load

Direct elimination of water column nitrate removed generally less than 4 % of the Elbe nitrate load, and agrees with the observed conservative mixing of nitrate-rich Elbe water and low-nitrate North Sea water. The observed N_2 production equalled 3-7 % of the Elbe nitrate discharge during late winter and 19-43 % during late summer, respectively (chapter 4). Observed N_2 production rates were up to one order of magnitude higher than is explainable with nitrate influx, which indicates intensive nitrification coupled to denitrification. Since the ammonium fuelling nitrification originates from the decomposition of particulate organic matter (POM), it implies that assimilation by phytoplankton during primary production is the most important process of nitrate removal in the German Bight. POM-bound nitrogen is either exported northward with the circulation of the North Sea, or deposited at the sediment-water interface. In permeable sediment, which represents the majority of North Sea sediment, deposited POM is efficiently degraded in the presence of high oxygen availability, and organic nitrogen is converted to nitrate via ammonification and subsequent nitrification. Depending on reactivity of the sediment and percolation rates, the recycled nitrate is subsequently either exported back into the water column or eliminated to N_2 by coupled nitrification-denitrification. As a result, the N_2 production rates in permeable sediment generally exceed the nitrate flux from the water column into the sediment by one order of magnitude (chapter 4). Model-based considerations further suggest that anoxic episodes of the Elbe estuary during past decades probably enhanced denitrification in permeable sediment and thus promoted the removal of nitrate by direct denitrification, which probably shifted the balance of denitrification and nitrate assimilation toward denitrification. However, the elimination of reactive nitrogen by coupled nitrification-denitrification is by far less efficient in fine-grained, diffusion-controlled sediment. Such sediment prevails in the mud aggregation areas near the island Helgoland and shallow intertidals of Wadden Sea and Elbe estuary (chapter 4). There, POM-bound nitrogen is transiently buried in anoxic sediment and slowly diffusing upward to the sediment-water interface as ammonium.

Future work: Overcoming diffusion

A limitation of the membrane inlet used for this study and other needle-type inlets (Lloyd et al. 1996, Hartnett & Seitzinger 2003) is the long measuring time compared to other techniques such as electrodes or optodes. One reason is that molecular diffusion transport the gaseous permeate from the membrane toward the mass spectrometer, which is slow in narrow tubes. A second reason is the application of relatively thick silicone membranes to provide the necessary mechanical strength for insertion into

sediment. But the membrane is to be crossed by the measured gases in a diffusion-type process (chapter 1) and response time is directly affected by the membrane thickness. The first issue can be addressed by purging the membrane with helium as illustrated in figure 6.2, which is basically an inverse flow-through inlet (compare: Fig 1.4). Purging with a high pressure gradient between membrane and roughing pump would result in viscous flow with higher flow velocities compared to molecular diffusion. The helium purge would further stabilize the pressure gradient across the membrane and would reduce the effect of stirring and porosity (chapter 2), but it won't eliminate this effect because diffusion still controls transport within sediment and different diffusivities will inevitably result in shifting concentration ratios.

The second reason of high response time can be addressed by replacing the solid silicone membrane by a porous hollow fibre coated with a very thin membrane film (e.g. Polyoctylmethylsiloxan, POMS). Such membranes are already successfully introduced for flow-through membrane inlets (Pohlmann 2010), but this membrane type is too fragile to be used for sediment probes. But the combination of helium purging and thin-film membrane may reduce the response time sufficiently below 1 s to enable application of the eddy correlation technique (Berg et al. 2003, Lorrai et al. 2010). This relatively novel, non-invasive method measures fluctuations of solute concentrations simultaneously with the three-dimensional water flow velocity, which enables establishing the exchange rates between sediment and water column under in-situ flow conditions. This technique is capable of measuring exchange rates just above the sediment under in-situ flow conditions, which yields more realistic turnover rates especially in advection-controlled permeable sediment. Recently, Johnson et al. (2011) demonstrated successful application of eddy-correlation technique to nitrate measurements, and combination of eddy-correlation technique with very fast MIMS will enable establishing rates of N-elimination in advection-controlled sediment under realistic conditions.

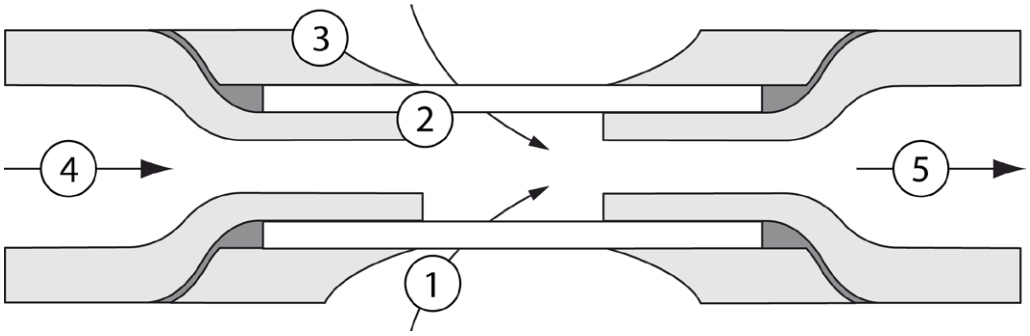

Fig. 6.2: Proposed inverse flow-through membrane inlet with helium-purged membrane for fast in-situ measurements. Dissolved gases (1) are diffusing through the thin-film membrane (2), which is protected by a jacket (3). A stream of helium (4) is purging the membrane and transporting the sample stream (5) toward the mass spectrometer.

Sketching a simple estimation model for N-elimination in permeable sediment

The development of a prediction model for diffusive nitrate uptake and N_2 release derived from basic transport considerations was demonstrated in chapter 4. However, a prediction model for diffusive fluxes is of limited use in permeable sediment. But the mindset underlying the diffusion model helps sketching a model for permeable sediment with advective pore water flow. Analogously to the diffusion model (chapter 4), denitrification commences when the local oxygen concentration is sufficiently low to loosen the inhibitory effects of oxygen on denitrification. The necessary time for oxygen depletion (t_1) is obviously dependent on initial oxygen concentration in the bottom water and the reactivity of the sediment. Subsequent nitrate consumption is likewise dependent on residence time (t_2) and initial nitrate concentration. The pore-water velocity varies along the sediment surface as result of pressure variation (Elliott & Brooks 1997). The horizontal coordinates of starting points of a flow paths with residence times t_1 and t_2 may be denoted X_1 and X_2, respectively. Flow field and position-dependent inflow velocity and residence time are illustrated in figure 6.X. For any point X along the sediment surface, it is possible to estimate the fraction of initially entering oxygen and nitrate that is consumed during the passage through the sediment. At high concentration and short residence, the perfusing oxygen / nitrate has not enough time for complete consumption ($t < t_1$ / $t < t_2$). Low concentration and long residence leaves parts of the sediment short of oxygen / nitrate ($t > t_1$ / $t > t_2$).

(6.1) $x \leq x_1$: $AOU = u \times c_{oxy} \times \frac{t}{t_1}$

$x > x_1$: $AOU = u \times c_{oxy}$

AOU: advective oxygen uptake
u: vertical inflow velocity at sediment surface
c_{oxy}: initial oxygen concentration
t: residence time in sediment
t_1: residence time for oxygen depletion

Employing the normalization of the Elliott & Brooks model (1997) enables estimating the uptake of oxygen and nitrate of a rippled bed. Briefly, bottom water entering at a position X* (0 < X* < 0.5 π) re-emerges at the position –X* after a time t*. X* scales with the ripple spacing, t* scales with permeability, dynamic head and ripple spacing as explained in detail in Elliott & Brooks (1997). See also figure 6.3.

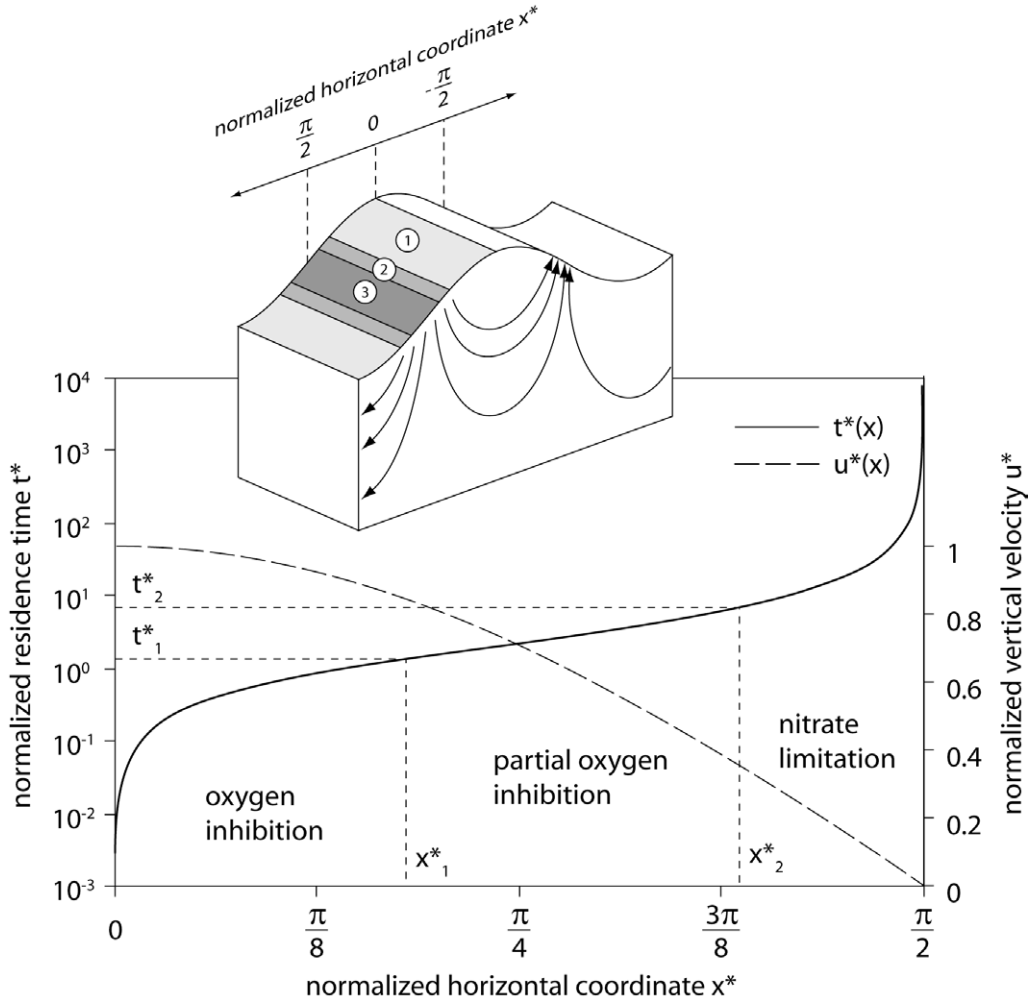

Fig. 6.3: Model-view of pore-water advection induced by flow over rippled sediment. The diagram shows residence time (t) and inflow velocity (u) as functions of the horizontal coordinate (X). Briefly: Bottom water enters the sediment at position x with a downward velocity u, and re-emerges at position –X after a time t. Water entering at X_1* resides just long enough for oxygen depletion (t_1*), water entering at X_2* resides just long enough for consecutive oxygen and nitrate depletion (t_2*). Illustration based on model of Elliott & Brooks (1997).

The areal uptake of oxygen can then be estimated with

$$AOU^* = \int_0^{x_1^*} \frac{t(x^*)}{t_1} \times u^*(x) \times c_{oxy}^* \, dx + \int_{x_1^*}^{0.5\pi} u^*(x) \times c_{oxy}^* \, dx \qquad (6.2)$$

AOU: advective oxygen uptake
X_1^*: normalized critical horizontal position where $t = t_1$
t_1^*: normalized time for oxygen depletion
u*(x): normalized position-dependent vertical velocity at surface
c_{oxy}: bottom water oxygen concentration
t*(x): normalized, position-dependent residence time

The flow path starting at x_1^* is the longest path without nitrate reduction, and any nitrate entering between 0 and x_1^* is passing unaffected through the sediment. The critical inflow position x_1^* is representative for the sediment fraction that remains oxygenated. The sediment is anoxic if x_1^* equals 0 and is close to full oxygenation if x_1^* approaches 0.5 π, respectively. The position x_2^* corresponds to the flow path where the residence time matches the necessary time for consecutive consumption of oxygen and nitrate. The normalized nitrate uptake is then

$$ANU^* = \int_{x_1^*}^{x_2^*} \frac{t(x^*)}{t_2} \times u^*(x) \times c_{nit}^* \, dx + \int_{x_2^*}^{0.5\pi} u^*(x) \times c_{nit}^* \, dx \qquad (6.3)$$

ANU: advective nitrate uptake
X_2^*: normalized critical horizontal position where $t = t_2$
t_2^*: normalized time for oxygen and nitrate depletion
u*(x): normalized position-dependent vertical velocity at surface
c_{nit}: bottom water nitrate concentration
t*(x): normalized, position-dependent residence time

Applying the equations 6.2 and 6.3 to various combinations of filtration rate, oxygen and nitrate concentrations yields the diagrams shown in figure 6.4, which mirror the results of Cardenas et al. (2008) featured in figure 4.11. Generally, nitrate consumption is a non-linear and non-monotonic function of filtration rate and concentrations of nitrate and oxygen. A high degree of sediment oxygenation expressed a high X_1^*

results in high oxygen consumption rates and low nitrate consumption rates, and the nitrate consumption is virtually independent from the nitrate concentration. In contrast, nitrate consumption is sensitive to nitrate and oxygen concentration at low sediment oxygenation (low X_1*).

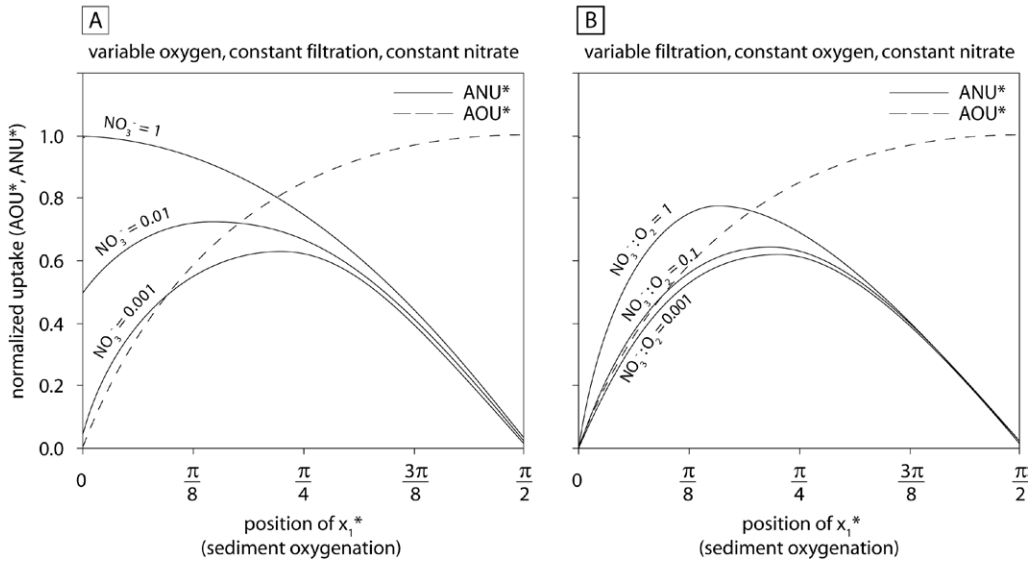

Fig. 6.4: Effect of variable sediment oxygenation on advective uptake of oxygen (AOU) and nitrate (ANU), calculated with equations 6.2 & 6.3. Left panel: Sediment oxygenation is function of initial oxygen concentration, filtration rate is constant. Solid lines represent ANU of different initial nitrate concentrations as function of sediment oxygenation. Right panel: Sediment oxygenation is function of filtration rate, oxygen concentration is constant. Solid lines represent ANU of different nitrate : oxygen ratios as function of sediment oxygenation.

In summary, direct measurement of sediment oxygenation (with planar optodes, Glud et al. 1996) or filtration rate (with tracer, Reimers et al. 2004) in addition to bottom water concentrations of nitrate and oxygen nitrate may be sufficient to fit a simple statistical model to spot measurements of nitrate consumption and N_2 production in advection-controlled sediment as has been demonstrated in chapter 4 for diffusion-controlled sediment. Once such model is established, it can be employed for ecosystem models or interpolations of spot-measurements as demonstrated in chapter 4.

7. Appendix

7.1 List of sampled stations

Tab. 7.1: Overview of the sampled stations in the Elbe estuary, German Bight and Wadden Sea. S: sediment sliced in 1 cm intervals, PW: pore water sampling; Ox: oxygen concentration profiles; MS: concentration profiles of N_2 measured with needle-type membrane inlet mass spectrometry.

Cruise	Station	Longitude	Latitude	Depth (m)	Processing
Pr-0309	ML	53° 32.6‘ N	9° 47.5‘ E	2	
	STS	53° 42.9‘ N	9° 26.5‘ E	3	
●	BR	53° 51.9‘ N	9° 13.6‘ E	3	
	NW	53° 53.0‘ N	9° 1.8‘ E	4	
	KL	53° 58.1‘ N	8° 41.6‘ E	5	
	TR	54° 3.8‘ N	8° 42.3‘ E	10	
	TS	54° 9.8‘ N	8° 40.0‘ E	6	
	WW	54° 15.1‘ N	8° 43.6‘ E	5	
	EI	54° 16.7‘ N	8° 54.9‘ E	3	
He-304	320	54° 5.2‘ N	8° 9.7‘ E	17	
	321	54° 14.1‘ N	7° 19.9‘ E	40	
★	324	54° 25.1‘ N	6° 0.1‘ E	37	
	327	54° 39.9‘ N	6° 0.2‘ E	38	
	332	54° 60.0‘ N	5° 29.9‘ E	37	
	334	54° 50.1‘ N	5° 30.0‘ E	39	
	335	54° 45.0‘ N	5° 30.0‘ E	40	
	336	54° 40.0‘ N	5° 30.1‘ E	40	
	337	54° 35.0‘ N	5° 30.1‘ E	40	
	338	54° 30.1‘ N	5° 29.9‘ E	39	
	339	54° 25.0‘ N	5° 30.0‘ E	39	
	341	54° 6.0‘ N	8° 0.1‘ E	26	
	343	54° 6.5‘ N	7° 45.0‘ E	38	
	350	54° 1.6‘ N	8° 15.1‘ E	11	
	351	54° 6.0‘ N	8° 15.1‘ E	14	
	353	54° 16.0‘ N	8° 15.0‘ E	10	
	354	54° 20.9‘ N	8° 14.9‘ E	12	

Overview of Multicorer-stations (continued)

Cruise	Station	Longitude	Latitude	Depth (m)	Processing
Pr-0909	ML	53° 32.7‘ N	9° 47.7‘ E	2	
	STS	53° 43.6‘ N	9° 25.7‘ E	3	
○	BR	53° 52.2‘ N	9° 12.7‘ E	3	
	NW	53° 53.0‘ N	9° 1.8‘ E	4	
	KL	53° 58.1‘ N	8° 41.6‘ E	5	
	TR	54° 3.8‘ N	8° 42.3‘ E	10	
	TS	54° 9.8‘ N	8° 39.9‘ E	6	
	BOS	54° 12.1‘ N	8° 35.2‘ E	5	
	FP	54° 13.8‘ N	8° 37.3‘ E	4	
	SOS	54° 25.1‘ N	8° 30.7‘ E	5	
	KO	54° 44.7‘ N	8° 20.9‘ E	4	
He-318	177	54° 14.5‘ N	7° 20.0‘ E	40	
	180	55° 48.3‘ N	3° 53.0‘ E	50	
☆	181	55° 40.2‘ N	4° 0.6‘ E	37	
	182	55° 30.1‘ N	3° 59.8‘ E	33	
	189	55° 10.0‘ N	5° 0.1‘ E	42	
	191	55° 0.0‘ N	4° 59.2‘ E	42	
	193	54° 50.0‘ N	5° 0.0‘ E	41	
	195	54° 39.7‘ N	5° 5.0‘ E	46	
	196	54° 5.7‘ N	8° 4.1‘ E	23	
	197	54° 5.3‘ N	8° 9.5‘ E	21	
	199	54° 21.0‘ N	8° 0.0‘ E	17	
	209	54° 45.0‘ N	7° 15.0‘ E	27	
	210	54° 45.0‘ N	7° 30.0‘ E	24	
	212	54° 45.0‘ N	8° 0.0‘ E	6	
	214	54° 53.0‘ N	7° 45.0‘ E	21	
	216	54° 53.0‘ N	7° 15.0‘ E	27	
List	1	55° 1.5‘ N	8° 25.9‘ E	1	
	2	55° 1.4‘ N	8° 26.2‘ E	1	
Büsum	1	54° 4.1‘ N	8° 58.4‘ E	1	
	2	54° 6.6‘ N	8° 56.4‘ E	1	

Tab. 7.2: Overview of Multicorer-stations of the cruise MSM 17/3, and the processing of retrieved sediment cores. S: sediment sliced in 1 cm intervals, PW: pore water sampling; Ox: oxygen concentration profiles; MS: concentration profiles of N_2 , CO_2, CH_4, H_2S measured with needle-type membrane inlet mass spectrometry; IP: isotope pairing incubation with ^{15}N-nitrate; B: survey of Macrozoobenthos.

Station	Latitude	Longitude	Depth (m)	Cores	Processing
224	23° 0.00‘ S	14° 3.00‘ E	135	Y	S, PW, B
225	23° 30.00‘ S	14° 0.00‘ E	165	Y	S, B
226	23° 30.77‘ S	13° 30.27‘ E	228	Y	S, PW, Ox, B
228	24° 2.68‘ S	14° 0.32‘ E	212	Y	S, B
229	24° 30.72‘ S	14° 20.10‘ E	120	Y	S, PW
230	25° 0.00‘ S	14° 0.00‘ E	180	N	-
231	26° 0.00‘ S	14° 30.00‘ E	190	Y	S, PW, Ox, B
232	26° 40.00‘ S	15° 3.60‘ E	39	N	-
233	26° 40.00‘ S	14° 45.59‘ E	180	Y	S, PW, IP, B
234	26° 40.00‘ S	14° 25.00‘ E	325	Y	S, PW
235	26° 40.00‘ S	14° 0.00‘ E	417	Y	S, PW, Ox, B
236	26° 40.00‘ S	13° 30.00‘ E	1100	Y	S, PW, Ox, IP, B
237	26° 0.00‘ S	13° 33.00‘ E	750	Y	S, PW, Ox
238	25° 0.00‘ S	13° 19.99‘ E	1080	Y	S, PW, Ox
239	24° 30.00‘ S	13° 42.00‘ E	356	N	-
240	24° 0.00‘ S	13° 6.60‘ E	735	Y	S, PW, Ox, B
241	23° 0.00‘ S	11° 45.00‘ E	2970	Y	S, PW, Ox, MS
242	23° 0.00‘ S	12° 30.00‘ E	1640	Y	S, PW, Ox
243	23° 0.00‘ S	12° 48.00‘ E	905	Y	S, PW, Ox, IP, B
246	23° 0.00‘ S	13° 3.00‘ E	410	Y	S, PW, Ox, B
250	22° 59.98‘ S	13° 20.01‘ E	350	Y	S, PW, Ox, MS, B
254	23° 0.00‘ S	13° 40.00‘ E	155	Y	S, PW, Ox, MS, B
264	22° 59.98‘ S	14° 20.02‘ E	66	Y	S, PW, MS
266	22° 45.90‘ S	13° 28.08‘ E	250	Y	S, Ox
267	22° 1.16‘ S	13° 10.78‘ E	205	Y	S, Ox, MS
268	21° 1.75‘ S	13° 29.18‘ E	23	Y	S, PW, Ox, MS, IP, B
269	20° 59.98‘ S	13° 20.00‘ E	98	Y	S, PW, Ox, MS, B
270	20° 59.93‘ S	13° 10.05‘ E	125	Y	S
271	20° 59.99‘ S	12° 50.01‘ E	196	Y	S, PW, MS, B
272	21° 0.00‘ S	12° 30.00‘ E	425	Y	S, PW, Ox, MS, B
274	20° 0.00‘ S	11° 50.00‘ E	408	Y	S, PW, Ox, MS, B
275	20° 0.00‘ S	12° 10.01‘ E	275	Y	S
276	20° 0.00‘ S	12° 30.00‘ E	153	Y	S, PW, Ox, MS, B
277	20° 0.00‘ S	12° 50.00‘ E	99	Y	S, IP

Overview of Multicorer-stations (continued)

Station	Latitude	Longitude	Depth (m)	Cores	Processing
278	20° 0.00‘ S	13° 0.00‘ E	30	Y	S, PW, Ox, MS, B
279	19° 0.08‘ S	12° 27.05‘ E	35	Y	S, PW, MS, B
292	19° 0.00‘ S	11° 26.00‘ E	416	Y	S, PW, Ox, MS, IP
295	19° 0.00‘ S	11° 0.00‘ E	1290	Y	S, PW, Ox, MS
298	19° 0.00‘ S	10° 30.00‘ E	2063	Y	S, PW, Ox, MS, B
299	18° 30.00‘ S	11° 25.00‘ E	436	Y	S, PW, Ox, MS, IP, B
300	18° 0.00‘ S	11° 30.00‘ E	237	Y	S, Ox, MS, B
304	17° 15.00‘ S	11° 43.00‘ E	35	Y	S, PW, Ox, MS, B
305	17° 15.24‘ S	11° 30.39‘ E	142	Y	S, PW, Ox, MS, B
306	17° 15.00‘ S	11° 17.30‘ E	500	Y	S, PW, Ox, MS, IP
307	17° 15.00‘ S	11° 11.00‘ E	915	N	-
308	17° 15.00‘ S	11° 0.00‘ E	2103	Y	S, PW, Ox, MS, B
309	17° 15.00‘ S	10° 47.00‘ E	2939	Y	S, PW, Ox, MS, B
310	17° 15.00‘ S	10° 30.00‘ E	3247	Y	S, PW, Ox, MS, B
311	17° 15.00‘ S	11° 11.00‘ E	922	Y	S, PW, Ox
316	17° 15.00‘ S	10° 0.00‘ E	3921	Y	S, PW, Ox, MS, B

7.2 List of figures

7.3 List of tables

7.4 List of used abbreviations

AAIW	Antarctic Intermediate Water
ABFZ	Angola-Benguela Frontal Zone
AIT	acetylene inhibition technique
Ar	argon
AOU	apparent oxygen utilization
ARGE	Elbe River Basin Community
BC	benthic flux chamber
BSH	Federal Maritime and Hydrographic Agency
C_{org}	organic carbon
CFI	core flux incubation
D_{50}	median grain diameter
DIN	dissolved inorganic nitrogen (ammonium, nitrate, nitrite)
DNRA	dissimilatory nitrate reduction to ammonium
DNU	diffusive nitrate uptake
DOU	diffusive oxygen uptake
ESACW	Eastern South Atlantic Central Water
HELCOM	Baltic Marine Environment Protection Commission
$HgCl_2$	mercury chloride
HZG	Helmholtz Centre for Materials and Coastal Research Geesthacht
ID	inner diameter
IL	isotopic labeling
IPI / IPT	isotope pairing incubation, isotope pairing technique
LLUR	State Agency for Agriculture, Environment and Rural Areas of Schleswig-Holstein
MIMS	membrane inlet mass spectrometry
$MgCl_2$	magnesium chloride
MUDAB	Marine Environmental Data Base
m/z	mass : charge ratio of ions

N	nitrogen
N*	apparent nitrogen deficit
^{14}N	stable nitrogen isotope with the the mass 14 amu
^{15}N	stable nitrogen isotope with the the mass 15 amu
N_2	dinitrogen gas
N_{tot}	total nitrogen
NADW	North Atlantic Deep Water
NCF	nitrate consumption factor
NH_4^+	ammonium ion
N_2O	nitrous oxide
NO_2^-	nitrite ion
NO_3^-	nitrate ion
O_2	oxygen molecule
OD	outer diameter
OPD	oxygen penetration depth
OSPAR	Convention for the Protection of the Marine Environment of the North-East Atlantic
P	phosphorous
Pb	lead
PPM	pore-water profile modeling technique
POC	particulate organic carbon
POM	particulate organic matter
RV	research vessel
SACW	South Atlantic Central Water
TOC	total organic carbon
WFD	European Water Framework Directive

8. References

Albers T. and N. von Lieberman (2007): Morphologische Veränderungen von Wattflächen am Beispiel des Neufelder Sandes in der Elbmündung. Coastline Reports 9, 81-92.

Allen S. E. and B. M. Hickey (2010): Dynamics of advection-driven upwelling over a shelf break submarine canyon. Journal of Geophysical Research, vol. 115, C08018, 1-20.

Aller R. C. (1980): Quantifying solute distributions in the bioturbated zone of marine-sediments by defining an average micro-environment. Geochim. Cosmochim. Acta, vol. 44, 1955–1965.

Ankele M. (2010): Evaluation of methods to balance oxygen concentration during sediment core incubations. Diplomarbeit, Fachbereich Naturwissenschaftliche Technik, Hochschule für Angewandte Wissenschaften Hamburg.

Amann T., A. Weiss, and J. Hartmann (2012): Carbon dynamics in the freshwater part of the Elbe estuary, Germany: Implications from improving water quality. Manuscript in preparation.

An S., W. S. Gardner and T. Kana (2001): Simultaneous measurement of denitrification and nitrogen fixation using isotope pairing with membrane inlet mass spectrometry analysis. Applied and Environmental Microbiology 67, 1171–1178.

An S., W. S. Gardner (2002): Dissimilatory nitrate reduction to ammonium (DNRA) as a nitrogen link, versus denitrification as a sink in a shallow estuary (Laguna Madre/ Baffin Bay, Texas). Marine Ecology Progress Series 237, 41–50.

ARGE (2007): Sauerstoffgehalte der Tideelbe. Arbeitsgemeinschaft zur Reinerhaltung der Elbe, 2007.

Axler R. P. and J. E. Reuter (1996): Nitrate uptake by phytoplankton and periphyton: Whole-lake enrichments and mesocosm-15N experiments in an oligotrophic lake. Limnology and Oceanography 41, no. 4, 659-671.

Barange M. and S. C. Pillar (1992): Cross-shelf circulation, zonation and maintenance mechanisms of Nyctiphanes capensis and Euphausia hanseni (Euphausiacea) in the northern Benguela upwelling system. Continental Shelf Research 12, no. 9, 1027–1042.

Bartlett R., R. J.G. Mortimer, and K. Morris (2008): Anoxic nitrification: Evidence from Humber Estuary sediments (UK). Chemical Geology 250, 29–39.

Beddig S., U.H. Brockmann, W. Dannecker, D. Körner, T. Pohlmann, W. Puls, G. Radach, A. Rebers, H.-J. Rick, M. Schatzmann, H. Schlünzen, and M. Schulz (1997): Nitrogen fluxes in the German Bight. Marine Pollution Bulletin 34, no. 6, 382-394.

Behrendt H. and D. Opitz (1999): Retention of nutrients in river systems: Dependence on specific runoff and hydraulic load. Hydrobiologia, 410, 111-122.

Berg P, N. Risgaard-Petersen, and S. Rysgaard (1998). Interpretation of measured concentration profiles in sediment pore water. Limnol. Oceanogr. 43 (7), 1500-1510.

Berg P., H. Røy, F. Janssen, V. Meyer, B. B. Jørgensen, M. Huettel, and D. de Beer (2003): Oxygen uptake by aquatic sediments measured with a novel non-invasive eddy-correlation technique. Marine Ecology Progress Series 261, 75-83.

Bernardo P., E. Drioli, and G. Golemme (2009): Membrane gas separation: A review/ State of the art. Industrial and Engineering Chemistry Research 48, 4638- 4663.

Beyer W (1964). Zur Bestimmung der Wasserdurchlässigkeit von Kiesen und Sanden aus der Kornverteilungskurve. WWT 14: 165-168, Berlin.

Billerbeck M., U. Werner, L. Polerecky, E. Walpersdorf, D. de Beer, and M. Huettel (2006): Surficial and deep pore water circulation governs spatial and temporal scales of nutrient recycling in intertidal sand flat sediment. Marine Ecology Progress Series 326, 61–76.

Blott S. J. and K. Pye (2001): GRADISTAT: a grain size distribution and statistics package for the analysis of unconsolidated sediments. Earth Surface Processes and Landforms, 26(11), 1237-1248.

Brandes J.A. and A. H. Devol (1997): Isotopic fractionation of oxygen and nitrogen in coastal marine sediments. Geochim. Cosmochim. Acta 61, no. 9, 1793– 1801.

Brandes J. A., A. H. Devol, and C. Deutsch (2007): New developments in the marine nitrogen cycle. Chem Rev 107, 577–589.

Bremner J. M. and J. P. Willis (1993): Mineralogy and geochemistry of the clay fraction of sediments from the Namibian continental margin and the adjacent hinterland. Marine Geology 115, 85-116.

Breton, M. and J. C. Salomon (1995) A 2D long term advection-dispersion model for the Channel and Southern North Sea Part A: Validation through comparison with artificial radionuclides. Journal of Marine Systems 6, 495-513.

Brion N., W. Baeyens, S. De Galan, M. Elskens, and R. W. Laane (2004): The North Sea: source or sink for nitrogen and phosphorus to the Atlantic Ocean? Biogeochemistry, vol. 68, no. 3, 277-296.

Broecker W. S. and T.-H. Peng (1974): Gas exchange rates between air and sea. Tellus 26, no. 1-2, 21-35.

Brunet R.C. and L. J. Garcia-Gil (1996): Sulfide-induced dissimilatory nitrate reduction to ammonia in anaerobic freshwater sediments. FEMS Microbiol Ecol 21, 131–138.

Bulla L. A., C. M. Gilmour, and W. B. Bollen (1970): Non- biological reduction of nitrite in soil. Nature 225, 664.

Bundy A., J. J. Heymans, L. Morissette, and C. Savenkoff (2009): Seals, cod and forage fish: A comparative exploration of variations in the theme of stock collapse and ecosystem change in four Northwest Atlantic ecosystems. Progress in Oceanography 81, 188–206.

Capone D. G., S. E. Dunham, S. G. Horrigan, and L. E. Duguay (1992): Microbial nitrogen transformations in unconsolidated coral reef sediments. Marine Ecology Progress Series 87, 75-88.

Cardenas M. B., P. L. M. Cook, H. Jiang, and P. Traykovski (2008): Constraining denitrification in permeable wave-influenced marine sediment using linked hydrodynamic and biogeochemical modeling. Earth Planet. Sci. Lett. 275: 127–137.

Carrera J., T. Vicent, and F. J. Lafuente (2003): Influence of temperature on denitrification of an industrial high-strength nitrogen wastewater in a two-sludge system. Water SA, vol. 29, no. 1, 11-16.

Cartaxana P. and D. Lloyd (1999): N2, N2O and O2 Profiles in a Tagus estuary salt Marsh. Estuarine, Coastal and Shelf Science 48, 751–756.

Christensen P. B., L. P. Nielsen, N. P. Revsbech, and J. Sørensen (1989): Microzonation of denitrification activity in stream sediments with a combined oxygen and nitrous oxide microsensor. Appl Environ Microbiol 55, 1234-1241.

Cook P. L. M., F. Wenzhöfer, S. Rysgaard, O. S. Galaktionov, F. J. R. Meysman, B. D. Eyre, J. Cornwell, M. Huettel, and R. N. Glud (2006): Quantification of denitrification in permeable sediments: Insights from a two-dimensional simulation analysis and experimental data. Limnol. Oceanogr.: Methods 4, 294–307.

Cook P. L. M., F. Wenzhöfer, R. N. Glud, F. Jansen, and M. Huettel (2007): Benthic solute exchange and carbon mineralization in two shallow subtidal sandy sediments: Effect of advective pore-water exchange. Limnol. Oceanogr. 52, no. 5, 1943–1963.

Cornwell J. C., W. M. Kemp, and T. M. Kana (1999): Denitrification in coastal ecosystems. Aquatic Ecology 33: 41-54.

Dähnke K., E. Bahlmann, and K.-C. Emeis (2008): A nitrate sink in estuaries? An assessment by means of stable nitrate isotopes in the Elbe estuary. Limnol. Oceanogr. vol. 53, no. 4, 1504–1511.

Dauwe B., J. J. Middelburg, P. M. J. Herman, and C. H. R. Heip (1999): Linking diagenetic alteration of aminoacids and bulk organic matter reactivity. Limnology and Oceanography 44, no. 7, 1809-1814.

de Beer D. and H. van den Heuvel (1988): Response of ammonium-selective microelectrodes based on the neutral carrier nonactin. Talanta 35, 728–730.

de Beer D., F . Wenzhöfer, T. G. Ferdelman, S. E. Boehme, M. Huettel, J. E. E. van Beusekom, M. E. Böttcher, N. Musat, and N. Dubilier (2005): Transport and mineralization rates in North Sea sandy intertidal sediments, Sylt-Römö Basin, Wadden Sea. Limnol. Oceanogr. 50 (1), 113-127.

Deek A. (2011): Sources and sinks of reactive nitrogen in the German Bight. PhD thesis, Universität Hamburg, Hamburg.

Deek A., K. Emeis, and J. van Beusekom (2012): Nitrogen removal in coastal sediments of the German Wadden Sea. Biogeochemistry 108, 467–483.

Deutsch C., N. Gruber, R. M. Key, J. L. Sarmiento, and A. Ganachaud A. (2001): Denitrification and N2 fixation in the Pacific Ocean. Glob. Biogeochem. Cycles 15, 483–506.

Deutsch B., S. Forster, M. Wilhelm, J. W. Dippner, and M. Voss (2010): Denitrification in sediments as a major nitrogen sink in the Baltic Sea: an extrapolation using sediment characteristics. Biogeosciences 7, 3259-3271.

Devol A. H. (1991): Direct measurements of nitrogen gas fluxes from continental shelf sediments. Nature 349, 319-321.

Devol A. H., L. A. Codispoti, and J. P. Christensen (1997): Summer and winter denitrification rates in western Arctic shelf sediments. Continental Shelf Research 17, no. 9, 1029-1050.

DHI Deutsches Hydrographisches Institut (1983): Atlas der Gezeitenströme in der Deutschen Bucht. Bundesamt für Seeschifffahrt und Hydrographie, Hamburg.

Dick S., U.H. Brockmann, J. E. E. van Beusekom, B. Fabiszisky, M. George, U. Hentschke, K.-J. Hesse, B. Mayer, T. Nitz, T. Pohlmann, K. Poremba, K. Schaumann, W. Schönfeld, A. Starke, U. Tillmann, and G. Weide (1999): Exchange of matter and energy between the Wadden Sea and the coastal waters of the German Bight- Estimations based on numerical simulations and field measurements. German Journal of Hydrography, vol. 51, no. 2/3, 181-219.

Dong L. F., D. C. O. Thornton, D. B. Nedwell, G. J. C. Underwood (2000): Denitrification in sediments of the River Colne esturay, England. Marine Ecology Progress Series 203, 109-122.

Dutkiewicz S., B. A. Ward, F. Monteiro, and M. J. Follows (2012): Interconnection of nitrogen fixers and iron in the Pacific Ocean: Theory and numerical simulations. Global Biogeochemical Cycles 26, GB1012.

Elliott A. H., and N. H. Brooks (1997): Transfer of nonsorbing solutes to a streambed with bed forms: Theory. Water Resources Research, Vol. 33, No. 1, 123-136.

Ekman V.W. (1905): On the influence of the earth‘s rotation on ocean currents. Arch. Math. Astron. Phys. 2, no. 11.

Emeis K.-C., V. Brüchert, B. Currie, R. Endler, T. Ferdelman, A. Kiessling, T. Leipe, K. Noli-Peard, U. Struck, and T. Vogt (2004): Shallow gas in shelf sediments of the Namibian coastal upwelling ecosystem. Continental Shelf Research 24, 627–642.

Enoksson V., F. Sörensson, and W. Granél (1990): Nitrogen Transformations in the Kattegat. Ambio, vol. 19, no. 3, 159-166.

Erisman J. W., M. A. Sutton, J. Galloway, Z. Klimont, and W. Winiwarter (2008): How a century of ammonia synthesis changed the world. Nature Geoscience, vol. 1, 636-639.

Ettwig K. F., M. K. Butler, D. Le Paslier, E. Pelletier, S. Mangenot, M. M. M. Kuypers, F. Schreiber, B. E. Dutilh, J. Zedelius, D. de Beer, H. J. Gloerich, C. T. Wessels, T. van Alen, F. Luesken, M. L. Wu, K. T. van de Pas-Schoonen, H. J. M. Op den Camp, E. M. Janssen-Megens, K.-J. Francoijs, H. Stunnenberg, J. Weissenbach, M. S. M. Jetten, and M. Strous. (2010): Nitrite-driven anaerobic methane oxidation by oxygenic bacteria. Nature 464, 543- 548.

Fick, A. (1855): Über Diffusion. Annalen der Physik, vol. 170, no.1, 59-86.

Figge, K. (1981): Karte der Sedimentverteilung in der Deutschen Bucht mit Beiheft. Karte Nr. 2900, DHI Hamburg.

Forster S, B Bobertz, and B Bohling (2003): Permeability of Sands in the Coastal Areas of the Southern Baltic Sea: Mapping a Grain-size Related Sediment Property. Aquatic Geochemistry 9: 171–190, 2003.

Fossing H., T. G. Ferdelman, and P. Berg (2000): Sulfate reduction and methane oxidation in continental margin sediments influenced by irrigation (South-East Atlantic off Namibia). Geochimica et Cosmochimica Acta, vol. 64, no. 5, 897–910.

Franke U, L. Polerecky, E. Precht, and Markus Huettel (2006): Wave tank study of particulate organic matter degradation in permeable sediments. Limnology and Oceanography 51, no. 2, 1084-1096.

Füssel J., P. Lam, G. Lavik, M. M. Jensen, M. Holtappels, M. Günter, and M. M. M. Kuypers (2011): Nitrite oxidation in the Namibian oxygen minimum zone. The ISME Journal, in press.

Garcia H. E. and L. I. Gordon (1992): Oxygen solubility in seawater: Better fitting equations. Limnology & Oceanography 37, 1307-1312.

Gao H., F. Schreiber, G. Collins, M. M. Jensen, J. E. Kostka, G. Lavik, D. de Beer, H. Zhou, and M. M. M. Kuypers (2010): Aerobic denitrification in permeable Wadden Sea sediments. The ISME Journal 4, 417–426.

Gao H., M. Matyka, B. Liu, A. Khalili, J. E. Kostka, G. Collins, S. Jansen, M. Holtappels, M. M. Jensen, T. H. Badewien, M. Beck, M. Grunwald, D. de Beer, G. Lavik, and M. M. M. Kuypers (2012): Intensive and extensive nitrogen loss from intertidal permeable sediments of the Wadden Sea. Limnol. Oceanogr. 57, no. 1, 185-198.

Gaye-Haake B., N. Lahajnar, K.-C. Emeis, T. Rixen, D. Unger, H. Schulz, V. Ramaswamy, A. L. Paropkari, M. V. S. Guptha, and V. Ittekkot (2005). Stable nitrogen isotopic ratios of sinking particles and sediments from the northern Indian Ocean. Marine Chemistry 96, 243-255.

Gideon R. A. and R. A. Hollister (1987): A rank correlation coefficient resistant to outliers. Journal of the American Statistical Association 82, no. 398, 656-666.

Gihring, T. M., A. Canion, A. Riggs, M. Huettel, and J. E. Kostka (2010a): Denitrification in shallow, sublittoral Gulf of Mexico permeable sediments. Limnol. Oceanogr., 55(1), 43–54.

Gihring T. M., G. Lavik, M. M. M. Kuypers, and J. E. Kostka (2010b): Direct determination of nitrogen cycling rates and pathways in Arctic fjord sediments (Svalbard, Norway). Limnol. Oceanogr., 55(2), 740–752.

Glud R. N., J. K. Gundersen, B. B. Jorgensen, N. P. Revsbech, and H. D. Schulz (1994): Diffusive and total oxygen uptake of deep-sea sediments in the eastern South Atlantic Ocean: in situ and laboratory measurements. Deep-Sea Research 1, vol. 41, no. 11, 1767-1788.

Glud R. N., N. B. Ramsing, J. K. Gundersen, and I. Klimant (1996): Planar optodes: a new tool for fine scale measurements of twodimensional O2 distribution in benthic communities. Marine Ecology Progress Series 140, 217-226.

Glud R. N., O. Holby, F. Hoffmann, D. E. Canfield (1998): Benthic mineralization and exchange in Arctic sediments (Svalbard, Norway). Marine Ecology Progress Series 173, 237-251.

Goldhammer T. V. Brüchert, T. G. Ferdelman, and M. Zabel (2010): Microbial sequestration of phosphorus in anoxic upwelling sediments. Nature Geoscience 3, 557-561.

Goldhammer T., B. Brunner, S. M. Bernasconi, T. G. Ferdelman, and Matthias Zabel (2011): Phosphate oxygen isotopes: Insights into sedimentary phosphorus cycling from the Benguela upwelling system. Geochimica et Cosmochimica Acta 75, 3741–3756.

Grasshoff K., M. Erhardt, and K. Kremling (1983): Methods of Seawater Analysis, Verlag Chemie, Weinheim.

Greenwood N., E. R. Parker, L. Fernand, D. B. Sivyer, K. Weston, S. J. Painting, S. Kröger, R. M. Forster, H. E. Lees, D. K. Mills, and R. W. P. M. Laane (2010): Detection of low bottom water oxygen concentrations in the North Sea; implications for monitoring and assessment of ecosystem health. Biogeosciences 7, 1357–1373.

Gruber N. and J. N. Galloway (2008): An Earth-system perspective of the global nitrogen cycle. Nature, vol. 451, 293-296.

Hamme R. C. and S. R. Emerson (2004): The solubility of neon, nitrogen and argon in distilled water and seawater. Deep-Sea Research, vol. 51, 1517–1528.

Harley C. D. G., A. R. Hughes, K. M. Hultgren, B. G. Miner, C. J. B. Sorte, C. S. Thornber, L. F. Rodriguez, L. Tomanek, and S. L. Williams (2006): The impacts of climate change in coastal marine systems. Ecology Letters 9, no. 2, 228–241.

Hartnett H. E. and S. P. Seitzinger (2003): High-resolution nitrogen gas profiles in sediment porewaters using a new membrane probe for membrane-inlet mass spectrometry. Marine Chemistry 83, 23– 30.

Hebbeln D., C. Scheurle, and F. Lamy (2003): Depositional history of the Helgoland mud area, German Bight, North Sea. Geo-Mar. Letters 23, 81–90.

Hensen C., M. Zabel, and H. D. Schulz (2000): A comparison of benthic nutrient fluxes from deep-sea sediments off Namibia and Argentina. Deep-Sea Research II 47, 2029-2050.

Hertweck G. (1983): Das Schlickgebiet in der inneren Deutschen Bucht. Aufnahme mit dem Sedimentechographen. Senckenbergiana maritima 15, 219–249.

Higashino, M. and H. Stefan (2008): Velocity pulse model for turbulent diffusion from flowing water into stream bed. Journal of Environmental Engineering, vol. 134, no. 7, 550-560.

Hoffman D., B. Singh, and J. H. Thomas III. (1997): Handbook of vacuum science and technology. Academic Press, London, 3-55.

Howarth R.W., G. Billen, D. Swaney, A. Townsend, N. Jarowski, K. Lajtha, J. A. Downing, R. Elmgren, N. Caracao, T. Jordan, F. Berendse, J. Freney, V. Kudeyarov, P. Murdoch, and Z. Zhao-Ling (1996): Regional nitrogen budgets and riverine N & P fluxes for the drainages to the North Atlantic Ocean: natural and human influences. Biogeochemistry 35, 75–139.

Huettel M., W. Ziebis, and S. Forster (1996): Flow-induced uptake of particulate matter in permeable sediments. Limnol. Oceanogr. 41(2), 309-322.

Huettel M., W. Ziebis, S. Forster, and G. W. Luther III (1998): Advective transport affecting metal and nutrient distributions and interfacial fluxes in permeable sediments. Geochimica et Cosmochimica Acta, vol. 62, no. 4, 613–631.

Huettel M. and A. Rusch (2000): Transport and degradation of phytoplankton in permeable sediment. Limniol. Oceanogr., vol. 45, no. 3, 534-549.

Hulth S., R. C. Aller, and F. Gilbert (1999): Coupled anoxic nitrification/ manganese reduction in marine sediments. Geochimica et Cosmochimica Acta, Vol. 63, No. 1, 49- 66.

Hydes D. J., B. A. Kelly-Gerreyn, A. C. Le Gall, and R. Proctor (1999): The balance of supply of nutrients and demands of biological production and denitrification in a temperate latitude shelf sea – a treatment of the southern North Sea as an extended estuary. Marine Chemistry, 68: 117–131.

Inthorn, M. T. Wagner, G. Scheeder, and M. Zabel (2006): Lateral transport controls distribution, quality, and burial of organic matter along continental slopes in high-productivity areas. Geology 34, no. 3, 205-208.

Inthorn M., V. Mohrholz, and M. Zabel (2006b): Nepheloid layer distribution in the Benguela upwelling area offshore Namibia. Deep-Sea Research I, vol. 53, 1423–1438.

Islas-Limaa S., F. Thalassoa, and J. Gómez-Hernandez (2004): Evidence of anoxic methane oxidation coupled to denitrification. Water Research 38, 13–16.

Janssen F., M. Huettel, and U. Witte (2005): Pore-water advection and solute fluxes in permeable marine sediments (II): Benthic respiration at three sandy sites with different permeabilities (German Bight, North Sea). Limnol. Oceanogr., vol. 50, no. 3, 779–792.

Jennerjahn T. C. and V. Ittekkot (1997): Organic Matter in sediments in the mangrove areas and adjacent continental margins of Brazil: I. Amino acids and hexosamines. Oceanologica Acta 20, no. 2, 359-369.

Jenkins M.C. and W. M. Kemp (1984): The coupling of nitrification and denitrification in two estuarine sediments. Limnol. Oceanogr. 29, 609-619.

Jensen K. M., M. H. Jensen, and E. Kristensen (1996): Nitrification and denitrification in Wadden Sea sediments (Königshaven, Island of Sylt, Germany) as measured by nitrogen isotope pairing and isotope dilution. AquaticMicrobial Ecology 11, 181-191.

Johannsen A., K. Dähnke, and K. Emeis (2008): Isotopic composition of nitrate in five German rivers discharging into the North Sea. Organic Geochemistry 39, 1678−1689.

Johnson K. S., J. P. Barry, L. J. Coletti, S. E. Fitzwater, H. W. Jannasch, and C. F. Love (2011): Nitrate and oxygen flux across the sediment-water interface observed by eddy correlation measurements on the open continental shelf. Limnology & Oceanography Methods 9, 543-553.

Joint I. and A. Pomroy (1993): Phytoplankton biomass and production in the southern North Sea. Marine Ecology Progress Series 99, 169-182.

Kalvelage T., M. M. Jensen, S. Contreras, N. P. Revsbech, P. Lam, M. Günter, J. La Roche, G. Lavik, and M. M. M. Kuypers (2011): Oxygen sensitivity of anammox and coupled N-cycle processes in oxygen minimum zones. PLoS ONE, vol. 6, no. 12, in press.

Kamp-Nielsen L. (1975): A kinetic approach to the aerobic sediment-water exchange of phosphorus in Lake Esrom. Ecological Modelling 1, no. 2, 153–160.

Kana T. M., C. Darkangelo, M. D. Hunt, J. B. Oldham, G. E. Bennett, and J. C. Cornwell (1994): Membrane inlet mass spectrometer for rapid high-precision determination of N2, O2, and Ar in environmental water samples. Analytical Chemistry 66, 4166−4170.

Kartal B., M. M. M. Kuypers, G. Lavik, J. Schalk, H. J. M. Op den Camp, M. S. M. Jetten, and M. Strous (2007): Anammox bacteria disguised as denitrifiers: nitrate reduction to dinitrogen gas via nitrite and ammonium. Environmental Microbiology, vol. 9, no. 3, 635–642.

Kessler A. J., R. N. Glud, M. Bayani Cardenas, M. Larsen, M. F. Bourke, and P. L. M. Cook (2012): Quantifying denitrification in rippled permeable sands through combined flume experiments and modelling. Limnol. Oceanogr. 57, no. 4, 1217–1232.

Kieskamp W. M., L. Lohse, E. Epping, and W. Helder (1991): Seasonal variation in denitrification rates and nitrous oxide fluxes in intertidal sediments of the western Wadden Sea. Mar. Ecol. Prog. Ser. Vol. 72: 145-151.

Klimant I., V. Meyer, and M. Kühl (1995): Fiber–optic oxygen microsensors, a new tool in aquatic biology. Limnol. Oceanogr 40, 1159–1165.

Koop K., W. R. Boynton, F. Wulff, and R. Carman (1990): Sediment water oxygen and nutrient exchanges along a depth gradient in the Baltic Sea, Mar. Ecol.-Prog. Series, 63, 65-77.

Köster R. (1998): Wattsedimente. In: Umweltatlas Wattenmeer, Bd I: Nordfriesisches und Dithmarscher Wattenmeer. Ulmer-Verlag, Stuttgart, pp. 40-41.

Kristensen E., F. Ø. Andersen, and T. H. Blackburn (1992): Effects of benthic macrofauna and temperature on degradation of macroalgal detritus: The fate of organic carbon. Limnology & Oceanography 37, no. 7, 1404-1419.

Kristensen E., M. H. Jensen, G. T. Banta, K. Hansen, M. Holmer, and G. M. King (1998): Transformation and transport of inorganic nitrogen in sediments of a southeast Asian mangrove forest. Aquatic Microbial Ecology 15, 165-175.

Larsen L. H., Niels Peter Revsbech, and S. J. Binnerup (1996): A microsensor for nitrate based on immobilized denitrifying bacteria. Applied and Environmental Microbiology 62, no. 4, 1248-1251.

Laursen A. E. and S. P. Seitzinger (2002): The role of denitrification in nitrogen removal and carbon mineralization in Mid-Atlantic Bight sediments. Continental Shelf Research 22, No. 9, 1397–1416.

Lehmann M. F., D. M. Sigman, and W. M. Berelson (2004): The effect of benthic nitrogen cycling on the 15N/14N and 18O/16O of oceanic nitrate. Marine Chemistry 88, 1-20.

Lehmann M. F., D. M. Sigman, D. C. McCorkle, J. Granger, S. Hoffmann, G. Cane, and B. G. Brunelle (2007): The distribution of nitrate 15N/14N in marine sediments and the impact of benthic nitrogen loss on the isotopic composition of oceanic nitrate. Geochimica et Cosmochimica Acta, vol. 71, no. 22, 5384-5404.

Lieberman N. and T. Albers (2009): Naturmessprogramm und Modellbildung zur Analyse morphodynamischer Veränderungen im Neufelder Watt, Phase 3, Abschlussbericht. Technische Universität Hamburg-Harburg, Institut für Wasserbau.

Lloyd D., K. Thomas, D. Price, B. O'Neil, K. Oliver,and T. N. Williams (1996): A membrane-inlet mass spectrometer miniprobe for the direct simultaneous measurement of multiple gas species with spatial resolution of 1 mm. Journal of Microbiological Methods Journal of Microbiological Methods 25, 145-151.

Lohse L., J. F. P. Malschaert, C. P. Slomp, W. Helder, and W. van Raaphorst (1993): Nitrogen cycling in North Sea sediments: interaction of denitrification and nitrification in offshore and coastal areas. Marine Ecology Progress Series 101, 283-296.

Lohse L., R. Kloosterhuis, W. van Raaphorst, and W. Helder (1996 a). Denitrification rates in continental shelf sediments of the North Sea: acetylene block technique versus isotope pairing. Marine Ecology Progress Series 132, 169-179.

Lohse L., E. H. G. Epping, W. Helder, and W. van Raaphorst (1996 b): Oxygen pore water profiles in continental shelf sediments of the North Sea: turbulent versus molecular diffusion. Marine Ecology Progress Series 145, 63-75.

Lorrai C., D. F. McGinnis, P. Berg, A. Brand, and A. Wüest (2010): Application of Oxygen Eddy Correlation in Aquatic Systems. Journal of Atmospheric and Oceanic Technology 27, no. 9, 1533-1546.

Luther III. G. W., Sundby B., Lewis B. L., Brendel P. J., and Silverberg N. (1997): Interactions of manganese with the nitrogen cycle: Alternative pathways to dinitrogen. Geochimica et Cosmochimica Acta, Vol. 61, No. 19, 4043-4052.

Lynam C. P., M. J. Gibbons, B. E. Axelsen, C. A. J. Sparks, J. Coetzee, B. G. Heywood, and A. S. Brierley (2006): Jellyfish overtake fish in a heavily fished ecosystem. Current Biology 16, R 492-493.

Manheim F.T. and L. S. Waterman (1974): Diffusimetry (diffusion coefficient estimation) on sediment cores by resistivity probe. Initial Rep. Deep-Sea Drilling Project 22, 663-670.

Meijboom F.W. and M.van Nordwijk (1992): Rhizon soil solution samplers as artificial roots. In: L. Kutschera et al. (Eds.): Root Ecology and its practical Application.- Proc 3rd ISSR Symp., 2.-6. Sep 1991, Wien Austria, 793-795.

Meysman, F. J. R., O. S. Galaktionov, B. Gribsholt, and J. J. Middelburg (2006): Bio-irrigation in permeable sediments: An assessment of model complexity. Journal of Marine Research, vol. 64, 589–627.

Meysman F. J. R., O. S. Galaktikov, R. N. Glud, and J. J. Middleburg (2010): Oxygen penetration around burrows and roots in aquatic sediment. Journal of Marine Research 68, 309 – 336.

Mohrholz V., M. Schmidt, and J. R. E. Lutjeharms (2001): The hydrography and dynamics of the Angola-Benguela Frontal Zone and environment in April 1999. South African Journal of Marine Science 97, 199–208.

Mohrholz V., C. H. Bartholomae, A. K. van der Plas, and H. U. Lass (2008): The seasonal variability of the northern Benguela undercurrent and its relation to the oxygen budget on the shelf. Continental Shelf Research 28, 424–441.

Mollenhauer G., R. R. Schneider, P. J. Müller, V. Spieß, and G. Wefer (2002): Glacial / interglacial variablity in the Benguela upwelling system: Spatial distribution and budgets of organic carbon accumulation. Global Biogeochemical Cycles 16, no 4, 1134-1149.

Mulder A., A. A. van de Graaf, L. A. Robertson, and J. G. Kuenen (1995): Anaerobic ammonoium oxidation discovered in a denitrifying fluidized bed reactor. FEMS Microbiol. Ecology 16, 177-183.

Myers, R. J. K. (1972): The effect of sulphide on nitrate reduction in soil. Plant and Soil 37, 431–433.

Nielsen L. P. (1992): Denitrification in sediment determined from nitrogen isotope pairing. FEMS Microbiol Ecol 86: 357- 362.

Nielsen K., L. P. Nielsen, and P. Rasmussen (1995): Estuarine nitrogen retention independently estimated by the denitrification rate and mass balance methods: a study of Norsminde Fjord, Denmark. Marine Ecology Progress Series 119, 275-283.

Nielsen L. P. and R. N. Glud (1996): Denitrification in a coastal sediment measured in situ by the nitrogen isotope pairing technique applied to a benthic flux chamber. Mar Ecol Prog Ser, Vol. 137: 181-186.

Niewöhner C., C. Hensen, S. Kasten M. Zabel, and H. D. Schulz (1998): Deep sulfate reduction completely mediated by anaerobic methane oxidation in sediments of the upwelling area off Namibia. Geochimica et Cosmochimica Acta, vol. 62, no. 3, 455-464.

Nishio T., I. Koike, and A. Hattori (1983): Estimates of denitrification and nitrification in coastal and estuarine sediments. Appl Environ Microbiol 45, 444-450.

OSPAR (2003): OSPAR integrated report 2003 on the Eutrophication Status of the OSPAR Maritime Area based upon the first application of the Comprehensive Procedure, OSPAR Commission 2003.

Owens N. J. P., E. M. S. Woodward, J. Aiken, I. E. Bellan, and A. P. Rees (1990): Primary production and nitrogen assimilation in the North Sea during July 1987. Netherlands Journal of Sea Research 25: 143-154.

Patel A. B (2008): Benthic denitrification and organic matter mineralization in intertidal flats of an enclosed coastal inlet, Ago Bay, Japan. Marine Pollution Bulletin 57, 116-124.

Pätsch J., A. Serna, K. Dähnke, T. Schlarbaum, A. Johannsen, and K.-C . Emeis (2010): Nitrogen cycling in the German Bight (SE North Sea) - Clues from modelling stable nitrogen isotopes. Continental Shelf Research 30, 203–213.

Peterson R. G. and L. Stramma (1991): Upper-level circulation in the South Atlantic Ocean. Progress in Oceanography 26, 1-73.

Pohlmann J. (2010): Optimierung eines Membraneinlasses für die Messung am Membran Inlet Massenspektrometer. Diplomarbeit (Thesis), Fachbereich Angewandte Naturwissenschaften, Fachhochschule Lübeck.

Poole R. and M. Tomczak (1999): Optimum multiparameter analysis of the water mass structure in the Atlantic Ocean thermocline. Deep-Sea Research I, no. 46, 1895–1921.

Postgate, J. (1998): Nitrogen Fixation, 3rd Edition. Cambridge University Press, Cambridge UK.

Precht E. and M. Huettel (2003): Advective pore-water exchange driven by surface gravity waves and its ecological implications. Limnol. Oceanogr. 48(4), 1674-1684.

Precht E., U. Franke, L. Polerecky, and Markus Huettel (2004): Oxygen dynamics in permeable sediments with wave-driven pore water exchange. Limnol. Oceanogr., 49, no. 3, 693–705.

Preisler A., D. de Beer, A. Lichtschlag, G. Lavik, A. Boetius, and B. B. Jørgensen (2007): Biological and chemical sulfide oxidation in a Beggiatoa inhabited marine sediment. The ISME Journal 1, 341–353.

Rao A. M. F., M. J. McCarthy, W. S. Gardner, and R. A. Jahnke (2007): Respiration and denitrification in permeable continental shelf deposits on the South Atlantic Bight: Rates of carbon and nitrogen cycling from sediment column experiments. Continental Shelf Research 27, 1801–1819.

Redfield, A. C., B. H. Ketchum, and F. A. Richards (1963): The influence of organisms on the composition of sea water, in The Sea, vol. 2, edited by M. N. Hill, Interscience New York, 26-77.

Reimers, C. E., H. A. Stecher, G. L. Taghon, C. M. Fuller, M. Huettel, A. Rusch, N. Ryckelyncka, and C. Wild (2004): In situ measurements of advective solute transport in permeable shelf sands. Continental Shelf Research 24, 183–201.

Revsbech N. P., L. P. Nielsen, P. B. Christensen, and J. Sørensen (1988): Combined oxygen and nitrous oxide microsensor for denitrification studies. Appl. Environ. Microbiol 54, 2245- 2249.

Revsbech N. P. (1989): An oxygen microsensor with a guard cathode. Limnol. Oceanogr. 34, no. 2, 474- 478.

Risgaard-Petersen N., L. P. Nielsen, and T. H. Blackburn (1998): Simultaneous measurement of benthic denitrification, with the isotope pairing technique and the N2 flux method in a continuous flow-through system. Water Research 32, no. 1, 3371-3377.

Risgaard-Petersen N., S. Skårup, and L. P. Nielsen (1999): Denitrification in a soft bottom lake: evaluation of laboratory incubations. Aquatic Microbial Ecology 17, 279-287.

Risgaard-Petersen N., L. P. Nielsen, S. Rysgaard, T. Dalsgaard, and R. L. Meyer (2003): Application of the isotope pairing technique in sediments where anammox and denitrification coexist. Limnol. Oceanogr.: Methods 1, 63–73.

Rysgaard S., N. Risgaard-Petersen, N. P. Sloth, K. Jensen, and L. P. Nielsen (1994): Oxygen regulation of nitrification and denitrification in sediments. Limnology & Oceanography 39, no. 7, 1643-1652.

Saunders D. L. and J. Kalff (2001): Denitrification rates in the sediments of Lake Memphremagog, Canada-USA. Water Resources 35, no. 8, 1897–1904.

Sayama, M. (2001): Presence of nitrate-accumulating sulfur bacteria and their influence on nitrogen cycling in a shallow coastal marine sediment. Applied and Environmental Microbiology, vol. 67, 3481–3487.

Schlitzer R. (2011): Ocean Data View. http://odv.awi.de

Schroeder F., K. H. Wiltshire, D. Klages, B. Mathieu, G. Blöcker, and H. D. Knauth (1996): Nitrogen and oxygen processes in sediments of the Elbe estuary. Arch. Hydrobiol. /Suppl. 110, 311-328.

Schulz H. and B. B. Jørgensen (2001): Big bacteria. Annual Review of Microbiology 55:105–37.

Schulz H. N. and H. D. Schulz (2005): Large sulfur bacteria and the formation of phosphorite. Science 307, 416-418.

Seeberg-Elverfeldt, J. M. Schlüter, T. Feseker, and M. Kölling (2005): Rhizon sampling of pore waters near the sediment/water interface of aquatic systems. Limnology and Oceanography: Methods, 3, 361-371.

Seiter K., C. Hensen, and M. Zabel (2005): Benthic carbon mineralization on a global scale. Global Biogeochemical Cycles 19, GB1010.

Seitzinger S., S. Nixon, M. E. Q. Pilson, and S. Burke (1980): Denitrification and N2O production in near-shore marine sediments. Geochim Cosmochim Acta 44, 1853-1860.

Seitzinger S. P., L. P. Nielsen, J. Caffrey, and P. B. Christensen (1993): Denitrification measurements in aquatic sediments: A comparison of three methods. Biogeochemistry 23, 147-167.

Seitzinger S. P. and A. Giblin (1996): Estimating denitrification in North Atlantic continental shelf sediments. Biogeochemistry, vol. 35, no. 1, 235-260.

Shannon L.V. (1985): The Benguela ecosystem part 1. Evolution of the Benguela, physical features and processes. Oceanography and Marine Biology: An Annual Review 23, 105–182.

Silió-Calzada A., A. Bricaud, J. Uitz, and B. Gentili (2008): Estimation of new primary production in the Benguela upwelling area, using ENVISAT satellite data and a model dependent on the phytoplankton community size structure. Journal of Geophysical Research, vol. 113, C11023, 1-19.

Sohm J. A., J. A. Hilton, A. E. Noble, J. P. Zehr, M. A. Saito, and E. A. Webb (2011): Nitrogen fixation in the South Atlantic Gyre and the Benguela Upwelling System. Geophysical Research Letters 38, L16608.

Sørensen J. (1978): Denitrification rates in a marine sediment as measured by the acetylene inhibition technique. Appl Environ Microbiol 36:139-14.

Stern S. A., F. J. Onorato, and C. Libove (1977): The permeation of gases through hollow silicone rubber fibers: effect of fiber elasticity on gas permeation. AIChE Journal, vol. 23, no. 4, 567-578.

Stockenberg A. and R. W. Johnstone (1997): Benthic denitrification in the Gulf of Bothnia. Estuar. Coast. Shelf S., 45, 835–843.

Stolper D. A., N. P. Revsbech, and D. E. Canfield (2010): Aerobic growth at nanomolar oxygen concentrations. Proceedings of the National Academy of Sciences USA 107: 18755–18760.

Stramma L. and M. England (1999): On the water masses and mean circulation of the South Atlantic Ocean. Journal of Geophysical Research 104, no. C9, 20863-20883.

Straub, K. L., M. Benz, B. Schink, and F. Widdel (1996): Anaerobic, nitrate-dependent microbial oxidation of ferrous iron. Applied and Environmental Microbiology, vol. 62, 1458–1460.

Sumaila U. R. and K. Stephanus (2006): Declines in Namibia's pilchard catch: the reasons and consequences. In: Climate change and the economics of the world's fisheries: examples of small pelagic stocks, edited by R. Hannesson, M. Barange & S. F. Herrick Jr., Edward Elgar Pub, 205-214.

Sundbäck K. and A. Miles (2000a): Balance between denitrification and microalgal incorporation of nitrogen in microtidal sediments, NE Kattegat. Aquatic Microbial Ecology 22, 291–300.

Sundbäck K., A. Miles, and E. Goransson (2000b): Nitrogen fluxes denitrification and the role of microphytobenthos in microtidal shallow-water sediments- an annual study. Marine Ecology Progress Series 200, 59-76.

Takahashi T., W.S. Broecker, and S. Langer (1985): Redfield ratio based on chemical data from isopycnal surfaces. Journal of Geophysical Research 90, 6907-6924.

Thamdrup B. and Dalsgaard T. (2000): The fate of ammonium in anoxic manganese oxide-rich marine sediment. Geochimica et Cosmochimica Acta, Vol. 64, No. 24, pp. 4157–4164.

Thamdrup B. and Dalsgaard T. (2002): Production of N2 through anaerobic ammonium oxidation coupled to nitrate reduction in marine sediments. Applied and Environmental Microbiology, vol. 68, no. 3, 1312–1318.

Thomas K. L. and D. Lloyd, D. (1995): Measurement of denitrification in estuarine sediment using membrane inlet mass spectrometry. FEMS Microbiol. Ecol. 16, 103– 114.

Timmermans P. and A. van Haute (1983): Denitrification with methanol. Fundamental work of the growth and denitrification capacity of Hyphomicrobium sp. Water Res. 17, no. 10, 1249-1255.

Timmermann K., G. T. Banta, and R. N. Glud (2006): Linking Arenicola marina irrigation behavior to oxygen transport and dynamics in sandy sediments. Journal of Marine Research 64, 915–938.

Tomaszek J. A. and E. Czerwieniec (2003): Denitrification and oxygen consumption in bottom sediments: factors influencing rates of the processes. Hydrobiologia 504, 59–65.

Trimmer M., D. B. Nedwell, D. B. Sivyer, and S. J. Malcolm (1998) Nitrogen fluxes through the lower estuary of the Great Ouse, England: the role of the bottom sediments. Marine Ecology Progress Series 163, 109-124.

Trimmer M., D. B. Nedwell, D. B. Sivyer, and S. J. Malcolm (2000): Seasonal benthic organic matter mineralisation measured by oxygen uptake and denitrification along a transect of the inner and outer River Thames estuary, UK. Marine Ecology Progress Series 197, 103-119.

Tyrrell T. and M. I. Lucas (2002): Geochemical evidence of denitrification in the Benguela upwelling system. Continental Shelf Research 22, 2497–2511.

Ullman W. J. and R. C. Aller (1982): Diffusion coefficients in near shore marine sediments. Limnology and Oceanogaphy, vol. 27, no. 3, 552-556.

van Beusekom J. E. E. and V. N. de Jonge (1998): Retention of phosphorus and nitrogen in the Ems estuary. Estuaries 21:527–539.

van Beusekom J. E. E, H. Fock, F. de Jong, S. Diel-Christiansen, and B. Christiansen (2001): Wadden Sea specific eutrophication criteria. Wadden Sea Ecosystem 14, 1-115.

van Beusekom J. E. E. and V. N. de Jonge (2002): Long-term changes in Wadden Sea nutrient cycles: importance of organic matter import from the North Sea. Hydrobiologia, 475/ 476, 185- 194.

van Beusekom J. E. E. (2005): A historic perspective on Wadden Sea eutrophication. Helgoland Marine Research 59: 45-54.

van Beusekom J. E. E., P. V. M. Bot, J. H. M. Goebel, H. Lenhart, J. Paetsch, L. Peperzak, T. Petenati, and K. Reise (2005): Eutrophication. In: K. Essink et al. (Editors), Wadden Sea Qualitiy Status Report 2004. Wadden Sea secretariat, Wilhelmshaven, 141-154.

van den Berg, J. H. and A. van Gelder (1993): A new bedform stability diagramm, with emphasis on the transition of ripples to plane bed in flows over fine sand and silt. Spec. Publs Int. Ass. Sediment 17, 11- 21.

van der Plas, A. K. , P. M. S. Monteiro, and A. Pascall (2007): Cross-shelf biogeochemical characteristics of sediments in the central Benguela and their relationship to overlying water column hypoxia. African Journal of Marine Science 29, no. 1, 37–47.

van Raaphorst, W., H. T. Kloosterhuis, A. Cramer, and K. J. M. Bakker (1990): Nutrient early diagenesis in the sandy sediments of the Dogger Bank area, North Sea: pore water results. Netherlands Journal of Sea Research 26, no. 1, 25-52.

Vance-Harris C. and E. Ingall (2005): Denitrification pathways and rates in the sandy sediments of the Georgia continental shelf, USA. Geochemical Transactions 6, 12-18.

Veraart A. J., J. J. M. de Klein, and M. Scheffer (2011): Warming can boost denitrification disproportionately due to altered oxygen dynamics. PLoS ONE 6, no. 3, e18508.

Volkenborn, N. L. Polerecky, D. S. Wethey, and S. A. Woodin (2010): Oscillatory porewater bioadvection in marine sediments induced by hydraulic activities of Arenicola marina. Limnol. Oceanogr., vol. 55, no. 3, 1231–1247.

von Liebig J. (1840): Die organische Chemie in ihrer Anwendung auf Agricultur und Physiologie. Verlag Vieweg und Sohn, Braunschweig, 143 pp.

Wang F., S. K. Junipera, S. P. Pelegri, S. A. Macko (2003): Denitrification in sediments of the Laurentian Trough, St. Lawrence Estuary, Quebec, Canada. Estuarine, Coastal and Shelf Science 57, 515–522.

Webster, I. T. (2003): Wave enhancement of diffusivities within surficial sediments. Environmental Fluid Mechanics 3, 269- 288.

Wiberg, P.L. and C. K. Harris (1994): Ripple geometry in wave-dominated environments. J. Geophys. Res. 99(C1), 775–789.

Wiesner M. G., B. Haake, and H. Wirth (1990): Organic facies of surface sediments in the North Sea. Organic Geochemistry 15, no. 4, 419-432.

Winogradsky S. (1892): Recherches sur les organismes de la nitrification. In: Annales de l'Institut Pasteur Bd. 4.

Wilson, A. M., M. Huettel, and S. Klein (2008): Grain size and depositional environment as predictors of permeability in coastal marine sands. Estuarine, Coastal and Shelf Science 80, 193-199.

Wirth H. and M. G. Wiesner (1988): Sedimentary facies in the North Sea. In: Biogeochemistry and distribution of suspended matter in the North Sea and implications to fisheries biology (edited by Kempe S. et al.). Mitt. Geol. -Paläont. Inst. Univ. Hamburg 65, 269-287.

Würgler Hansen J., B. Thamdrup, and B. B. Jørgensen (2000): Anoxic incubation of sediment in gas-tight plastic bags: a method for biogeochemical process studies. Marine Ecology Progress Series, vol. 208, 273–282.

Zabel M., A. Dahmke, and H. D. Schulz (1998): Regional distribution of diffusive phosphate and silicate fluxes through the sediment-water interface: the eastern South Atlantic. Deep-Sea Research 1, vol. 45, 277-300.

Zimmerman A. R. and R. Benner (1994): Denitrification, nutrient regeneration and carbon mineralization in sediments of Galveston Bay, Texas, USA. Marine Ecology Progress Series, vol. 114: 275-288.

Acknowledgements

As usual for projects like this dissertation, it would have been impossible without the many helpful hands. I want to thank my advisors, colleagues and fellow students for all the fruitful discussions, even the scientific ones. I am indebted especially to (in alphabetical order): Markus Ankele, Justus van Beusekom, Kay Emeis, Astrid Deek, Niko Lahajnar, Frauke Langenberg, Jürgen Möbius, Stefanie Schnell. Thanks for your technical assistance, your patience, your guidance and lessons in geology. Thanks for scientific freedom, and thanks for all the nitrate. I am grateful for the support by the crews of the research vessels Prandtl, Heincke, Africana and Maria S. Merian, I further appreciate access to and support by the laboratories at the AWI Wadden Sea Station List, the FTZ Büsum and the HZG Geesthacht.

This research received financial support by German Research Foundation (DENISE project, Em 37/29) and Federal Ministry of Education and Research (GENUS project, 03F0497A).

Curriculum vitae

Entfällt aus datenschutzrechtlichen Gründen.

Eidesstattliche Versicherung

Hiermit erkläre ich an Eides statt, dass ich die vorliegende Dissertationsschrift selbst verfasst und keine anderen als die angegebenen Quellen und Hilfsmittel benutzt habe.

Hamburg, 20. Oktober 2012 Andreas Neumann